DETERMINATION OF APOLLO EMERGENCY IMPACT LIMITS

C. F. Lombard, S. H. Advani,
A. Roy, M. S. Estes

Prepared under Contract No. NAS 9-4539 by
NORTHROP SPACE LABORATORIES
3401 West Broadway
Hawthorne, California

for

NATIONAL AERONAUTICS AND SPACE ADMINISTRATION

DETERMINATION OF APOLLO EMERGENCY IMPACT LIMITS

C. F. Lombard, S. H. Advani,
A. Roy, M. S. Estes

Prepared under Contract No. NAS 9-4539 by
NORTHROP SPACE LABORATORIES
3401 West Broadway
Hawthorne, California

for

NATIONAL AERONAUTICS AND SPACE ADMINISTRATION

FOREWORD

This report describes the experimental and analytical investigations of the pathophysiological responses to tailward acting impact accelerations ($-G_z$) performed for NASA Manned Spacecraft Center under Contract NAS 9-4539. Mr. H. F. Scherer served as Technical Monitor for NASA.

The objective of the work reported herein was to develop, using small animal experimental data, a theoretical model of the mechanisms of injury to the heart and great vessels of subjects exposed to $-G_z$ impact forces. The ultimate goal of this program is to refine the current model through experiments with larger animals, so that it may be applied to accurate prediction of human impact response.

This study was performed by Northrop Space Laboratories, Hawthorne, California. Dr. C. F. Lombard served as Program Manager. Contributions to this program were made by Mssrs. J. Beattie, J. Felder, R. Hubbard, J. Schuessler, G. Branch, H. Bell, K. Dart, G. Potter, E. Nez, A. D'Aquila, and T. Buser.

All animal research accomplished in the performance of this contract was conducted according to the National Society for Medical Research "Principles of Laboratory Animal Care."

This report is cataloged by Northrop Space Laboratories as document number NSL 65-179.

TABLE OF CONTENTS

LIST OF ILLUSTRATIONS

LIST OF ILLUSTRATIONS (CONT'D)

LIST OF TABLES

SECTION 1.0
INTRODUCTION

Tolerance and survival limits of the human to impact accelerations have increased in importance in the operation of space vehicles and for emergency survival in all manned vehicles. Tolerance limits, using the subjective "ouch factor," have been established for all practical orientations of the body to the accelerative force as shown by Brown (1) and Stapp (2). The lack of objective findings, except for transient bradycardia noted when the the orientation is such that the impact force has a tailward component, indicates that the majority of the tolerance limits are probably related to mechanical distortion of the body which can be minimized by improved containment. However, bradycardia was noted to increase in duration and magnitude with the onset and magnitude of the $-G_z$ impact (1) and could be an indicator of potential injury to the heart or great vessels. Bradycardia has been shown to be abolished by blocking the action of the vagus by the use of atropine (3). Fear of rupture of blood vessels in the chest or brain, and the general discomfort which is produced by a strong vagal stimulation could be factors which would cause a human test subject to reach a voluntary limit to $-G_z$ impact at a relatively low exposure level. Thus two factors are present which may lead to low subjective (tolerance) limits to $-G_z$ impact. Limited experiments using animal subjects have shown that the survival limit in the $-G_z$ orientation is lower than in the other orientations (4). However, a comparison of ratios of no injury level to survival limit in animals indicates that the tolerance level of the human should be higher then presently accepted. Perhaps the true tolerance level of the human is higher and, disregarding the "fear level", can be established for an emergency situation in space vehicle operations. To do this, additional information is needed on the mechanisms which cause injury and produce physiological responses. This information can be used in formulating objective criteria to establish the preinjury limits.

Since the direct approach using human test subjects can not be employed, and since data from accidental exposures to $-G_z$ impact is inadequate, it is

necessary to employ the indirect method to establish realistic human emergency impact limits for tailward acting forces ($-G_z$). The approach selected was to develop a theoretical analog of the mechanisms of injury to the heart and great vessels of humans subjected to $-G_z$ impact to the degree that it can be used to estimate possible impact injury levels. This analog would utilize anatomical and objective physiological data derived from human test subjects at low $-G_z$ impact level exposures to predict the minor and major injury levels.

To develop this analog, a program is required in which (a) both the physiological responses and the pathological findings of animal subjects exposed to $-G_z$ impact are established for the variables of the impact profiles (rate of onset, peak level of G, and duration), (b) the significance of both size and species of animal subjects in relation to the physiological responses and the pathological findings is determined, (c) the tissue strength characteristics of the great vessels of the animals and the human are obtained, (d) the theoretical analog is developed, based on information from several species of small animals, (e) the model is verified using large animals (i.e., bears or chimpanzees), and (f) the model is refined so that it can be applied to man to predict at least the minor impact injury level. To accomplish these objectives, and to facilitate planning, the overall program tasks were grouped into phases as follows:

Phase I Conduct small animal studies or experiments

Phase II Develop a theoretical analog of the mechanisms of injury

Phase III Verify the analog using large animals

Phase IV Refine the model so that it can be applied to man

Phases I and II when accomplished would indicate the feasibility of the approach, thereby permitting planning for the additional Phases III and IV, if indicated. Consequently these two phases were performed first and constitute the program reported herein.

1.1 PHASE I - SMALL ANIMAL STUDIES

A series of $-G_z$ impact tests were conducted using one pound male guinea pigs as test subjects. The purpose of this series was to explore major responses (survival, ECG, and gross pathology) to $-G_z$ impact stress. The profile of the impact acceleration (deceleration) was varied with respect

to rate of onset and peak G, commensurate with velocity changes of 20, 40, and 60 ft/sec. Onset rates used were 5, 10 and 20 thousand G/sec with the peak G of 20, 40, 60, etc., up to that required to give approximately 50% mortality, where possible within the energy envelope. Before, during, and for several minutes following the impact exposure, a modified ECG was obtained. Thirty-one of the 70 subjects impacted at a velocity change of 40 ft/sec were re-exposed to provide additional data on ECG and survival. Gross pathological examinations were conducted on non-survivors and also survivors after euthanasia with sodium pentobarbital; particular attention was given to the heart and great vessels. Alterations in the ECG and the gross pathology incurred were tabulated and correlated with the variables of the forcing function.

Following the guinea pig experiments, a series of $-G_z$ impact tests were conducted using 10 to 13 pound young adult male monkeys (Macaca speciosa) as test subjects. The profile of the impact was varied primarily to give a desired peak G with velocity changes of 20, 40, and 60 ft/sec and to enable study of the correlation between the degrees of bradycardia and the levels of impact. Some animals had repeated exposures while some at the higher levels were exposed only once before being euthanised and necropsied for gross pathological findings. Particular attention was given to the injuries of the heart and great vessels (which did not rupture as predicted). This altered the original plan of determining the pressure and G level at which rupture of the great vessels would occur. Experiments were, therefore, conducted to determine the pressure differential across the aortic arch and the thorax during the $-G_z$ impact. Tissue strength characteristics of the great vessels of the monkey were obtained from literature and other projects. The mechanical and physiological mechanisms which cause the bradycardia were studied in the laboratory and through an extensive literature survey. The results of these experiments and studies were most encouraging and provided a sound basis for the Phase II development of a theoretical analog of the mechanisms of injury.

1.2 PHASE II - DEVELOPMENT OF THEORETICAL ANALOG OF THE MECHANISMS OF INJURY

The results of the small animal studies in Phase I, and the additional information gathered from the literature surveys and other projects provided

basic data for the development of the analog. The guinea pig studies provided pertinent pathological information while the monkeys provided more useful physiological response data. As will be shown, definite progress has been made indicating the feasibility of using a theoretical analog to predict tolerance and injury levels of humans to exposure of $-G_z$ (tailward acting) impact. This will permit the planning of Phases III and IV required to verify and refine the analog so that it can be applied to man.

SECTION 2.0
APPARATUS AND PROCEDURE

2.1 DECELERATORS

A horizontal decelerator and a vertical decelerator were used for the guinea pig and monkey experiments. The impact series requiring a velocity change of 20 ft/sec or 40 ft/sec were conducted on a horizontal decelerator while those requiring a velocity change of 60 ft/sec were conducted on a vertical decelerator.

2.1.1 Horizontal Decelerator

The horizontal decelerator used in these experiments is essentially the same as reported by Lombard (4, 5, 6) with some modifications to upgrade performance. The decelerator (Figure 1) consists basically of a support and restraint system (SARS) for holding the animal, a sled assembly with means for mounting the SARS, a track upon which the sled runs, a 3/4-inch diameter bungee cord to accelerate the sled, and a 20-ton concrete anvil upon which the aluminum honeycomb to be impacted by the sled, as a means of controlling the deceleration G profile, is mounted. In operation, the sled is drawn back by a power winch, stretching the bungee into the firing position. The sled is then attached to the release mechanism and the power winch cable removed. When released, the sled accelerates along the track until its broad, flat face contacts the honeycomb. The honeycomb crushes progressively and, depending upon its cross sectional area, frontal contour, and basic crush strength produces the desired deceleration G profile (rate of onset and peak or plateau value), commensurate with the velocity changes.

2.1.2 Vertical Decelerator

The vertical decelerator consists basically of an 80-foot tower, support and restraint system (SARS), a drop vehicle assembly with means for mounting the SARS and with a hoist cable attachment point, SARS rotating device, a hoist cable and crane to raise the drop vehicle to the desired height, guide cables to reduce transverse motion when the drop vehicle was decending, and a steel anvil secured to a reinforced concrete base upon which

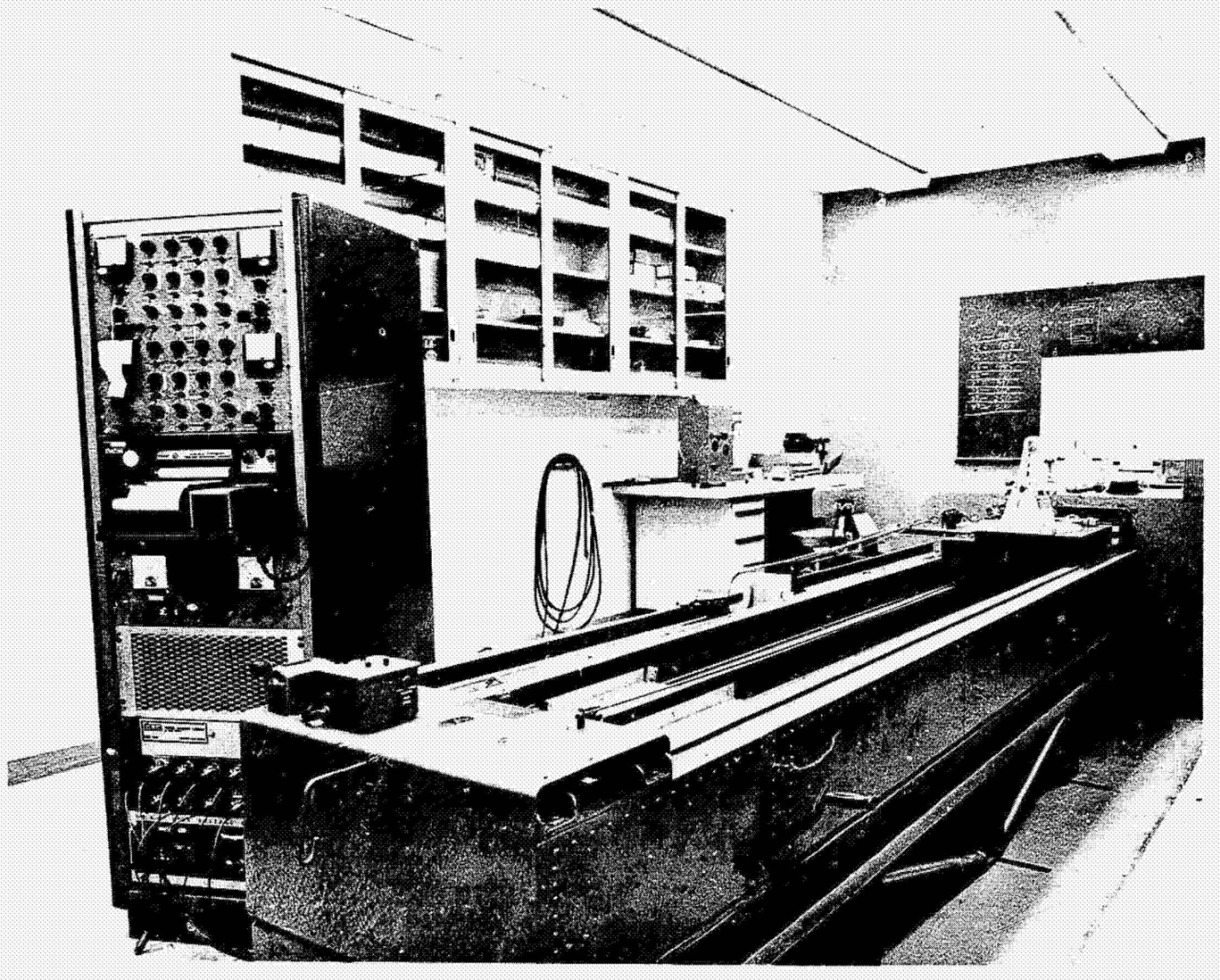

FIGURE 1 HORIZONTAL DECELERATOR SLED

the aluminum honeycomb was placed. In operation, the test animal is placed in the appropriate SARS which in turn is secured in the drop vehicle. The drop vehicle is raised to the desired height by means of a winch and the SARS rotated from the horizontal to the vertical position. The drop vehicle is then released and accelerates at approximately 1 G until it contacts the honeycomb. The honeycomb crushes progressively producing the desired deceleration profile.

2.2 SUPPORT AND RESTRAINT SYSTEMS (SARS)

Two support and restraint systems were used in these experiments. One provided impact protection for guinea pigs and the other for monkeys. Each was designed to be used with either decelerator.

2.2.1 Guinea Pig SARS

The support and restraint system used to contain guinea pig subjects for these experiments is shown in Figure 2 . The SARS consisted of a dorsal support and a torso restraint. The dorsal support was constructed of epoxy plastic reinforced with fiber glass cloth around steel frame members welded to heavy steel pivots. The surface in contact with the subject was semi-contoured to conform to the animal's dorsal form and was lined with 1/8-inch Ensolite semi-resiliant vinyl foam. The torso restraint was made of dacron with 1/2-inch by 1/16-inch nylon webbing (1000 lb test rating) to secure the subject to the dorsal support. A head restraint of nylon webbing (1000 lb) with a three point suspension was provided to reduce whiplash and lateral head rotation.

2.2.2 Monkey SARS

The support and restraint system used for monkey subjects (Figure 3) consisted of a basic dorsal support, nylon webbing, a head and shoulder restraint fixture, and a welded tubular truss. Part way through the experiment, the head and shoulder restraint fixture was replaced by a "muzzle type" head restraint and shoulder and chest restraint of nylon webbing. The basic dorsal support was designed to maintain the subject in a seated posture and directly supported the animal's feet, legs, buttocks and lower back. The dorsal support was semi-contoured to fit the dorsal side of the monkey and an 1/8-inch layer of Ensolite was provided in the torso region. Semi-contoured torso panels conforming to the subject's abdomen and lower

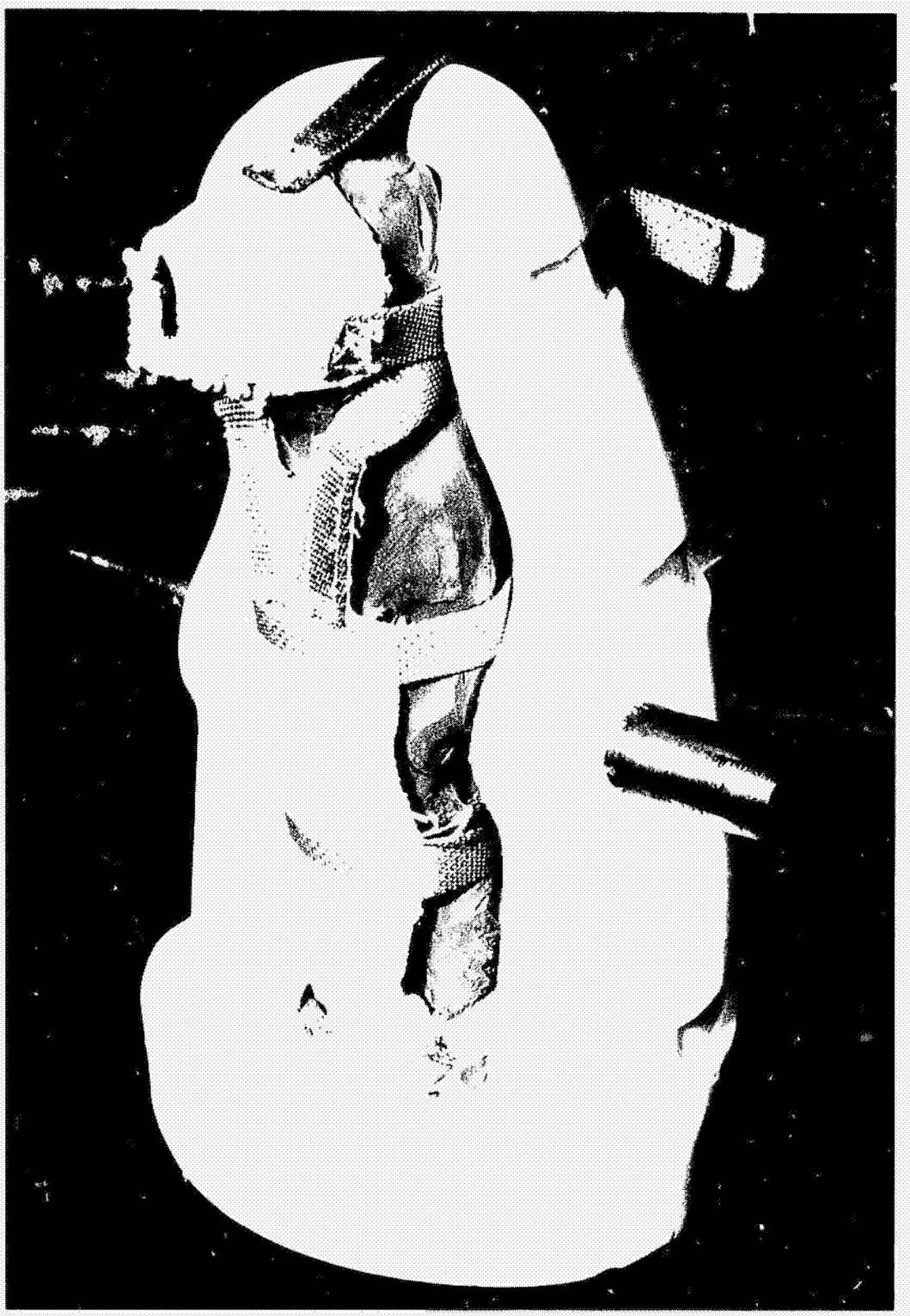

FIGURE 2 SUPPORT AND RESTRAINT SYSTEM USED FOR GUINEA PIG SUBJECTS

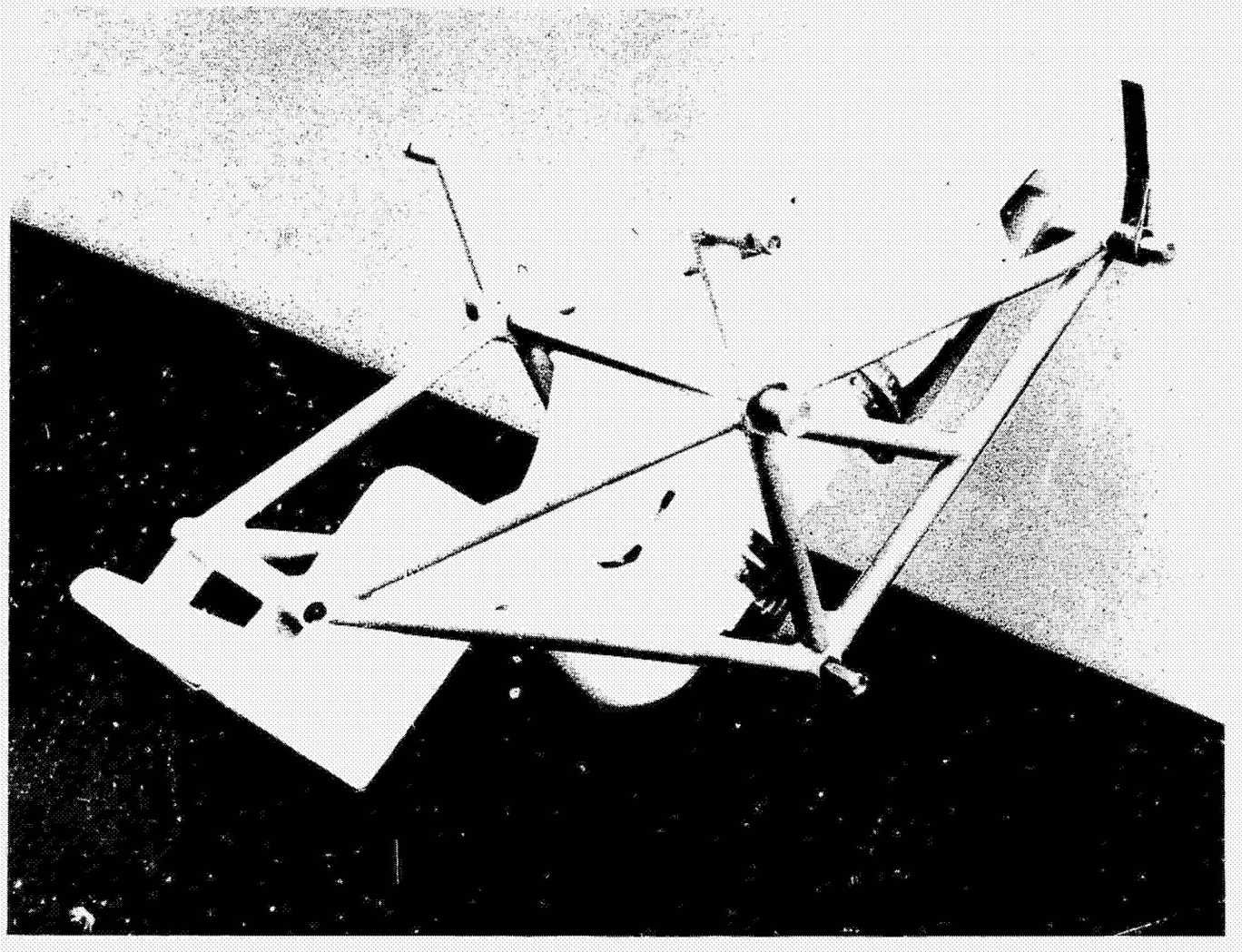

FIGURE 3 SUPPORT AND RESTRAINT SYSTEM USED FOR MONKEY SUBJECTS (WITH HEAD AND SHOULDER RESTRAINT FIXTURE)

chest were attached by means of hinges to the basic dorsal support to provide uniform containment of the subject. The dorsal support and torso panels were constructed of 3/16-inch epoxy plastic reinforced with fiberglass cloth. Nylon webbing (2500 lb) 1-inch by 1/16-inch, was used to restraint the subject's feet and legs and the upper and lower ends of the torso panels. A dacron webbing lap belt, 1 3/4-inch by 1/16-inch with a tensile strength of 6300 pounds was used for additional restraint. The arms were restrained by tying the subject's wrists to the supporting truss with 1/2-inch by 1/32-inch nylon webbing. The head and shoulder restraint fixture consisted of a channel which cradled the head and had curved flanges at the lower end which conformed to fit the subject's shoulders. The head and shoulder restraint fixture was constructed of epoxy plastic reinforced with fiberglass cloth and was approximately 3/16-inch in thickness. The head and shoulder restraint fixture was mounted on a braking mechanism which was attached to the welded tubular truss. This allowed the subject's head and shoulders to translate up to one inch along the "Z" axis under $-G_z$ loading to reduce compression loading on the spine. An Eccosphere pad* sealed in an impermeable latex bag was used and was evacuated to provide a rigid, custom-contoured support for the head and shoulder area of each individual subject. The welded tubular truss enabled the SARS to be used in either decelerator. The truss attached to the basic dorsal support at the footrest and at the upper and lower ends of the back, thus joining the two together into a framework which provided maximum support for the basic dorsal support. After welding, the tubular frame was stress relieved and heat treated to insure the structural integrity of the system.

After the first 25 runs, the SARS was modified to simulate a restraint system more readily adaptable to man. A flaccid (un-evacuated) 1/2-inch Eccosphere torso pad was substituted for the Ensolite torso pad and the head and shoulder restraint fixture was removed and replaced by a shoulder restraint of 2500-lb, 1-inch by 1/16-inch nylon webbing (see Figure 4a,b). Two straps were secured to the anterior portion of the basic dorsal support just below the shoulders. The straps ran over the shoulders, under the torso pad, and were attached to the truss beside the thighs. They were laced together

*(Small hollow plastic spheres in a cover, somewhat resembling a bean bag. After being contoured to the individual subject, bag evacuation rigidizes the assembly. See NSL Report No. 66-109 for details.)

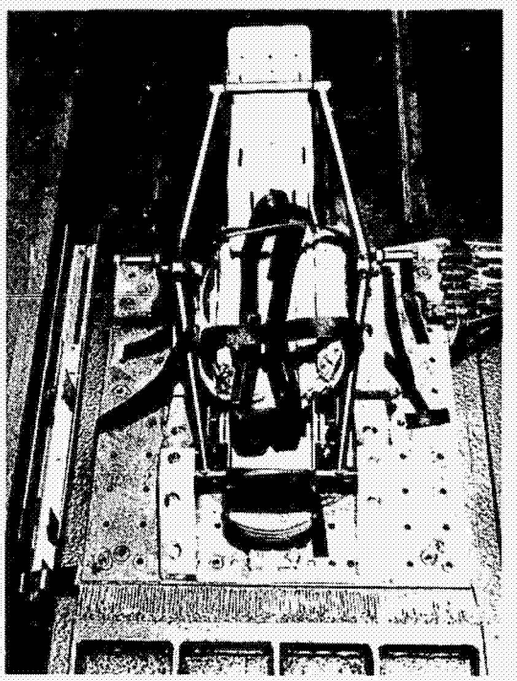

A. TOP FRONT VIEW

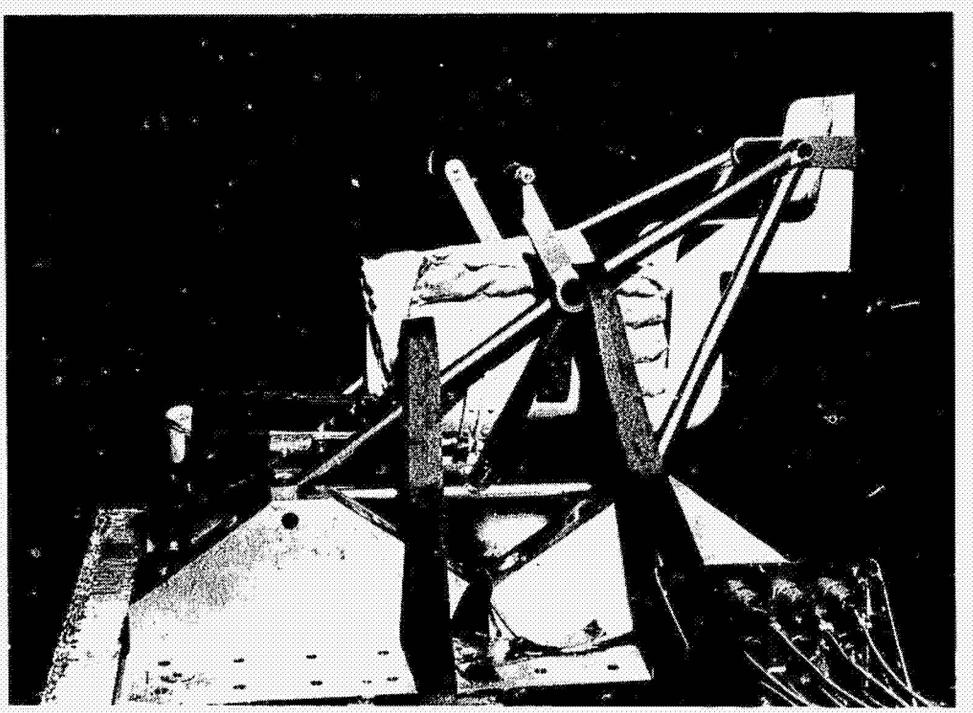

B. SIDE VIEW

FIGURE 4 SUPPORT AND RESTRAINT SYSTEM USED FOR MONKEY SUBJECTS (WITH SHOULDER HARNESS) MOUNTED ON SLED

across the chest to prevent them from slipping off the shoulders under load. A wedge of rigid epoxy foam was attached to the welded tubular truss to position the subject's head in the proper orientation. A three point dacron head restraint was used to reduce lateral head motion and whiplash under loading.

2.3 INSTRUMENTATION

Acceleration transducers and a recording oscillograph were used to record the deceleration G profile. The three types of transducers used were (a) Statham model A52-150-300 ±150 G with a natural frequency of more than 1000 cps, (b) CEC model 4-202-0001 ±250 G with a natural frequency of 2000 cps, and (c) CEC model 4-202-0001 ±500 G with a natural frequency of 2900 cps. The frequency response of all transducers is flat to one-half of their frequency. The output from the transducers was fed through a balance box to a CEC Model 5-124 recording oscillograph. The galvanometer used in the oscillograph in conjunction with the acceleration transducers was a CEC 7-342 which has a flat response to frequencies up to 135 cps.* Typical G profiles are shown in Figure 5.

For recording internal pressures from the test subject Statham SF-1 physiological pressure transducers were used. These strain gage devices have an operating range of ±300 mm Hg and a design limit of ±500 mm Hg with a natural frequency of 1200 cps. The outputs of the transducers were fed into CEC Model 3101B wideband DC amplifiers, then through a balance box and into a recording oscillograph. The oscillograph was the same as that used to record the deceleration G profile. The galvanometers used in the oscillograph in conjunction with the pressure transducers were CEC 7-364 with a flat response to a frequency of 500 cps.

Electrocardiograms were obtained on guinea pig subjects impacted at 20 and 40 ft/sec using a Beck-Lee "Cardi-O-Mite". Electrodes were attached

*The minimum frequency response requirement for the deceleration profile is determined by the equation $f = \omega/2\pi$ where ω is equal to the onset divided by the peak G (ω = onset/G). Since the highest frequency attained by the forcing function was 90 cps at a peak G of 446 with an onset of 250,000 G/sec, a flat response to 135 cps was sufficient.

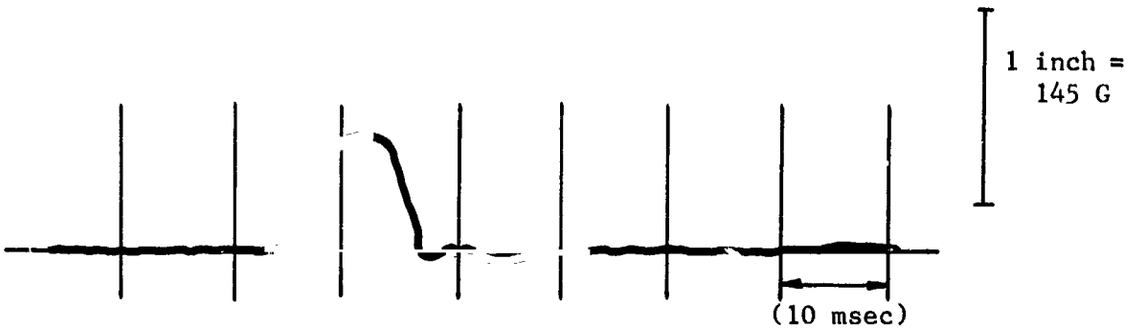

A. - ΔV = 20 ft/sec, Peak G = 85, Onset = 20,000 G/sec

B. - ΔV = 40 ft/sec, Peak G = 80, Onset = 20,000 G/sec

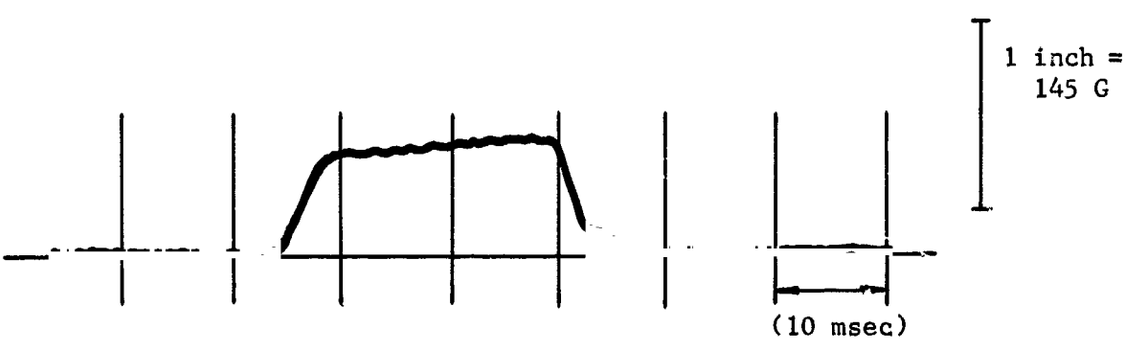

C. - ΔV = 60 ft/sec, Peak G = 85, Onset = 20,000 G/sec

FIGURE 5 TYPICAL IMPACT DECELERATION PROFILES FOR GUINEA PIG AND MONKEY SUBJECTS

to skin folds in the axillary region using spring type clips. Electrocardiograms were obtained on guinea pig subjects impacted at 60 ft/sec using a Sanborn recorder (Model 296) in conjunction with a Sanborn 350-3200A ECG preamplifier. Four spring clip electrodes were used on these subjects, attached on the chest and groin. A continuous recording was obtained on all subjects before, during, and after impact using the lead one configuration.

Electrocardiograms were obtained on all monkey subjects using the same Sanborn recorder and preamplifier system that was used in the guinea pig 60 ft/sec series. Four Telemedic adhesive electrodes were used on the chest and lower abdomen. A lead one configuration was used in obtaining continuous recordings from the subjects.

2.4 TEST SUBJECTS

Two types of test subjects were used in this study. In the first phase, 266 tests were conducted with adult male guinea pigs (Cavy porcellus). The second phase used young adult male monkeys (Macaca speciosa).

2.4.1 Guinea Pigs

Guinea pigs were obtained from a local breeder. These animals were of good pedigree and were raised with the care and attention required for research animals. When received the animals were examined for outward signs of illness. Periodically, animals were sacrificed and examined for both gross and microscopic pathological findings for controls.

2.4.2 Monkeys

Research quality monkeys, weighing from 10 to 13 pounds, were obtained via air freight from an importer. The animals had been conditioned for at least six seeks before delivery.* Upon receipt, all animals were examined for outward signs of disease or injury. If needed, therapeutic measures were taken. Animals not meeting quality standards were returned to the importer. Subjects selected were housed in an air conditioned laboratory holding facility for further observation before being tested.

2.5 HANDLING PROCEDURES

Two-hundred and sixty-six (266) guinea pig runs and 42 monkey runs were conducted with planned deceleration G profiles to study the threshold of

*Asiatic Animal Imports, Inc., Burlingame, California conducts tests and treats animals to provide a "conditioned" or certified test subject.

bradycardia and the tolerance limits of the subjects. An additional 19 tests were conducted on surgically prepared monkeys to record intrathoracic and intra-aortic pressures during impact.

2.5.1 Guinea Pig Tests

A preliminary clinical examination was given each animal immediately before being exposed. The subject was then placed in the appropriate SARS and restrained. The ECG electrodes were attached and the animal impacted with the planned G profile. The heart rate was monitored throughout the test and the recording was continued until it became constant. The subject was then removed from the SARS and examined for clinical signs of injury. Non-survivors were necropsied the day of impact. Subjects that lived for 24 hours were considered to be survivors. In the 20 and 60 ft/sec series, the subjects were euthanized after the survival period. In the 40 ft/sec series the subjects were either euthanized at the end of the survival period or held for reexposure. The subjects were euthanized with 1 cc of sodium pentobarbital (50 mg/cc) intraperitoneally. After the subjects were euthanized they were necropsied and a gross pathological examination of the major organs and blood vessels was made.

2.5.2 Monkey Tests

Each subject was given a preliminary examination and shaved for the ECG electrodes which were then attached. The subject was then placed in the SARS and impacted with the planned G profile. The ECG was monitored throughout the test and continued until the heart rate returned to the pre-run level. The subject was then removed from the SARS and examined clinically for injuries, and observed further for two hours. At the end of this time, if the subject was scheduled to be necropsied, it was euthanized with a 10 cc intravenous injection of sodium pentobarbital (50 mg/cc). If the subject was to be tested again, it was returned to the holding facility and observed for at least three days before being re-exposed. Any subject that was injured was euthanized and necropsied immediately. During necropsy, special attention was given to the heart, major vessels, and CNS.

2.5.3 Monkey Preparations for Pressure Measurements

Subjects scheduled to be surgically prepared for pressure measurements were anesthetized with sodium pentobarbital (50 mg/cc) administered intravenously using a dosage of 10 mg per pound of body weight. Additional 1 cc dosages of the anesthetic were injected throughout the experiment to maintain

the subject at an adequate level of surgical anesthesia. The subject was then given an intravenous injection of 3000 USP units of heparin to prevent blood clotting. The subject's neck, chest, abdomen, thighs, and elbows were shaved to facilitate surgery and electrode placement. A tracheotomy was then performed and an endotracheal tube inserted. At this point the subject was ready for the introduction of the SF-1 pressure transducer catheters.

The catheterization of the aortic arch was performed first. A skin incision was made in the left inguinal region and the iliac artery exposed by blunt dissection. The vessel was ligated at the distal end and occluded at the proximal end with "0" silk sutures. An incision was then made in the vessel wall and the catheter inserted. The proximal end of the vessel was released slowly to permit the passage of the catheter. The catheter was then passed through the iliac artery into the aorta to the desired level. The suture at the proximal end of the incision in the vessel wall was tied, thus securing the catheter in the vessel. The catheter was then anchored to the deep tissue and skin by proximal and distal ligatures to prevent displacement at impact. The skin incision was closed with wound clips and the catheter was then sutured along the length of the thigh to improve stability.

In two preparations the iliac artery was found to be too small to permit introduction of the catheter. In these cases, the initial skin incision was extended anteriorly to the lumbar region and blunt dissection was performed retroperitoneally to expose the abdominal aorta. The aorta was then ligated distally just above the bifurcation and was occluded proximally. An incision was made in the vessel wall and the catheter was inserted. Once the catheter was in place the proximal ligature was tied to anchor the catheter to the deep tissue. The muscle layers were closed with "0" silk sutures and the skin incision was closed with wound clips.

Catheterization of the intrathoracic space began with a skin incision in the right chest at the second intercostal space. A trocar-like needle was used for blunt dissection of the chest wall into the intrathoracic space. Once the needle was in place, the catheter was passed from the needle into the cavity. The needle was then withdrawn and the skin incision

was closed with wound clips. The catheter was then anchored to the skin at two points with "0" silk sutures.

The ECG electrodes were then attached. The plug in the distal end of the aortic catheter was then opened and the catheter was bled to remove trapped air. The plug was then replaced and the subject was secured in the SARS on the sled. The instrumentation leads were then connected and the sled was pulled into the firing position. Instrumentation recording was then begun and after 60 seconds, the subject was impacted. Instrumentation was monitored throughout the run and continued until the pre-run baseline was reached. The subject was observed in the SARS for at least thirty minutes before re-exposure. The number of exposures for each of the six subjects varied from two to six. At the completion of the runs, the subject was removed from the SARS and euthanized with 10 cc of sodium pentobarbital (50 mg/cc) intravenously. The subject was necropsied with care taken to note the location and orientation of the catheter tips in relation to the G vector.

SECTION 3.0
EXPERIMENTAL RESULTS

In this section, experimental results describing pathophysiological responses of subjects exposed to $-G_z$ (tailward acting) accelerations are presented. The results include the electrocardiographic findings and clinical and pathological observations of the guinea pig and monkey impact subjects.

3.1 GUINEA PIG (Cavy porcellus) IMPACT RUNS

3.1.1 Clinical Observations

Two subjects impacted at a velocity change of 20 ft/sec expired immediately following the exposure, one at 40 G and 5,000 G/sec and one at 40 G and 10,000 G/sec. The remainder of the subjects in this series appeared to be essentially normal at post-impact examination. Tabulation was not considered necessary.

During the series of tests conducted at a velocity change of 40 ft/sec the survival rate decreased at higher G levels. It was noted that all non-survivors in this series were dead within two minutes after impact. Thus, no animals expired between two minutes and the 24 hours defined as the time of survival. Respiratory difficulty was noted more frequently at higher G levels. Injury to the forelimbs occurred in three out of seven subjects at 120 G and 20,000 G/sec and injury to both the hindlimbs and forelimbs was apparent in one subject out of ten at 150 G and 20,000 G/sec. Tabulation was not considered necessary.

Clinical observations noted during tests with a velocity change of 60 ft/sec are listed in Table I. An examination of these observations shows that the number of non-survivors increases with higher G levels. A column for leg injuries has also been included to differentiate between true paralysis and inability to move the legs. Large hematomas, severe muscle contusions, and hemorrhage of the brachial arteries are causes of foreleg injuries often confused with paralysis.

3.1.2 General Trends and Patterns of Electrocardiograms

The general trend of the electrocardiographic tracings showed mainly a change in rate. The majority of the subjects manifested bradycardia with

TABLE I - CLINICAL OBSERVATIONS - GUINEA PIG
RUNS - VELOCITY CHANGE (ΔV) = 60 FT/SEC

G Level	80	100		120		140		160
Onset (G/sec)	20,000	10,000	20,000	10,000	20,000	10,000	20,000	20,000
No. of Subject	9	10	10	10	10	10	8	10
No. of Non-Survivors			2	1	2	2	4	5
Fatal at Impact			2	1	2	2	4	4
Fatal 0-24 hours								1
Paralysis								
Forelimb	2		1		1			
Hindlimb					1			2
Both					1			1
Respiratory Distress							1	2
Leg Injury								
Forelimb	2	4	4	3	2	1	3	3
Hindlimb						1		
Normal	5	6	3	6	3	6	2	

a few exhibiting tachycardia or alternating tachycardia and bradycardia. The tracings were also examined for abnormalities other than change in rate. These findings are listed in Tables II, III, and IV and are summarized below.

20 Ft/Sec Series - Bradycardia was incident in 76 subjects out of 84 (90%) in varying degrees of severity. Severe bradycardia appeared in only 13% of the subjects with 34% exhibiting moderate bradycardia and 43% showing minimal bradycardia.

Transient auricular flutter and atrioventricular block were common observations as was the occurrence of asystole. Extrasystoles, evidence of subendocardial damage, and tachycardia were also observed in a few incidences and were all of a transient character.

40 Ft/Sec Series - Bradycardia was incident in 84 out of 105 subjects (80%), severe degree in 27%, moderate degree in 30%, and minimal degree in 23%. Tachycardia was more prevalent at this energy level, occurring in 26% of the subjects.

The incidence of transient auricular flutter, extrasystoles, and evidence of subendocardial damage increased in this series over the 20 ft/sec series. Atrioventricular block, a common finding in subjects exposed with a velocity change of 20 ft/sec, occurred in only three cases in this series. There appear to be no significant differences in the ECG tracings of multiple and single exposure animals.

60 Ft/Sec Series - As seen in Table IV (given in more detail to bring out the causes of non-survival) 57 guinea pigs out of 77 (74%) exhibited bradycardia, 29% to a severe degree, 30% to a moderate degree, and 15% to a mild degree. Tachycardia was evident in only five of the subjects tested in this series. The incidence of auricular flutter and atrioventricular block increased at higher G levels. Extrasystoles and evidence of subendocardial damage were common findings throughout the series. Five animals demonstrated ventricular tachycardia out of which three survived. One subject died of ventricular fibrillation following ventricular tachycardia, while another died with evidence of severe subendocardial damage and extrasystoles following ventricular tachycardia.

TABLE II - ECG OBSERVATIONS - GUINEA PIG RUNS -

VELOCITY CHANGE (ΔV) = 20 FT/SEC

G Level		20		40			60		
Onset (G/Sec)		5,000	10,000	5,000	10,000	20,000	5,000	10,000	20,000
No. of Subjects		11	10	10	10	11	10	10	12
No. of Non-Survivors		0	0	1	1	0	0	0	0
Brady-cardia	Severe	1			2	4	2	2	
	Moderate	5	1	3	5	3	3	2	7
	Minimal	4	7	7	3	3	3	4	5
Tachycardia*							2	3	1
Auricular Flutter		3	1	2	4	6	2	3	5
Atrioventricular Block		1	1	2	4	5		1	2
Subendocardial Damage					1	2			
Extrasystole					1			2	1
Asystole				3	1	1	2	2	3
No Change in Rate		1	2			1	1		

* Tachycardia may follow original bradycardia

TABLE III - ECG OBSERVATIONS - GUINEA PIG RUNS -

VELOCITY CHANGE (ΔV) = 40 FT/SEC

G Level		40			60			100		120	130	150
Onset (G/sec)		5,000	10,000	20,000	5,000	10,000	20,000	5,000	20,000	20,000	20,000	20,000
No. of Subjects		10	10	10	10	10	10	10	8	7	10	10
No. of Non-Survivors		0	0	0	0	0	0	0	0	0	2	6
Brady-cardia	Severe	3		2	3	1	3	2	4	3	7	1
	Moderate	1	1	3	6	4	1	5	3	1	1	5
	Minimal	4	6	1	1	2	4	2	1	1	1	1
Tachycardia*		1	2	1		4	2	1	1	2	1	9
Auricular Flutter		1	3	3	3	5	5	6	8	4	5	6
Atrioventricular Block						1					2	
Subendocardial Damage						3	2	7	3	2	3	3
Extrasystole		2	1	1			2	2	3	2	1	1
Asystole		1				2	2	2				
No Change in Rate		1	2	3		1				1		

*Tachycardia may follow original bradycardia.

TABLE IV - ECG OBSERVATIONS - GUINEA PIG RUNS -
VELOCITY CHANGE (ΔV) = 60 FT/SEC

G Level		80		100				120				140				160	
Onset (G/sec)		20,000		10,000		20,000		10,000		20,000		10,000		20,000		20,000	
No. of Subjects		9		10		10		10		10		10		8		10	
		S*	NS*	S	NS	S	NS	S	NS	S	NS	S	NS	S	NS	S	NS
		9		10		8	2	9	1	8	2	8	2	4	4	5	5
Brady-cardia	Severe	2		1		1	2	1	1	2	2		2		2	3	3
	Moderate	2		4		4		5		3				2	1	1	1
	Minimal	3		1		3						4		1			
Tachycardia**						1	1			1				1	1		
Auricular Flutter		3		6		5		6	1	5	1	5	2	3	3	3	5
Atrioventricular Block		2		6		4	2	5	1	3	2	3	2	2	3	3	5
Subendocardial Damage		1		3		4	2	4		5	2		2	1	3	4	2
Extrasystole		3		3		3	1	5	1	3	2	4		3	2	3	3
No Change in Rate		2		4				3		2		4				1	1

*S and NS refer to Survivors and Non-Survivors respectively.

**Tachycardia may follow original bradycardia.

3.1.3 Pathological Observations

The gross pathology observed in the subjects exposed to impact with a velocity change of 40 ft/sec is not tabulated because 31 of the 70 subjects were exposed more than once to yield additional data on ECG patterns and survival limits. The gross pathology observed at velocity changes of 20 and 60 ft/sec is listed in Tables V and VI A,B,C,D and is summarized under three major headings: Head and Neck, Thorax, and Abdomen.

Head and Neck - Congestion of the cerebral vessels and hemorrhage of the meningeal vessels tended to increase at higher G levels. Hemorrhage of the neck vessels was not observed at 20 ft/sec, but was a common finding at a velocity change of 60 ft/sec.

Thorax - Pulmonary hemorrhage was a major finding. The degree of such hemorrhage varied, occurring primarily in the periphery of the individual lobes and less frequently in the hilum. Subpleural hemorrhage in the area where the azygos vein joins the superior vena cava was observed at 60 ft/sec, but was not found at a velocity change of 20 ft/sec. Major vessel laceration did not occur in the 20 or 40 ft/sec series and was noted only twice in the 60 ft/sec series, once as pulmonary vessel laceration and once as aortic laceration.

Abdomen - Hemorrhage of the abdominal organs such as liver, kidney, stomach, pancreas, and spleen was noted to increase at higher G levels. Lacerations of the stomach and liver were also detected.

TABLE V - PATHOLOGICAL OBSERVATIONS - GUINEA PIG

RUNS - VELOCITY CHANGE (ΔV) = 20 FT/SEC

G Level	20		40			60		
Onset (G/sec)	5,000	10,000	5,000	10,000	20,000	5,000	10,000	20,000
No. of Subjects	11	10	10	10	11	10	10	12
No. of Non-Survivors	0	0	1	1	0	0	0	0
Hemorrhage								
Meningeal	2	1		1		1	1	1
Pulmonary	2	1	2	1	1	1	4	5
Laceration								
Gastric vessels		1			1			
Pancreatic vessels		1	1	1		1	2	2

TABLE VI - PATHOLOGICAL OBSERVATIONS - GUINEA PIG

RUNS VELOCITY CHANGE (ΔV) = 60 FT/SEC

A - 100 G

G Level	100						100					
Onset (G/Sec)	10,000						20,000					
No. of Subjects	10						10					
No. of Non-Survivors	0						2					
Pathology	Minimal		Moderate		Severe		Minimal		Moderate		Severe	
	S	NS	S	NS	S	NS	S	NS	S	NS	S	NS
Hemorrhage												
Meningeal	3		1				1		1			2
Neck Vessel			1				1	1			1	1
Subpleural					1							
Pulmonary	1		1				2					1
Laceration												
Pulmonary			1									
Hepatic									1			

B - 120 G

G Level	120						120					
Onset (G/Sec)	10,000						20,000					
No. of Subjects	10						10					
No. of Non-Survivors	1						2					
Pathology	Minimal		Moderate		Severe		Minimal		Moderate		Severe	
	S	NS	S	NS	S	NS	S	NS	S	NS	S	NS
Hemorrhage												
Meningeal	2	1	2				2		1			2
Neck Vessel			1	1	1		2				1	
Subpleural					1				2		6	
Pulmonary												2
Hemothorax				1								1
Renal	1											
Intestinal			1						1			
Laceration												
Pulmonary Vessel						1						
Fracture												
Spinal											2	

TABLE VI (Continued)

C - 140 G

G Level	140						140					
Onset (G/Sec)	10,000						20,000					
No. of Subjects	10						8					
No. of Non-Survivors	2						4					
Pathology	Minimal		Moderate		Severe		Minimal		Moderate		Severe	
	S	NS	S	NS	S	NS	S	NS	S	NS	S	NS
Hemorrhage												
Meningeal	2			1			1			2		
Neck Vessel		1	1		1				1			2
Subpleural					1							
Pulmonary									1			1
Precaval												1
Hemopericardium												1
Hemothorax										1		
Intestinal	2		1				2					
Laceration												
Hepatic										1		
Aortic												1
Gastric												1

D - 80 & 160 G

G Level	80						160					
Onset (G/Sec)	20,000						20,000					
No. of Subjects	9						10					
No. of Non-Survivors	0						5					
Pathology	Minimal		Moderate		Severe		Minimal		Moderate		Severe	
	S	NS	S	NS	S	NS	S	NS	S	NS	S	NS
Hemorrhage												
Meningeal	3		1					1	1	1		2
Neck Vessel	1		1						1	2	1	
Subpleural										1		1
Pulmonary	1				1						1	1
Gastric											2	1
Renal	1											
Intestinal	3						1				1	
Laceration												
Gastric								1				
Hepatic								1		1		

3.2 MONKEY (Macaca speciosa) IMPACT RUNS

3.2.1 Clinical Observations

At a velocity change of 20 ft/sec, six runs were conducted with no apparent change in the clinical condition of the subjects.

At a velocity change of 40 ft/sec, twenty-two runs were conducted. Immediate post-impact observations included distention of the jugular veins and a cessation of respiration which usually resumed within two minutes. Most of the subjects observed had a moderate degree of paleness of the cheeks and were moderately to slightly dazed after impact. The mobility of the subjects did not appear impaired except in one test where a fractured femur occurred.

At a velocity change of 60 ft/sec, the subject's respiration ceased at impact in all fourteen runs. When it returned, within two minutes, it was slow and irregular for up to five minutes before returning to normal. In one subject abdominal breathing was noted post-impact. The subject was later found to have a moderate degree of pneumothorax. The gums and tongues of six subjects appeard bluish in color immediately post-impact. Within a minute or two the bluish color disappeared. The cheeks of all subjects looked moderately pale after impact and the jugular and axillary veins appeared engorged. Changes in the size of the pupils in two subjects were observed. In both subjects the left pupil was constricted and appeared smaller in size than the right, but reacted to light reflex in both cases. Accommodation reflex was present in both. It took five minutes and ten minutes for the pupils to regain normal size. Loss of muscle tone of varying degree after impact was a notable feature in some subjects. Myalgia occurred commonly after impact and contributed to the lack of voluntary mobility. Fracture of femur occurred in two subjects.

3.2.2 General Trends in Electrocardiograms

The observations obtained from examination of the electrocardiograph tracings of monkey subjects are listed in Table VII and are summarized here.

At a velocity change of 20 ft/sec, no change in heart rate or rhythm was observed. Six runs were conducted at various G levels ranging from 40 to 130 G.

TABLE VII ECG EVALUATIONS - MONKEY RUNS

A. Velocity Change = 20 Ft/Sec

G	Onset	Evaluations
39	16,300	No change
59	26,400	No change
88	20,300	No change
111	23,200	No change
117	19,100	No change
131	20,150	No change

B. Velocity Change = 40 Ft/Sec

G	Onset	Evaluations
40	19,400	No change
55	30,700	No change
58	21,400	Mild tachycardia
62	40,600	No change
78	18,350	Severe bradycardia, auricular fibrillation, extrasystoles, subendocardial damage
79	31,700	Mild tachycardia
99	18,100	Bradycardia at impact and auricular fibrillation
122	14,200	No change
124	41,600	Bradycardia at impact; mild tachycardia later
125	19,400	Mild tachycardia
152	18,100	No change
177	14,900	No change
189	21,600	Moderate tachycardia
201	41,500	Bradycardia at impact; mild tachycardia later

(Continued)

(TABLE VII Continued)

(B. Velocity Change = 40 Ft/Sec Continued)

G	Onset	Evaluations
234	37,000	No change
258	38,500	Mild tachycardia
339	38,000	Mild tachycardia
413	175,500	Severe to moderate bradycardia, auricular fibrillation at impact
430	210,200	Mild bradycardia followed by mild tachycardia
433	205,000	Bradycardia at impact only
446	250,000	No change
450	223,000	No change

C. Velocity Change = 60 Ft/Sec

G	Onset	Evaluations
98	57,300	Mild tachycardia, subendocardial damage
100	No Record	Mild tachycardia
153	69,100	Mild tachycardia, subendocardial damage
159	85,000	Moderate tachycardia
166	95,200	Severe bradycardia
175	No Record	Moderate bradycardia, extrasystoles
193	90,250	Severe bradycardia, extrasystoles, subendocardial damage
200	No Record	Severe bradycardia, subendocardial damage
200	No Record	Severe bradycardia, auricular fibrillation at impact, extrasystoles, subendocardial damage
254	120,000	Moderate to severe bradycardia, ventricular tachycardia, subendocardial damage
306	169,100	Severe bradycardia, subendocardial damage
325	151,000	Severe bradycardia

At a velocity change of 40 ft/sec, 22 runs were conducted. Nine subjects showed no change, six mild tachycardia, five transient (2-3 sec) bradycardia, and two showed mild to moderate bradycardia for one minute or longer.

At a velocity change of 60 ft/sec, 14 runs were conducted at various G levels from 98 to 325 G. No ECG was obtained in two runs (not included in Table VII) as the leads parted at impact. Bradycardia of a moderate to severe degree was noted in subjects exposed above 160 G. Mild to moderate tachycardia was observed below 160 G.

The results of the electrocardiograms obtained from the surgically prepared subjects for pressure measurements are not included in Table VII. However, no change in rate or rhythm was observed.

3.2.3 Pathological Observations

With one exception, M-24, all of the monkey subjects used in this project are listed with an individual history of exposures arranged below in sequential order. M-24 was maintained to study possible long term effect of multiple exposure. This subject has sustained exposures of 413 G (40 ft/sec); 20 days then 100 G (60 ft/sec); 40 days then 193 G (60 ft/sec); 3 days then 175 G (60 ft/sec); 67 days then 450 G (40 ft/sec). One month after the last exposure the subject appeared in good health.

M-27 - 258 G (40 ft/sec)

Minimal hemorrhage at the hilar area of left lung. Minimal degree of congestion in the right kidney and small intestines. Comminuted fracture of the right femur in the mid-shaft area. Contusions, minimal in degree over the left wrist and left thigh.

M-18 - 280 G (60 ft/sec)

Severe hemorrhage in the apical segment of the superior lobe of the left lung. Moderate hemorrhage on the dorsal surface of the left superior lobe along with rupture. Adhesions extending from the dorsal surface of the left inferior lobe of the lung to the chest wall. Moderate hemorrhage on the right superior lobe dorsally along with rupture. Recent pulmonary embolism of the right lung. Hepatic laceration near the entry of portal vein. A small cyst in the gall bladder. Full urinary bladder. Minimal

to moderate hematoma on the right side of the vertebral column extending from the level of fourth thoracic vertebra to the eleventh thoracic vertebra anteriorly. Comminuted fracture of the right femur one-third of the way down from the proximal end.

M-29 - 300 G (60 ft/sec)

Severe hemorrhage at the hilar areas of both the lungs. Severe hemorrhage of the apical segments of right and left superior lobes of the lungs (right greater than left). Moderate degree of collapse of both lungs. Minimal degree of distention of the right atrium with moderate congestion. Severe degree of hematoma lateral to the vertebral column between the levels of sixth and tenth thoracic vertebra. Minimal degree of "sago" spleen. Minimal contusions on the dorsal surface of right kidney. Full urinary bladder. Moderate distention of the jugular veins. Minimal to moderate contusions over the supra-orbital crests of both eyes, right corner of right eye, right and left shoulders, right axilla, mid-arm, wrist, flexor surface of left wrist, anterior surface of chest along the costal cartilages of both sides, left ankle, and vertex of skull. The right clavicle fractured in the mid-shaft area. Minor degree of capillary hemorrhage on the dura of the occipital region. Subdural vessels severely congested.

M-22 - 325 G (60 ft/sec)

Severe hemorrhage in the apical segments of the right and left superior lobes of the lungs in the apical segment of right superior lobe. Moderate degree of hemothorax present. Moderate emphysema on the inferior division of left superior lobe. Right atrium grossly distended. Moderate distention of the coronary vessels. Severe hematoma extending from the level of the second to the eleventh thoracic vertebra on both sides of the vertebral column indicating presence of possible compression fracture of intervertebral disks of this area. Moderate hematoma on the right side of manubrium sterni. Moderate degree of splenic and hepatic congestion. Minimal congestion of right kidney. Full urinary bladder. Contusions of minimal degree on both maxillae, lower jaw, right and left shoulders and the left wrist. Moderate degree of edema around each eye (right side greater than left). Severe congestion of subdural vessels. Hemorrhage on the dura over longitudinal fissure at the base of occipital lobe.

M-26 - 430 G (40 ft/sec); 70 days then surgically prepared for pressure measurement runs (20 ft/sec) at 11 G, 15 G, 9 G, 14 G.

Left superior lobe of the lung fused to the inferior lobe with severe infection at the hilum. Emphysematous bullae in the left inferior lobe towards the periphery. The right inferior lobe of the lung adhered to the diaphragm. Small nodules in the small intestine. Full urinary bladder.

M-19 - 339 (40 ft/sec); 60 days then 306 (60 ft/sec)

Severe hemorrhage on the apical segment of right superior lobe of the lung. Severe spotted hemorrhages over the dorsal and ventral surfaces of the right inferior and middle lobes. Thick fibrous adhesions over the dorsal and ventral surfaces of the right inferior lobe. Moderate spotted hemorrhage in areas over dorsal and ventral surfaces of left superior and inferior lobes. Moderate hepatic congestion. Comminuted fracture of the right femur at the mid-shaft region.

M-31 - 433 G (40 ft/sec); 19 days then 200 G (60 ft/sec)

Moderate degree of congestion of the apical segment of the left superior lobe of the lung. Fibrous adhesions extending from the periphery of the lobes of both lungs to chest wall (left greater than right). The pulmonary vessels distended moderately. Excessive clear fluid in the pericardial sac. The coronary vessels congested minimally. The intercostal vessels moderately distended. Excessive clear perioneal fluid. Minimal degree of hepatic and splenic congestion.

M-20 - 39 G (20 ft/sec); 9 days then 40 G (40 ft/sec); 5 days then 55 G (40 ft/sec); 71 days then surgically prepared for pressure measurement runs (20 ft/sec) at 9 G, 15 G.

Adhesions between superior, middle and inferior lobes of the right lung. Adhesions between the left superior and inferior lobes and also with the pericardium. Adhesions from the superior lobe extending to the parietal thoracic wall. "Sago" spleen.

M-21 - 234 G (40 ft/sec); 62 days then 152 G (60 ft/sec); 67 days then 44 G (40 ft/sec); 1 day then surgically prepared for pressure measurement runs (20 ft/sec) at 16 G, 12 G, 11 G, 12 G, 15 G, 17 G.

Severe degree of adhesions over dorsal surface of all the lobes of right and left lungs to the chest wall and diaphragm. Severe collapse of mid-lobe of right lung. Small areas of fibrosis and hemorrhage in spleen, Urinary bladder full. Fracture right clavicle at junction of lateral one-third and medial two-thirds. Severe hematoma right axilla.

M-23 - 88 G (20 ft/sec); 8 days then 58 G (40 ft/sec); 4 days then 177 G (40 ft/sec).

Mild hemorrhage on the right superior lobe and adhesion from right inferior lobe to the pericardium. Adhesion between left superior and inferior lobes. Mild distention of coronary vessels. Mild degree of splenic congestion. The mesenteric vessels moderately congested. The large and small intestines distended with fecal matter. A band-like structure in the lower six inches of the colon extending for two and one half inches. (This caused a functional obstruction to proper evacuation of the bowels.)

M-25 - 111 G (20 ft/sec); 9 days then 122 G (40 ft/sec); 4 days then 123 G (40 ft/sec); 77 days then surgically prepared for pressure measurements runs (20 ft/sec) at 11 G, 16 G, 17 G.

Moderate degree of congestion of the inferior division of the superior lobe of the left lung. Small cyst in the large intestine. Chronic obstruction in a small section of the small intestine.

M-30 - 131 G (20 ft/sec); 8 days then 78 G (40 ft/sec); 5 days then 201 G (40 ft/sec); 16 days then 200 G (60 ft/sec).

Severe degree of hemorrhage in the apical segment of the right superior lobe of the lung. Moderate hemorrhage in the apical segment of the left superior of the lung. Moderate congestion of the coronary vessels of left ventricle. Moderate hematoma at level of the ninth and tenth thoracic vertebra in the region of the vertebral column bilaterally. Moderate distention of the intercostal vessels. Minimal degree of free

fluid in the peritoneal cavity. The spleen and the liver, and the left kidney minimally congested. Empty urinary bladder. Minimal contusions over the frontal area of the skull, left axilla, tips of right and left shoulders (right greater than left), and right and left wrists. Moderate congestion of the subdural vessels of the right parietal lobe.

M-28 - 117 G (20 ft/sec); 9 days then 99 G (40 ft/sec); 3 days then 152 G (40 ft/sec); 4 days then 61 G (40 ft/sec); 59 days then 98 G (60 ft/sec); 3 days then 166 G (60 ft/sec); 62 days then surgically prepared for pressure measurement runs (20 ft/sec) at 11 G, 16 G, 18 G, 11 G.

Small area of collapse from left inferior lobe to pericardium. Minor adhesions between lobes of liver. Urinary bladder full.

M-32 - 59 G (20 ft/sec), 9 days then 124 G (40 ft/sec); 3 days then 188 G (40 ft/sec); 4 days then 79 G (40 ft/sec); 60 days then 158 G (60 ft/sec); 6 days then 254 G (60 ft/sec).

Severe hemorrhage around the hilum of left superior lobe of the lung extending into the apical segment. Severe hemorrhage in the hilar area of left inferior lobe. Mild to moderate hemorrhage in the superior, mid and inferior lobes of the right lung. Severe hemorrhage in the right inferior lobe at the periphery. Mild degree of hematoma at the level of ninth thoracic vertebra on both sides of the vertebral column anteriorly. Hemoperitoneum of mild to moderate degree. Laceration of spleen at the region of lieno-renal ligament. Small cysts throughout the small and the large intestines. Ulcer formation of unknown cause in parts of the small intestine, caecum, and the large intestine. Five small (one hemorrhagic) cauliflower-like growths were found inside the stomach.

3.2.4 Monkeys Surgically Prepared for Pressure Measurements

The purpose of these runs was to obtain simultaneous pressure measurements within the aortic arch and intrathoracic space. Techniques were developed to accomplish this using the Statham SF-1 physiological pressure transducer. Aortic arch catheterization was accomplished as described in the preceeding section with very little difficulty in technique. Many

techniques, however, were tried before an acceptable method for obtaining intrathoracic pressure was found. The accepted technique used a fluid-filled catheter with an open tip. This was introduced through a trocar-like needle into the right chest through the second intercostal space to the apex of the thoracic cavity. This system yielded acceptable results and eleven runs were made in which useful data was obtained. These runs are summarized in Table VIII and typical pressure profiles obtained at impact are found in Figures 6, 7, and 8. These profiles are presented to give an indication of the transient pressure changes following impact and are not intended to furnish a numerical representation of the absolute pressures.

The existing state of the art for measuring pressures in biological systems under extreme dynamic conditions precludes any definitive statements as to the validity of the numerical values obtained. However, a quantitative interpretation must consider that the profiles reflect changes from mean baseline pressures of approximately -10 to -5 mm Hg. for the intrathoracic pressure and 100 to 120 mm Hg. for the aortic pressure. The aortic and intrathoracic pressure profiles in Figures 8a, b, and c provide significant indication that the total aortic pressure (P mean + ΔP) is compensated by the increased intrathoracic pressure during impact. The intrathoracic profiles in these figures display damped harmonic characteristics which appear after a delay of approximately 20 milliseconds following the end of impact exposures. This damped spring mass system behavior may possibly be explained by considering the restoring effects of restraint and tissue elasticy and the dynamic interplay of the abdominal fluid mass, elastic diaphragm, and the air elasticity in the lungs. However, further investigation is necessary to conclusively establish the course of these wide variations in the intrathoracic pressure.

An attempt was made to obtain pressure measurements from the jugular vein and the carotid artery under impact. The vessel diameters were too small to permit proper insertion of the catheter and no further attempts were made adequate. Adequate pressure measuring instrumentation could not be obtained.

TABLE VIII - MONKEY RUNS FOR PRESSURE MEASUREMENTS
ΔV = 20 FT/SEC

Run Number	G Level	Onset G/Sec	Pressure Instrumentation
1	9	8,700	SF-1 Catheter introduced through left iliac artery into abdominal aorta with tip 3/4 inch below aortic arch to record aortic pressure.
2	15	9,300	
3	11	7,000	SF-1 Catheter introduced through left iliac artery in abdominal aorta with tip seated about 1 inch below diaphragm to record aortic pressure.
4	16	9,600	
5	17	10,100	
6	12	5,400	SF-1 Catheter, fluid filled with open tip, introduced through chest wall at 2nd intercostal space to record intrathoracic pressure.
7	16	9,500	
8	11	7,500	(1) SF-1 Catheter, fluid filled with open tip, introduced through chest wall at 2nd intercostal space. (2) SF-1 Catheter introduced retroperitoneally into abdominal aorta just above bifurcation of aorta. Catheter tip seated at base of aortic arch.
9	12	6,000	
10	15	10,500	
11	17	11,300	

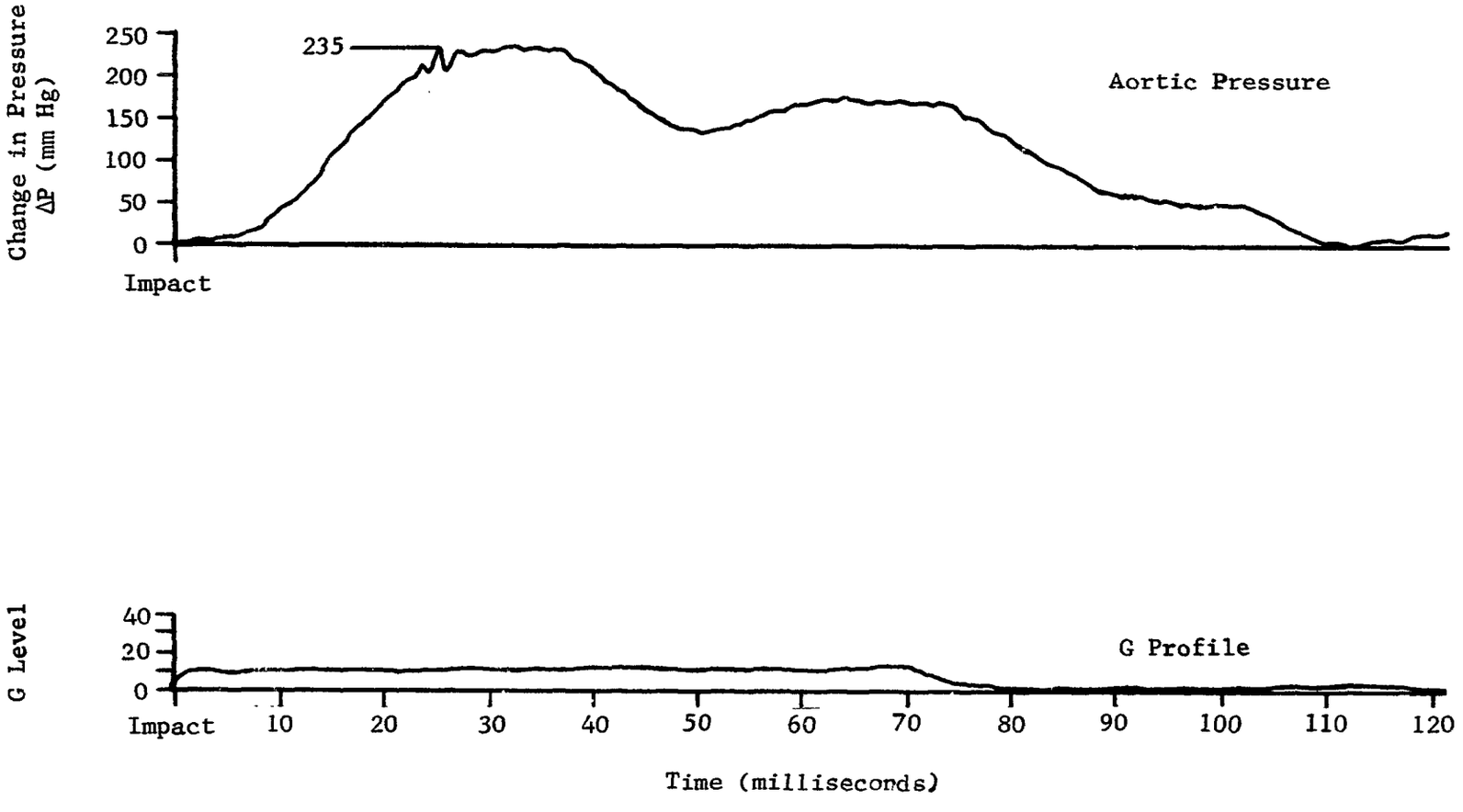

FIGURE 6a AORTIC PRESSURE PROFILE FOR MONKEY SUBJECT EXPOSED TO $-G_z$ IMPACT

RUN #1, ΔV = 20 FT/SEC, G = 9, ONSET = 8,700 G/SEC

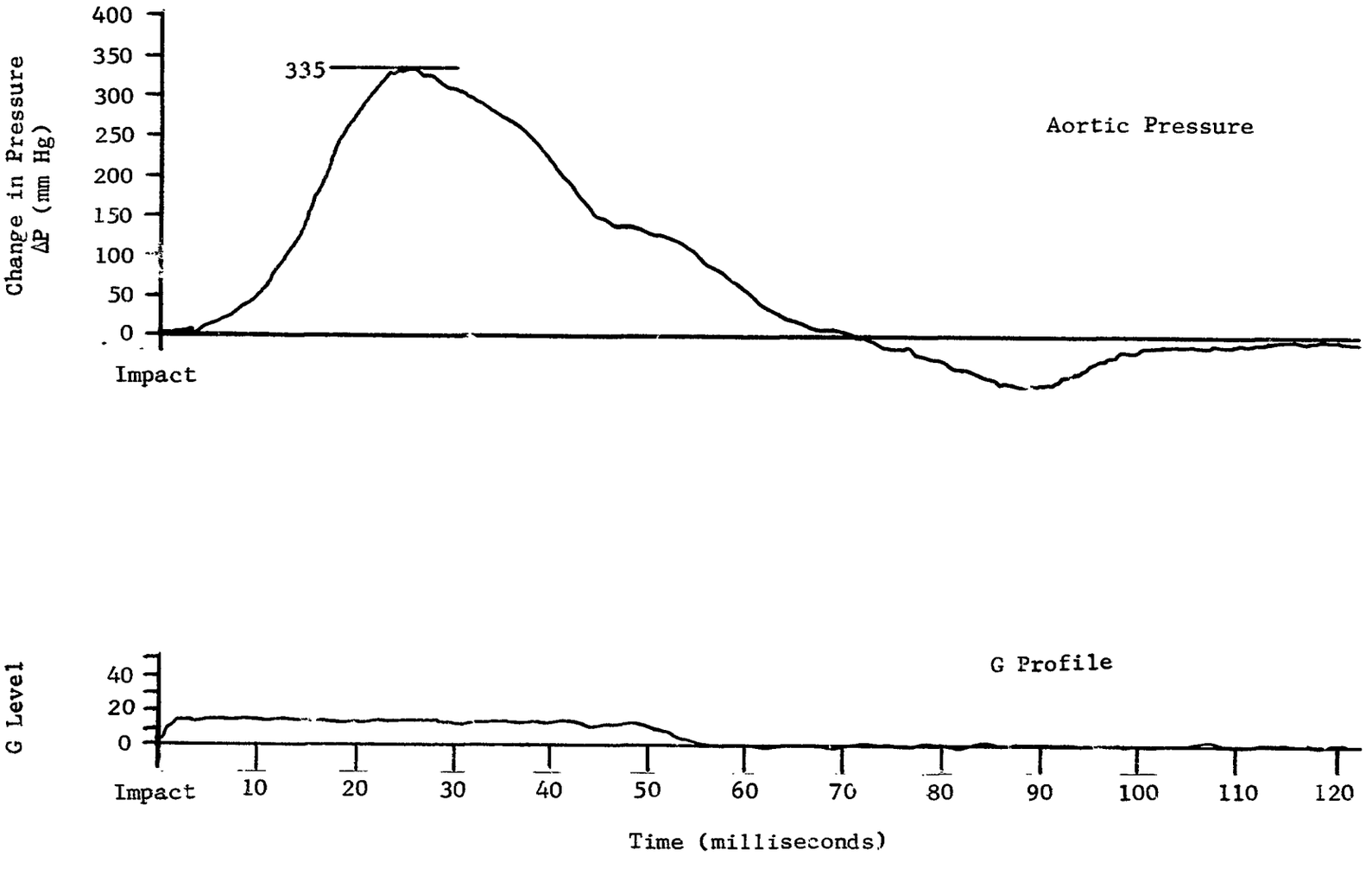

FIGURE 6b AORTIC PRESSURE PROFILE FOR MONKEY SUBJECT EXPOSED TO $-G_z$ IMPACT

RUN #2, ΔV = 20 FT/SEC, G = 15, ONSET = 9,300 G/SEC

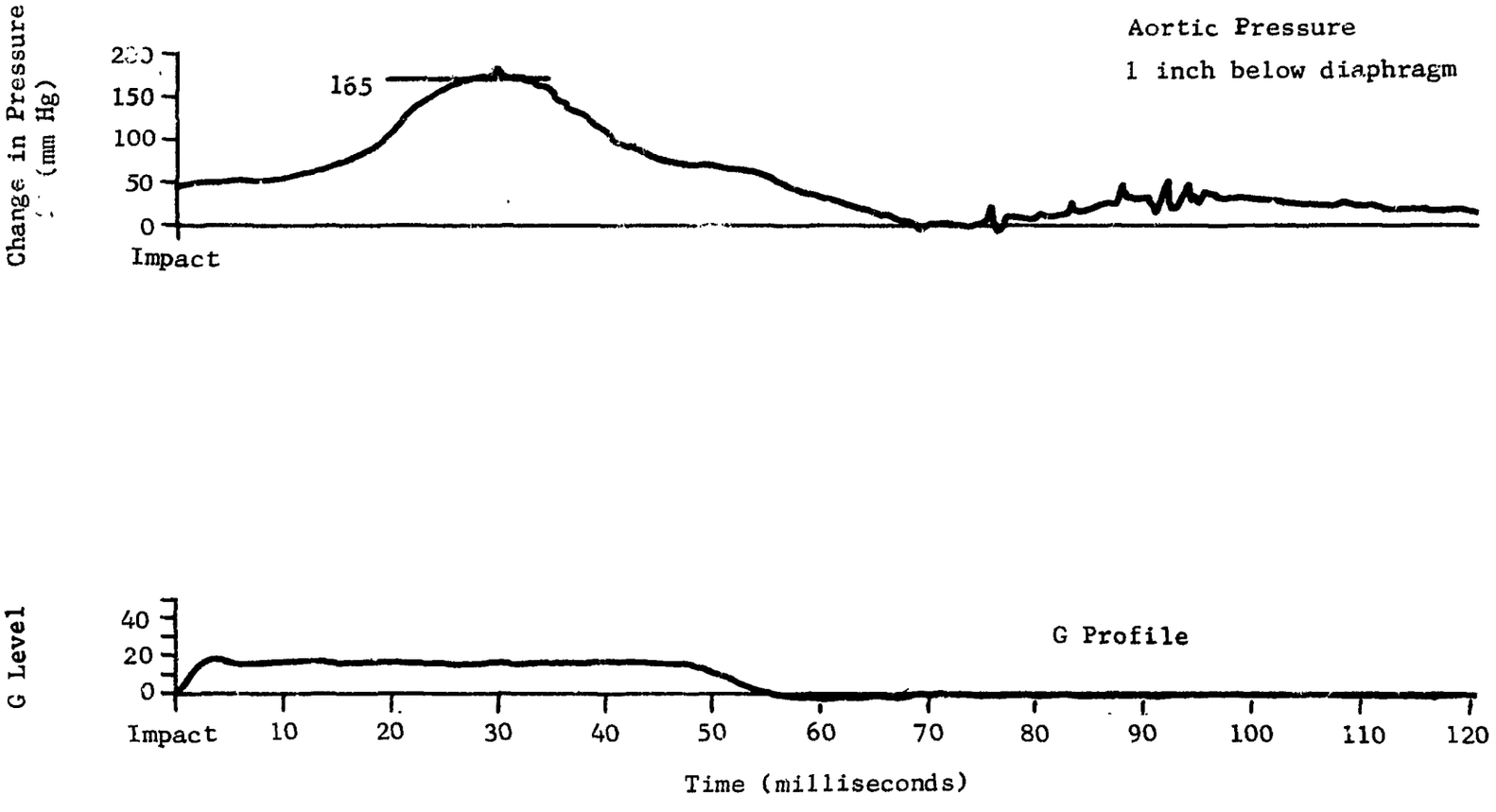

FIGURE 6c AORTIC PRESSURE PROFILE FOR MONKEY SUBJECT EXPOSED TO $-G_z$ IMPACT

RUN #5, ΔV = 20 FT/SEC, G = 17, ONSET 10,000 G/SEC

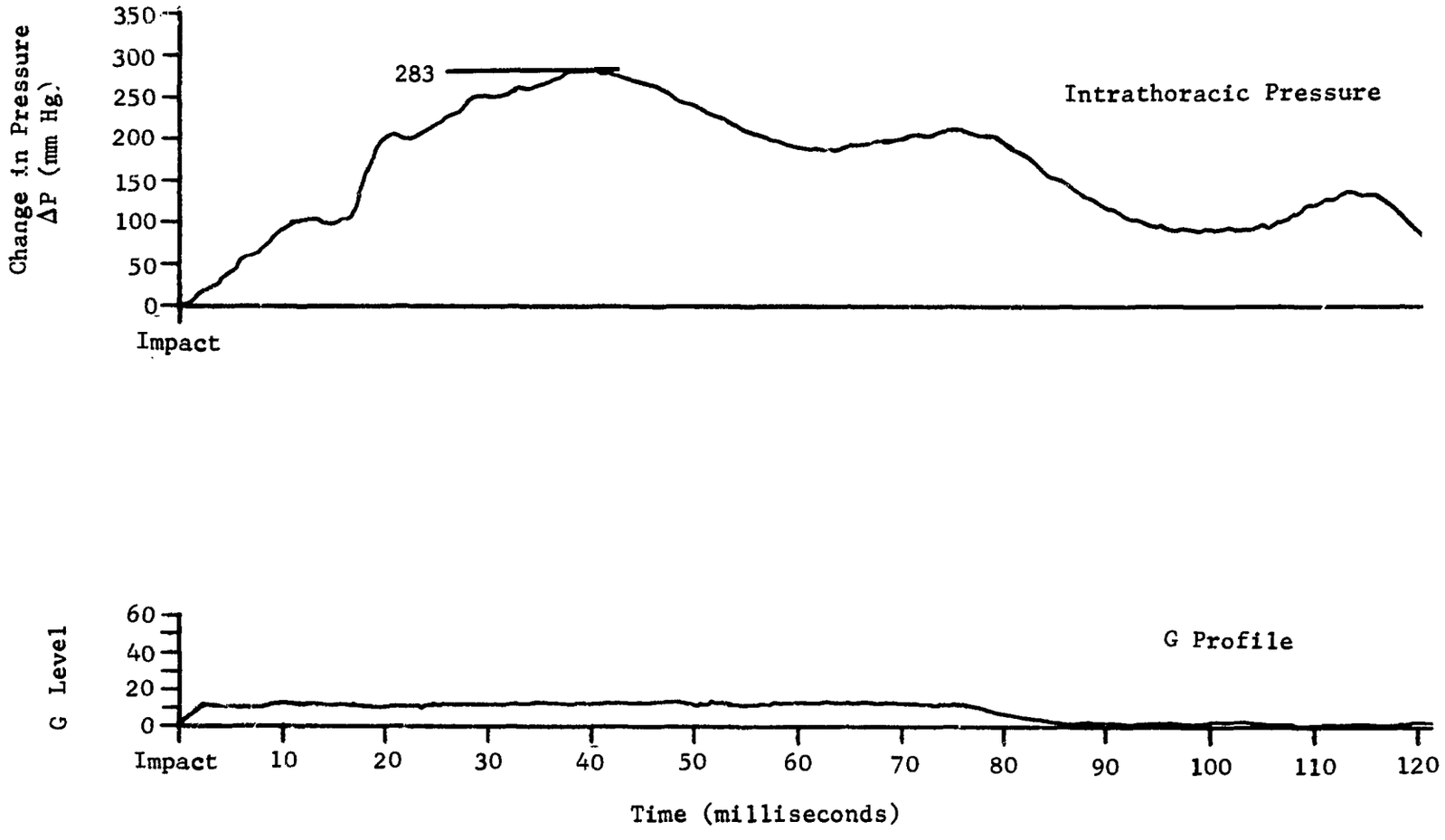

FIGURE 7 INTRATHORACIC PRESSURE PROFILE FOR MONKEY SUBJECT EXPOSED TO $-G_z$ IMPACT

RUN # 6, ΔV = 20 FT/SEC, G=12 , ONSET = 5,400 G/SEC

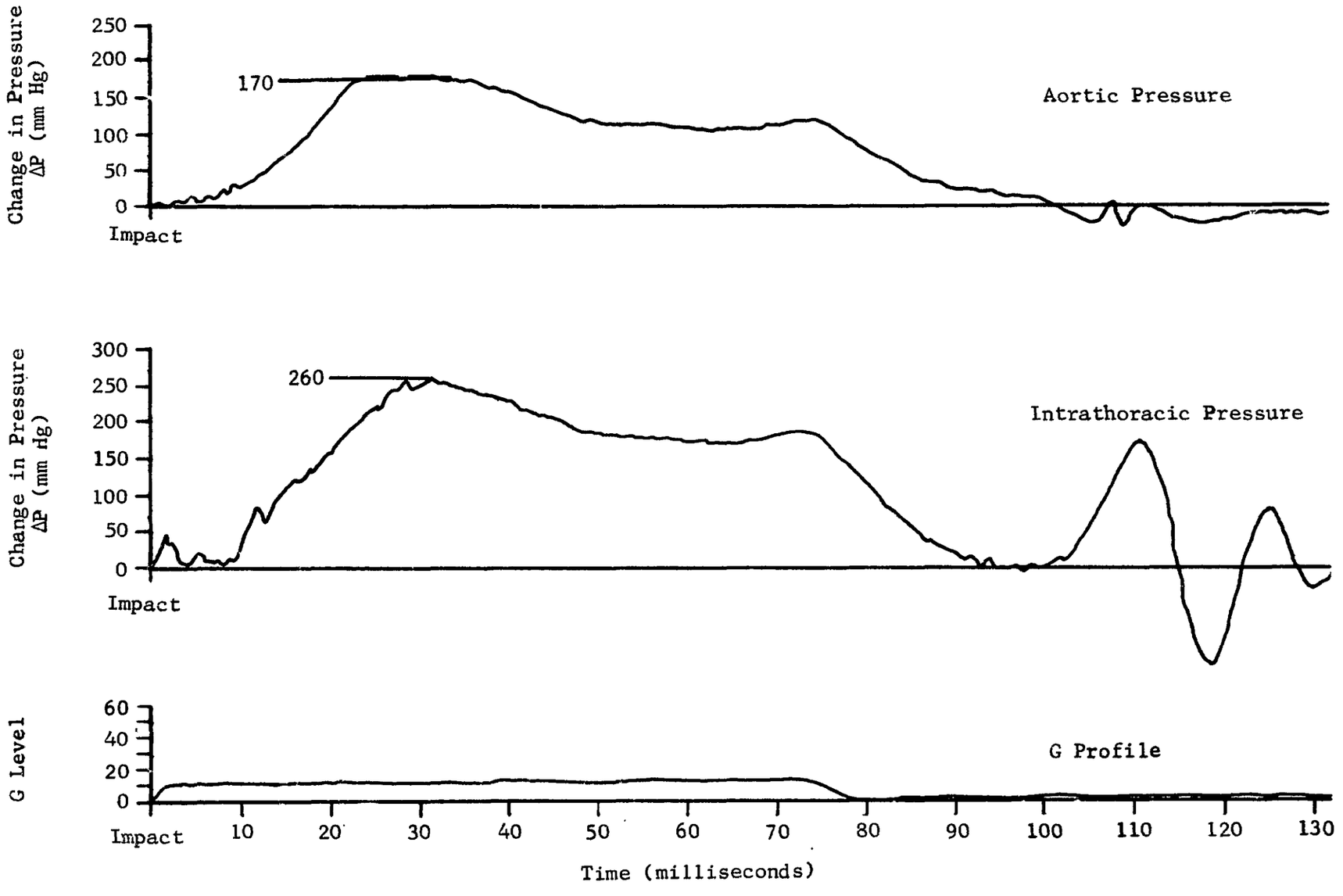

FIGURE 8a AORTIC AND INTRATHORACIC PRESSURE PROFILES FOR MONKEY SUBJECT EXPOSED TO $-G_z$ IMPACT

RUN #8, ΔV = 20 FT/SEC, G = 11, ONSET = 7,500 G/SEC

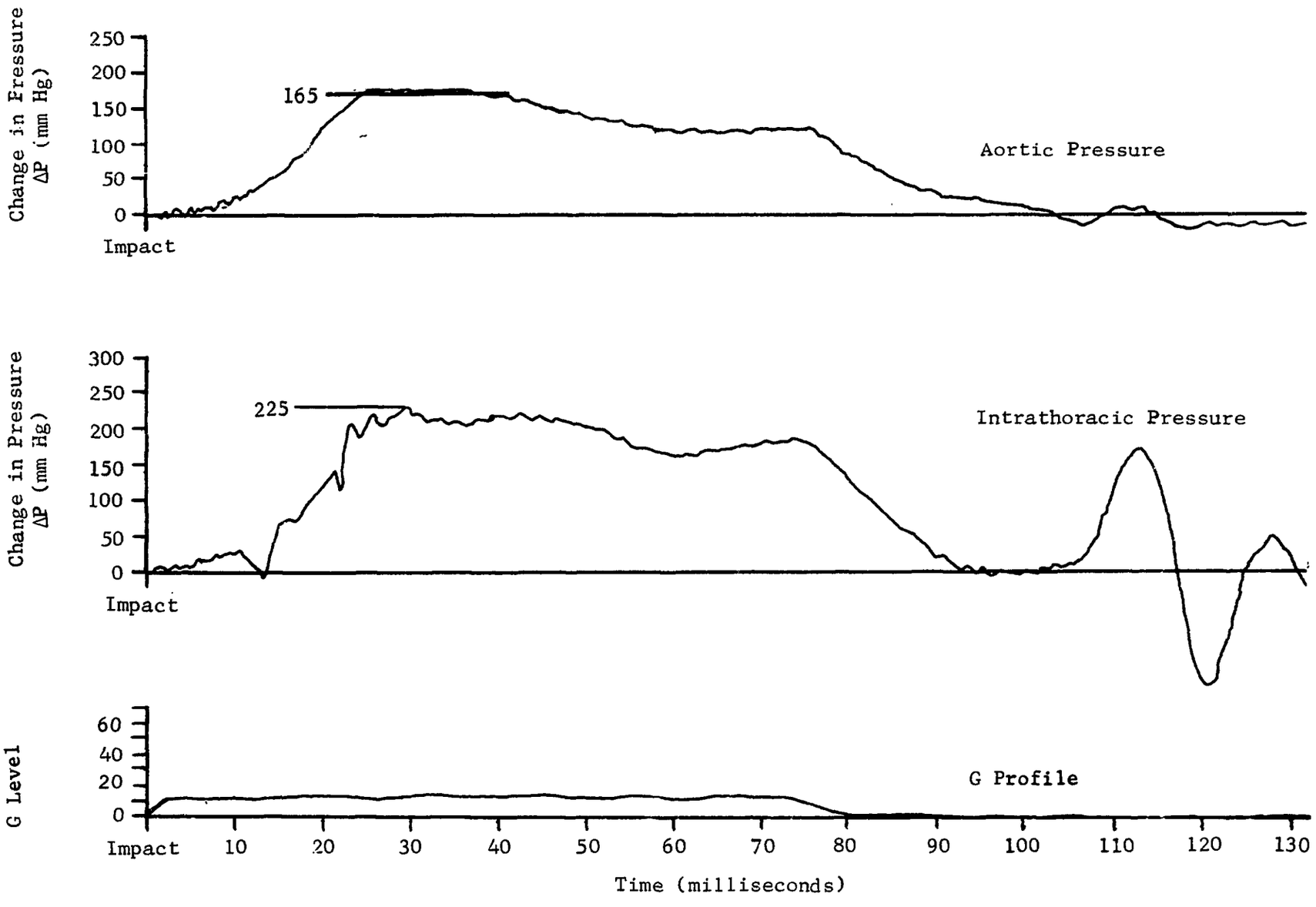

FIGURE 8b AORTIC AND INTRATHORACIC PRESSURE PROFILES FOR MONKEY SUBJECT EXPOSED TO $-G_z$ IMPACT
RUN #9, ΔV = 20 FT/SEC, G = 12, ONSET = 6,000 G/SEC

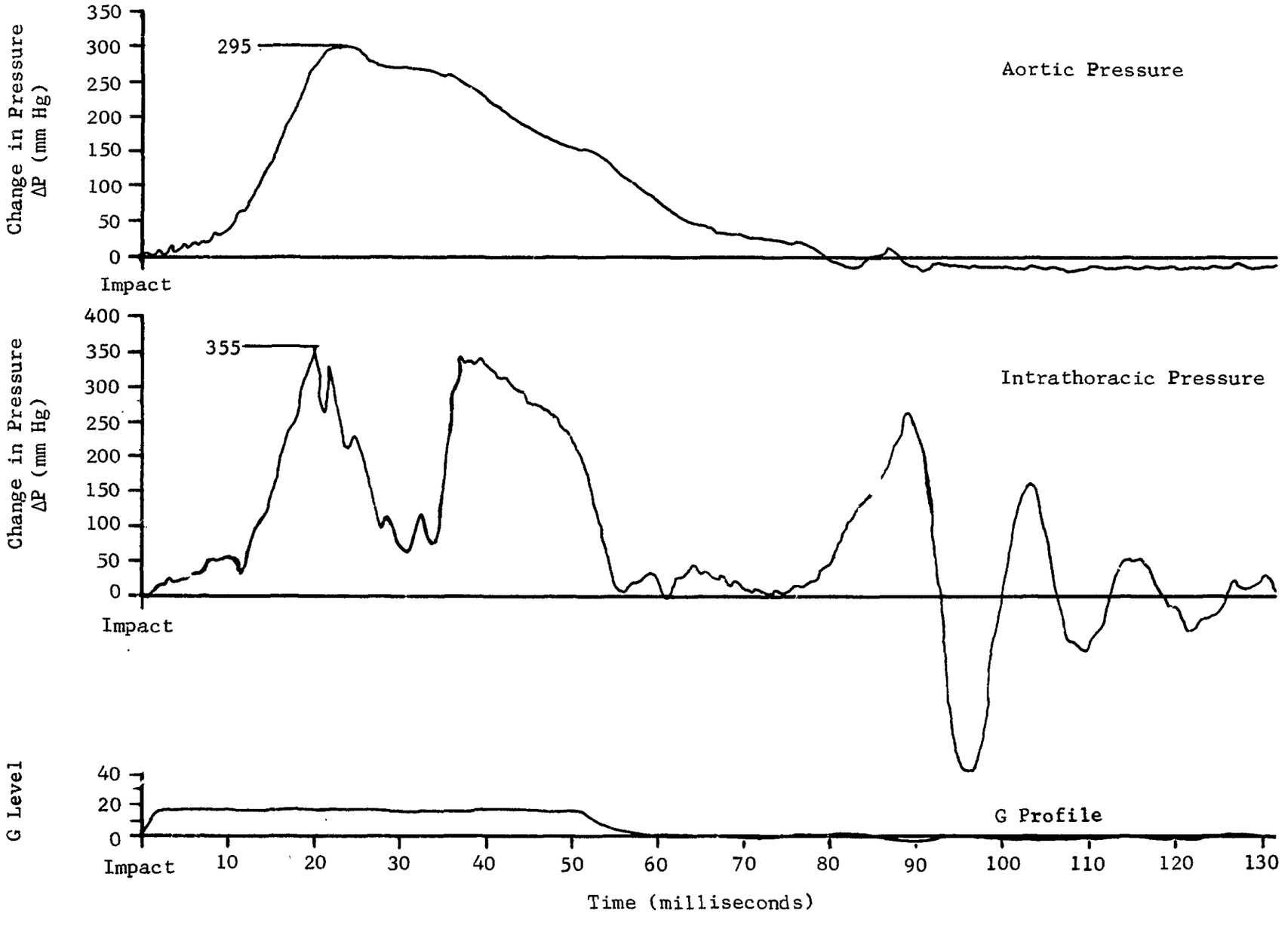

FIGURE 8c AORTIC AND INTRATHORACIC PRESSURE PROFILES FOR MONKEY SUBJECT EXPOSED TO $-G_z$ IMPACT

RUN #10, ΔV = 20 FT/SEC, G = 15, ONSET = 10,500 G/SEC

SECTION 4.0
ANALYTICAL INVESTIGATIONS

In this section, analytical considerations pertaining to the patho-physiological responses of the cardiovascular system (CVS) to tailward acting impact accelerations are given. The analysis is presented in three subsections. First, a review of mathematical models of the CVS and their applicability to transient forcing functions is presented. Second, the CVS is treated as a one-degree-of-freedom mechanical relaxation oscillator corresponding to a modified version of the van der Pol equation. In such a general analogy, the CVS, under steady state (normal) conditions behaves as a stable oscillator with a fixed limit cycle. Under the influence of the impact forcing function, the phase plane trajectory representing the directional and time dependent element of blood motion is altered. Numerical values of changes in flow caused by impact for guinea pig and monkey subjects are obtained and the applicability of the limit cycle oscillator for studying such transient changes is given. Finally, dynamic considerations of the aorta are investigated. The analysis includes study of the radial dilatation of the aortic wall, aortic pressure, aortic dynamic response, and wave stability of the aorta.

4.1 MATHEMATICAL MODELS OF THE CVS

Mathematical models of the CVS are based on two classical theories:

(a) Transmission theory initiated by Moens and Korteweg in the second half of the nineteenth century.

(b) Windkessel theory proposed by Euler in 1775 and promoted by Weber and Frank.

These theories diverge in their basic assumptions; the transmission theory starts out from a finite pulse wave velocity, while the Windkessel theory assumes an infinite pulse wave velocity (pressure independent of the position in the chamber). Considerable effort was devoted by Frank to reconcile these theories. However, recent efforts have been mostly concerned with extension and refinement of the individual theories.

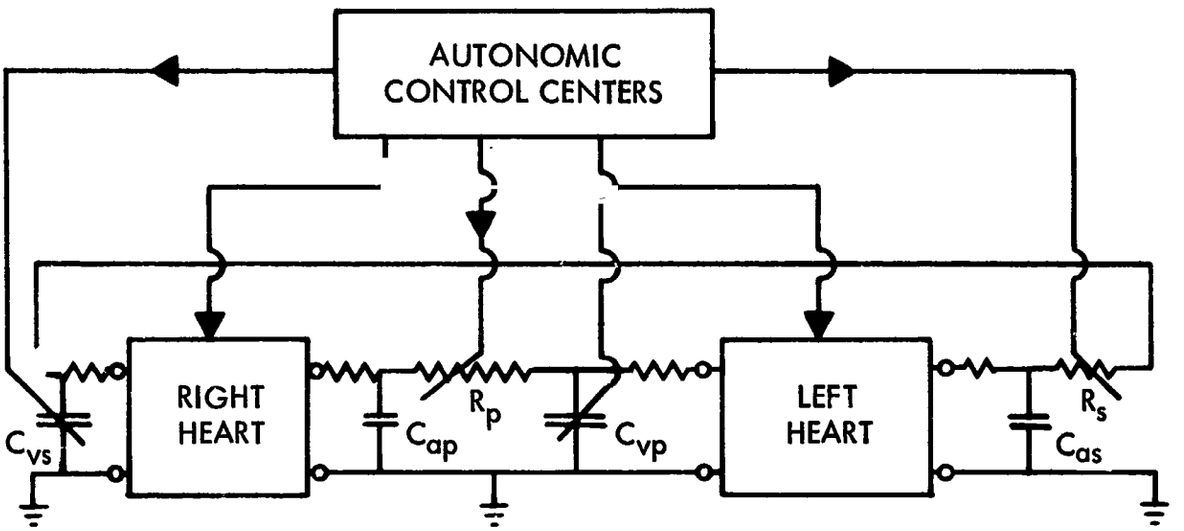

R_s - Resistance of systemic vascular bed

R_p - Resistance of pulmonary vascular bed

C_{as} - Compliance of systemic arteries

C_{ap} - Compliance of pulmonary arteries

C_{vp} - Pulmonary blood reservoir

C_{vs} - Systemic blood reservoir

FIGURE 9 ELECTRICAL MODEL OF THE CARDIOVASCULAR SYSTEM

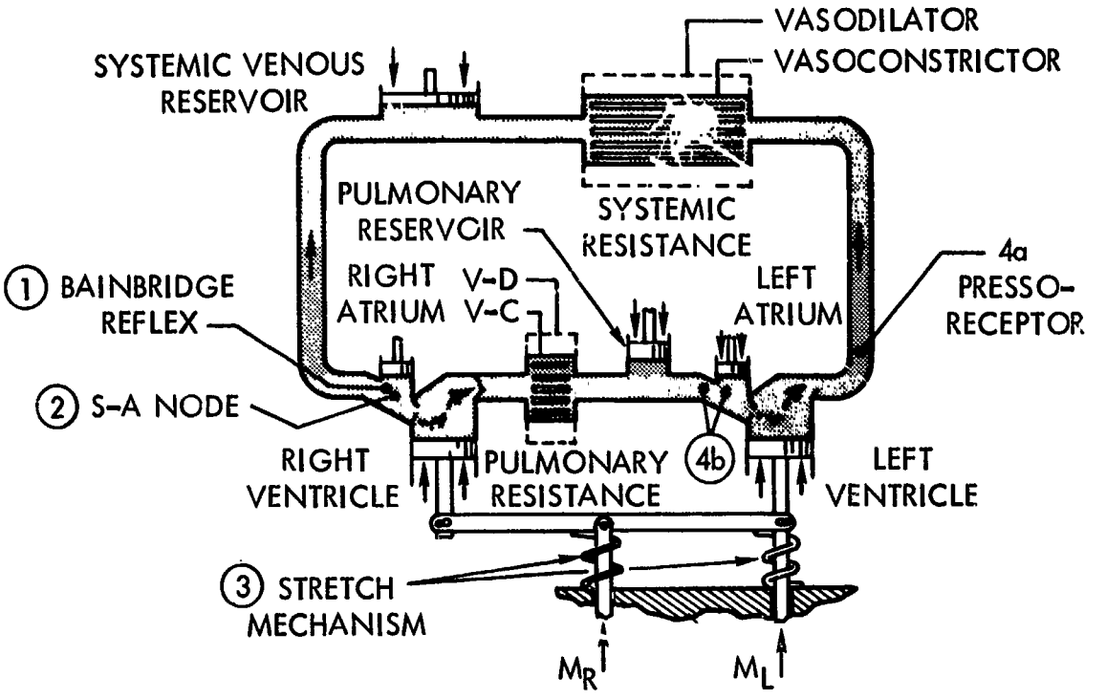

1 Bainbridge Reflex: Pressoreceptor senses increased filling pressures causing pulse rate to increase "up" only

2 S-A Node: Receives signal from brain initiates de-polarizing action of AV node. Signals control pulse rate "up" and "down"

3 Stretch Mechanism: Increased filling pressures cause increased contractile forces and vice versa

3 Pressoreceptor:
- 4a - Senses Arterial Pressures: Heart rate and systemic resistance are regulated to maintain constant arterial pressures
- 4b - Increased Filling Pressures: Systemic resistance is caused to increase and vice versa

FIGURE 10 -MECHANICAL-EQUIVALENT DIAGRAM OF THE HUMAN CARDIOVASCULAR SYSTEM (7)

The CVS can be considered to be composed of two coordinated systems: (a) the blood conducting systen and (b) the regulatory system. Electrical and mechanical models of the CVS illustrating these systems are shown in Figures 9 and 10 . These models do not include chemoreceptors.

4.1.1 Blood Conducting System

The blood conducting system consists basically of two heart pumps, resistance, and capacitance vessels. A block diagram of this system is illustrated in Figure 11. The mechanical elements of the system are lumped as follows: left atrium and pulmonary veins, left ventricle, systemic arteries, peripheral resistance (systemic arterioles and capillaries),

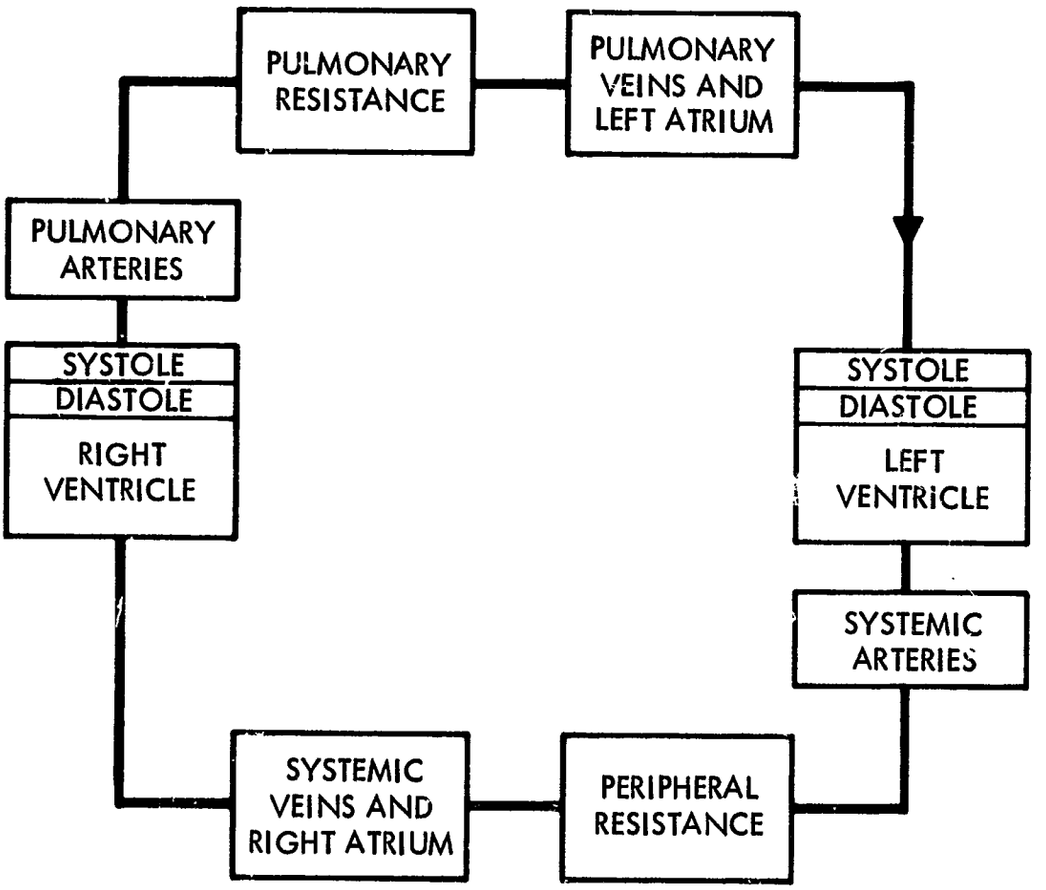

FIGURE 11 BLOCK DIAGRAM OF BLOOD CONDUCTING SYSTEM

systemic veins and right atrium, right ventricle,pulmonary arteries, and pulmonary resistance (pulmonary arterioles and capillaries). Physical support of these components of the blood conducting system is provided by hydraulic, pneumatic and structural means.

The blood conducting system can be represented by 18 coupled equacions which take into account the properties of blood and vessels (inertia, viscosity, pressure-volume relationship, elastic properties etc.),. time relaxation between systole and diastole, contractile properties of the heart muscles, and blood volume. These 18 equations are characterized by the following classes of equations.

Conservation of Mass The conservation law may be expressed as

$$\frac{\partial}{\partial t} \quad (m_{cv}) = \int d\omega_{in} - \int d\omega_{out} \qquad [1]$$

which states that the rate of accumulation of mass within the considered volume is equal to the excess of the incoming rate of flow over the outgoing rate of flow.

Pressure-Volume Relation. -

$$V = V(p) \qquad [2]$$

Momentum Equation. -

$$\frac{\partial p}{\partial x} = \rho\left[\frac{\partial v}{\partial t} + \bar{V}\cdot\nabla\bar{V}\right] + \mu\nabla^2\bar{V} \qquad [3]$$

$$\text{Pressure gradient} = \text{density}\left[\begin{matrix}\text{local}\\ \text{acceleration}\end{matrix} + \begin{matrix}\text{convective}\\ \text{acceleration}\end{matrix}\right] + \begin{matrix}\text{viscous pressure}\\ \text{losses}\end{matrix}$$

For a Newtonian fluid, the coefficient of viscosity is assumed constant.

Using these equations, a prediction may be made of the response of the whole system to a transient disturbance. Warner (8) has indicated a method of solution wherein the transient disturbance is introduced by the subject's

attempting a forced expiration against a closed glottis. Since the system is a closed loop, an accurate prediction of the dynamic response of each component of the CVS to stress involves the solution of 18 coupled equations of the system simultaneously, in addition to the governing regulatory system equations.

4.1.2 Regulatory System

The regulatory system controls the blood conducting system and maintains certain values or ranges of blood flows and pressures. This control is exercised through both stretch and chemo-receptors by mechanisms of arterial and venous vasoconstrictions (or dilatations), by variation of the heart rate and by change of the contractile properties of the heart muscle.

The formulation of a quantitative theory of the regulating mechanism requires a knowledge of the response or output of each element in a given reflex as a function of the frequency of nerve impulses or other stimuli (input). Macey (9) has derived an equation relating the heart rate to the frequency of nerve impulses traveling along the cardiac nerves. His equation relating the excitatory state $\mathcal{E}$ of the heart and the intensity S(t) of the stimulating agent is of the form

$$\frac{d\mathcal{E}}{dt} = \varphi\left[S(t)\right] - K\mathcal{E} \qquad [4]$$

where φ is a function of S(t)
and K is a constant

A equation relating heart rate and frequencies of nerve impulses traveling down the vagus and sympathetic nerves, has been obtained from equation [4], Macey (op.cit.). This relationship is graphically illustrated in Figure 12.

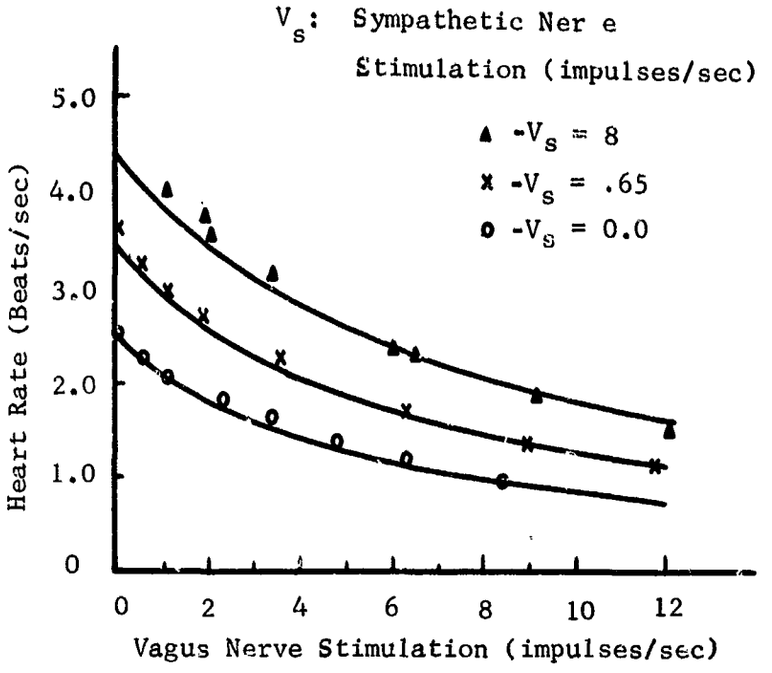

FIGURE 12 HEART RATE VERSUS FREQUENCY OF STIMULATION

Analog simulation has been performed on the baroreceptor feedback mechanism by Warner (8). In his study, variations in pressure were induced by varying the flow. The variation in flow was induced by stimulating the vagus nerve.

Studies on the carotid sinus have yielded an equation similar to [4]. The relationship between the output frequency on the carotid sinus and the hemodynamic pressure on the carotid sinus is

$$K_1 \frac{dp}{dt} = K_2 (p_o - p) + s \qquad [5]$$

where

K_1 and K_2 are constants

s is the frequency of impulses on the carotid sinus nerve

p is the pressure in the carotid artery

p_o is the minimum static pressure capable of producing stimulus of the carotid sinus vasopressor mechanism

Mathematical studies on pressure receptors in the aortic arch and atria have not been conducted. However, most investigators have assumed that all pressure receptors behave similarly.

The vascular system consisting of the volume compliance, arterial (C_a) and venous (C_v), separated by the arteriole resistance R_s, can be similarly modeled by the approximate relations

$$\frac{dp_a}{dt} = \frac{1}{C_a}\left[Q - \frac{p_a - p_v}{R_s + Ks}\right] \qquad [6]$$

$$\frac{dp_v}{dt} = \frac{1}{C_v}\left[-Q + \frac{p_a - p_v}{R_s + Ks}\right] \qquad [7]$$

where

p_a is the arterial pressure

p_v is the venous pressure

s is the pulse frequency of the vasoconductor nerves

Q is the volume flow of the heart

K is a constant

Since the degree of regulation excercised by pressoreceptors is governed by pressure differentials across the components of the blood conducting system, their physical support plays an important role at impact.

4.1.3 Comprehensive Model of the CVS

In developing a comprehensive model of the CVS valid for impact injury analysis, the blood conducting and regulating system must be accounted for in a unified manner. A simplified representation of such a model, obtained by lumping the blood conducting components and the reflex elements of the CVS, is shown in Figure 13.

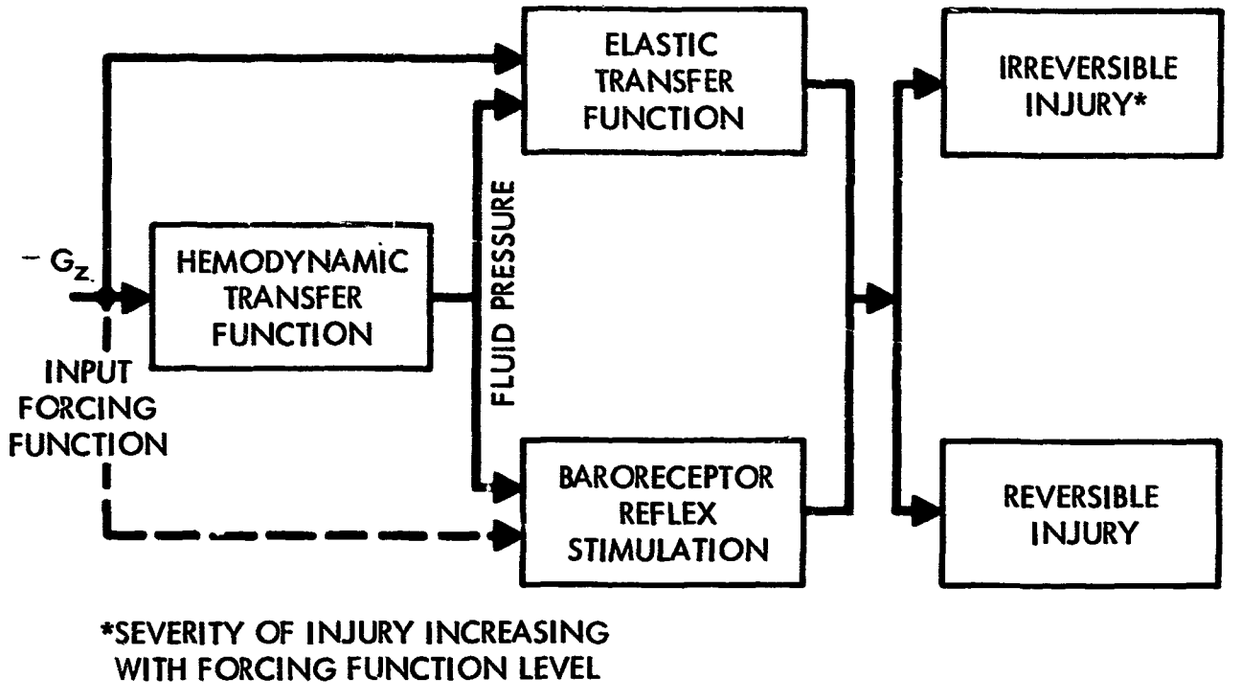

FIGURE 13 BLOCK DIAGRAM REPRESENTATION OF THE CARDIOVASCULAR MODEL

4.2 LIMIT CYCLE RELAXATION OSCILLATOR

The class of differential equations mathematically representing the comprehensive model (Figure 13) is restricted since the variables of the system are governed by baroreceptor reflex stimulation. Of particular interest is the van der Pol equation. The applicability of this equation to physiological systems was pointed out by van der Pol (10) who suggested that the heart behaved like a non-linear relaxation oscillator and showed networks that could simulate a P, R, and T wave. Brinks (11) in his study of the general behavior of the circulatory system extended this line of thought by assuming that the entire system of heart and blood vessels could be treated as a one-degree-of-freedom mechanical relaxation oscillator. The modified van der Pol equation used in his analysis is of the form

$$m\ddot{x} - \lambda^2 \dot{x} + \alpha^2 \dot{x}^2 \operatorname{sgn} \dot{x} + kx + f \operatorname{sgn} \dot{x} = 0 \qquad [8]$$

where

m	is the mass of the blood
x	is the blood displacement
λ^2, α^2	are constants
k	is the spring constant
f	is the coulomb damping force

and $\operatorname{sgn} \dot{x} = \begin{matrix} +1 \text{ for } \dot{x}>0 \\ -1 \text{ for } \dot{x}<0 \end{matrix}$

Equation [8] is a statement of the dynamic equilibrium of the system, namely: the blood motion imparted by the heart is resisted by the dynamic fluid friction, coulomb static friction, blood vessel elasticity and inertia of the blood mass. The quantities in this equation can be physically interpreted in the following manner. The quantity λ^2 is assumed to be proportional to the energy available to the heart muscle. The velocity $\dot{x}$ is proportional to the strength of the heart thrust. The spring constant k represents the lumped restoring force (elasticity of the system). The quantities α^2 and f represent the dynamic and static coulomb friction coefficients of the blood vessels. The addition of the coulomb friction term provides a situation where energy must be initially fed to the system to start motion (example: heart massage). A mechanical model of the modified van der Pol relaxation oscillator is shown in Figure 14. Dynamic friction and coulomb friction characteristics are illustrated in Figure 15.

The validity of the relaxation oscillator as a mathematical model for the CVS is not directly seen from the planar representation of the trajectories. The periodicity of the motion is, however, apparent when the phase plane representation of the circulatory system is wrapped on a circular cylinder (see Reference (12) for a detailed description). Figure 16 shows two types of trajectories on the cylindrical phase surface. Trajectories of the first kind are just ordinary planar closed trajectories traced on the surface of the cylinder. Trajectories of the second kind, however, do not require the existence of singular points. They are wrapped around the cylinder and represent blood motion around the CVS.

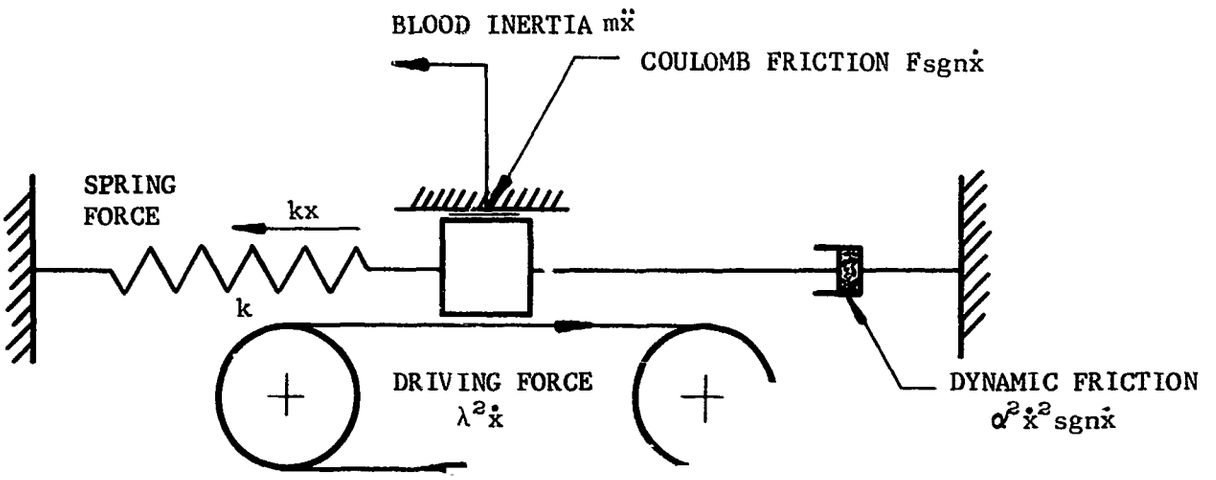

FIGURE 14 MECHANICAL MODEL OF MODIFIED VAN DER POL RELAXATION OSCILLATOR

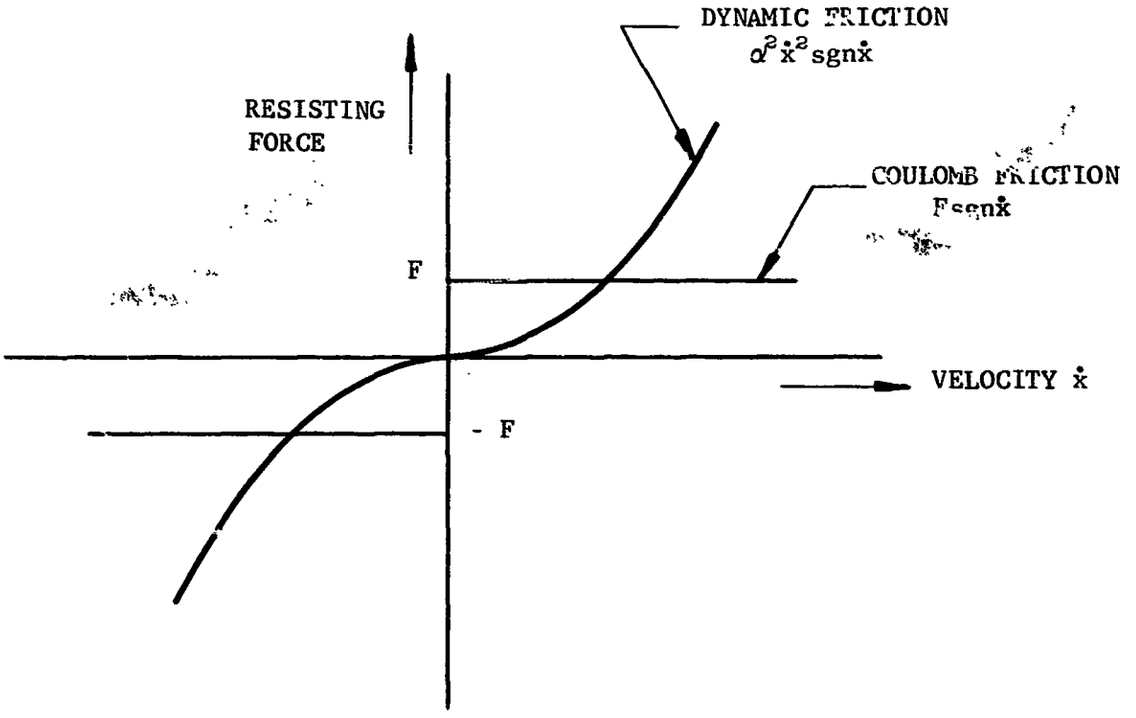

FIGURE 15 DYNAMIC FRICTION AND COULOMB FRICTION CHARACTERISTICS

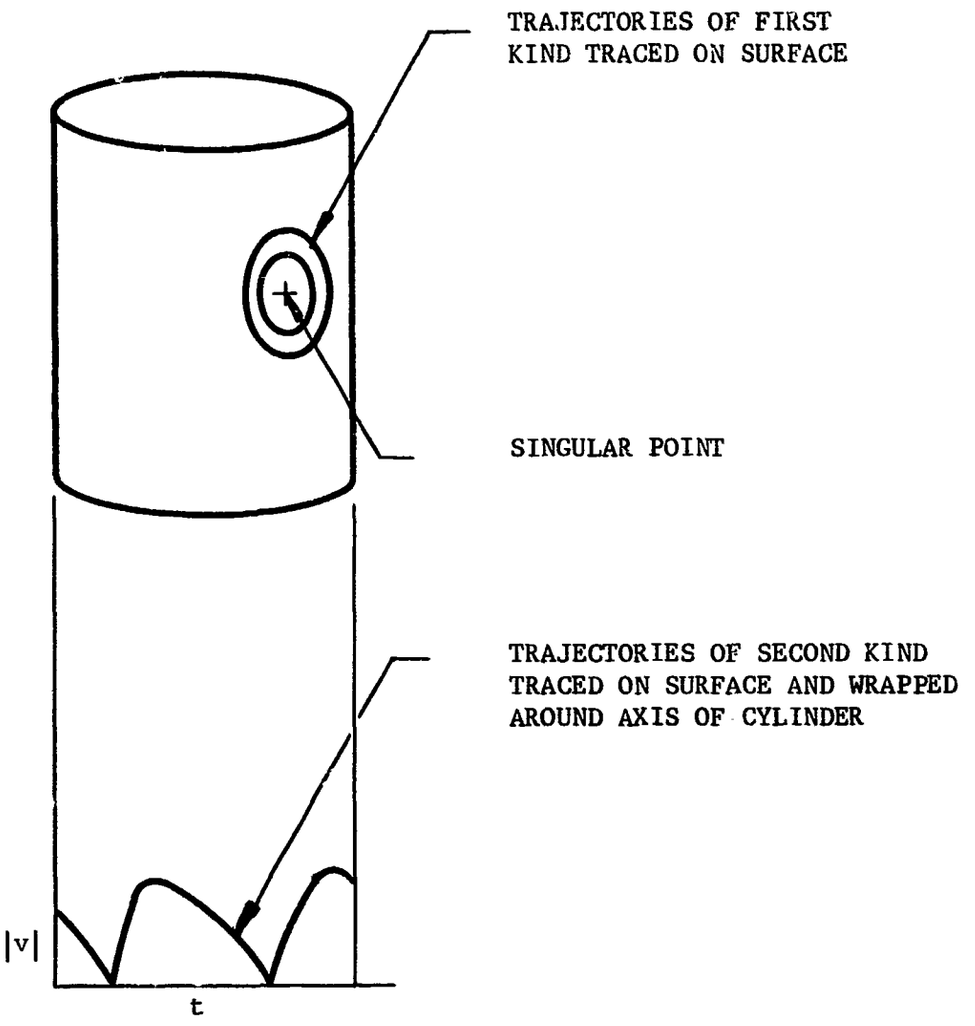

FIGURE 16 CYLINDRICAL PHASE OF CIRCULATORY SYSTEM

The system governing equation [8] can be non-dimensionalized by defining

$$\Omega^2 = \frac{k}{m} \text{ and } \tau = \Omega t \qquad [9]$$

Using these definitions, equation [8] can be re-written as

$$x'' - a^2 x' (1-b^2 x' \text{sgn} x') + x + F \text{sgn} x' = 0$$

where

$$a^2 = \frac{\lambda^2}{\sqrt{km}}, \quad b^2 = \frac{\alpha^2}{\lambda^2}\Omega, \quad F = \frac{f}{k}$$

and primes denote differentiation with respect to τ

Equation [9] can be reduced to two first order equations

$$x' = v$$
$$v' = -x + a^2 v (1-b^2 v \text{sgn} v) + F\text{sgn}v = -x + \varphi(v) \qquad [10]$$

The limit cycle and a typical trajectory for this system, obtained by Liénard's construction (12) are shown in Figure 17.

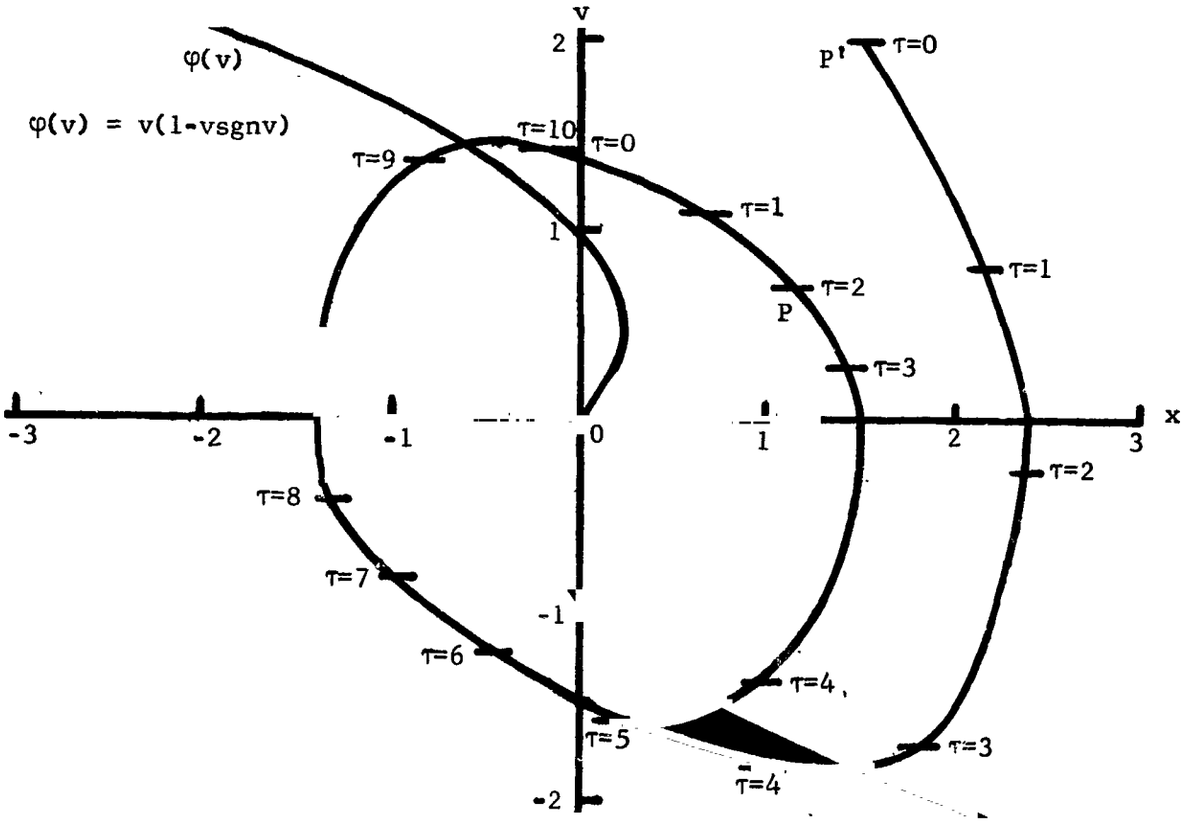

FIGURE 17 TYPICAL LIMIT CYCLE AND TRAJECTORY FOR RELAXATION OSCILLATOR

The limit cycle represents a stable "stationary" oscillation of the physical system. We note that the quantity ($1-b^2 v\,sgn\,v$) in equation [10] is positive for small v and negative for large v, i.e. the resistance is negative for small v and positive for large v. Consequently, the system releases energy for small v and absorbs energy for large v.

Before studying the applicability of this mathematical model to impact, the effect of different system variables on the frequency of the system (cardiac rate) will be qualitatively stated.

a. Decreasing m is equivalent to bleeding. It can be reasoned that the pulse rate will increase since the linear natural frequency $\frac{1}{2\pi}\sqrt{\frac{k}{m}}$ of the system is increased. Similarly, an increase in k will increase the natural frequency of the system.

b. Decreasing α is equivalent to decreasing the external resistance (by dilation of vessels). It can be shown analytically that the pulse rate will increase.

c. Increasing λ is equivalent to increasing the energy available to the heart muscle. This increase of energy results in a reduced pulse rate. The energy available to the cardiac muscles is governed by their initial length rather than their initial tension. Consequently the end-diastolic volume has a significant effect on the pulse rate.

4.2.1 Applicability of the Limit Cycle Oscillator to Impact

Study of the applicability of the limit cycle oscillator to impact can be made by investigating its perturbation from dynamic equilibrium. It is worth noting that motion of the relaxation oscillator during impact is not governed by the modified van der Pol equation. Impact can be specified by a relation between conditions immediately before it and immediately following it. This results from the existence of certain invariants (theorems of momentum and kinetic energy which are not related to the process differential equation).

The average velocity of blood $\bar{V}$ flowing past a point in a unit time before impact can be represented by

$$\bar{V} = \frac{2}{T}\int_{\alpha}^{\alpha+\frac{T}{2}} V\,dt \qquad [11]$$

where α is a constant
and T is the period of oscillation

After impact, there is a transient velocity change followed by an impulsive pressure gradiant. A study of the magnitude of the perturbation can be made by investigating the flow characteristics in the aorta. The condition for back flow in the aorta is

$$\eta(\tau) < o \qquad [12]$$

where $$\eta(\tau) = \int_o^\tau \left(Q(t) - \pi r_o^2 \int_o^\tau F(\xi)\, d\xi \right) dt$$

$Q(t)$ is the volume flow rate before impact

$F(t)$ is the impact acceleration experienced by the blood stream in aorta

τ is the time interval over which F (t) acts

r_o is the resting radius of the aorta

Assumed values for guinea pig and monkey subjects are:

guinea pig	monkey
r_o = .08 cms	r_o = 0.50 cms
$Q_{average}$ = 35 cc/min	$Q_{average}$ = 350 cc/min

We further assume that there is no flow into the aorta during diastole and that the systolic phase covers approximately 0.6 of the cycle. As a result, the flow rate into the aorta is approximately 1 cc/sec for a guinea pig and 10 cc/sec for a monkey subject.

Approximating F (ξ) by a constant force F_o, we obtain from equation [12]

$$\eta(\tau) = \int_o^\tau Q dt - \frac{\pi r_o^2}{2} F_o \tau^2 \qquad [13]$$

For a forcing function profile defined by F_o = 100 G and τ = 0.01 sec., we have

for guinea pig subjects:

$$\eta(\tau) = \left(.01 - \frac{\pi x (.08)^2}{2} \times 100 \times 980 \times \frac{1}{10^4} \right) = - .0886 \text{ cm}^3 \qquad [14]$$

for monkey subjects:

$$\eta(\tau) = \left(0.1 - \frac{\pi x(.5)^2}{2} \times 100 \times 980 \times \frac{1}{10^4}\right) = -3.84 \text{ cm}^3 \qquad [15]$$

We note from [14], and [15] that considerable back flow occurs in the aorta during impact both for the guinea pig and monkey subjects.

For a curved tube such as the aorta, the friction factor is given by (13)

$$f_c = \frac{6.2}{\sqrt{Re}}\left(\frac{R}{r_o}\right)^{1/5} \qquad [16]$$

where f_c = curved friction factor

r_o = radius of the aorta

R = radius of the aortic arch

R_e = Reynolds number

For $\frac{R}{r_o} = 6$, the friction factor from equation [16] is approximately seven times as great as in a straight tube in the Reynolds number range of 2,000 to 10,000. Therefore, when backflow occurs through the straight part of the aorta it must flow through a resistance approximately seven times the resistance at the site at which the backflow originated. This implies that we would expect a rapid flow through the branching vessels of the aortic arch along with an expansion of the aortic arch. Simultaneously, we would expect a surge on the venous side through the precava and jugulars. As a result, a large amount of energy may be dissipated in the vessels of the head and neck.

Considering now the limit cycle representation in Figure 17 , we note that impact produces a transient velocity change and, thereby, displaces the point P on the limit cycle to the corresponding point P'. Unless injury occurs, the trajectory through the displaced point P' returns to the limit cycle because of the inherent stability of the mechanical oscillator. The energy dissipation for the return trajectory is higher since it acts for a longer time. When the return trajectory approaches the limit cycle, the energy absorbed is balanced by the energy released and the system performs

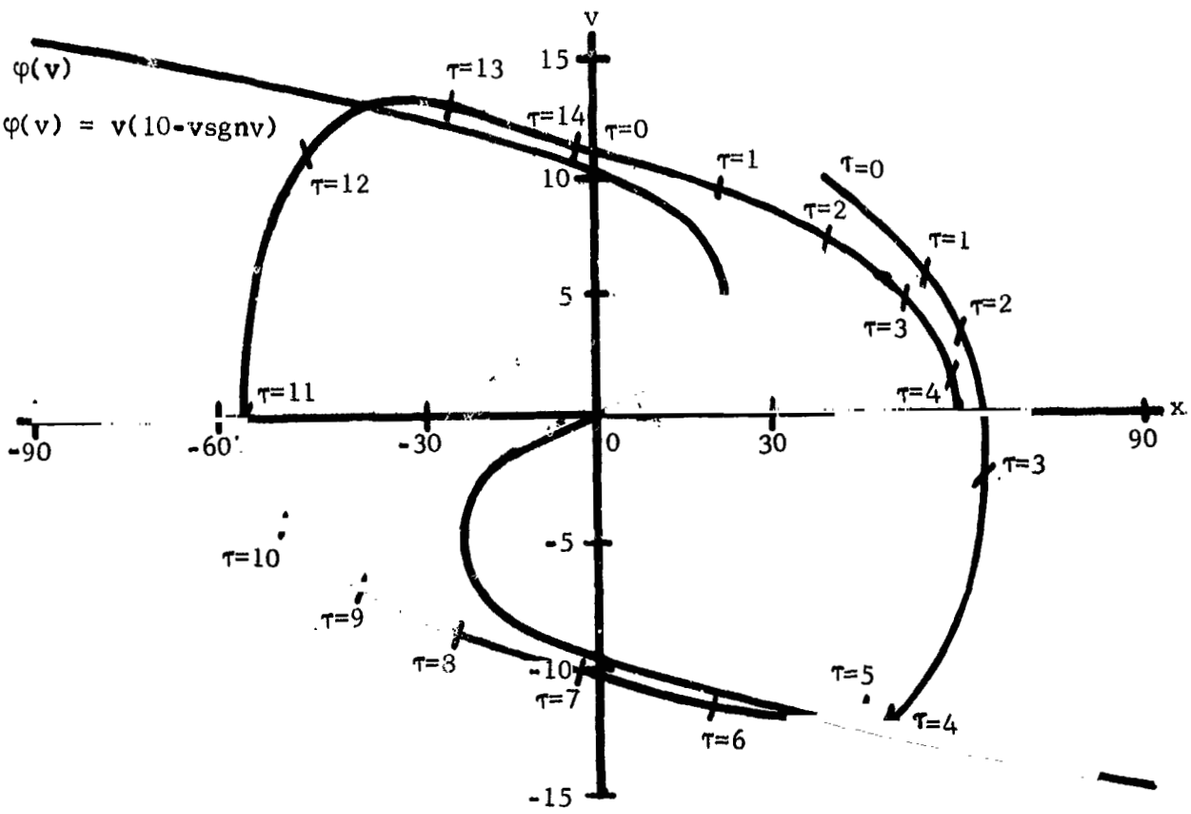

FIGURE 18a LIMIT CYCLE AND TRAJECTORY

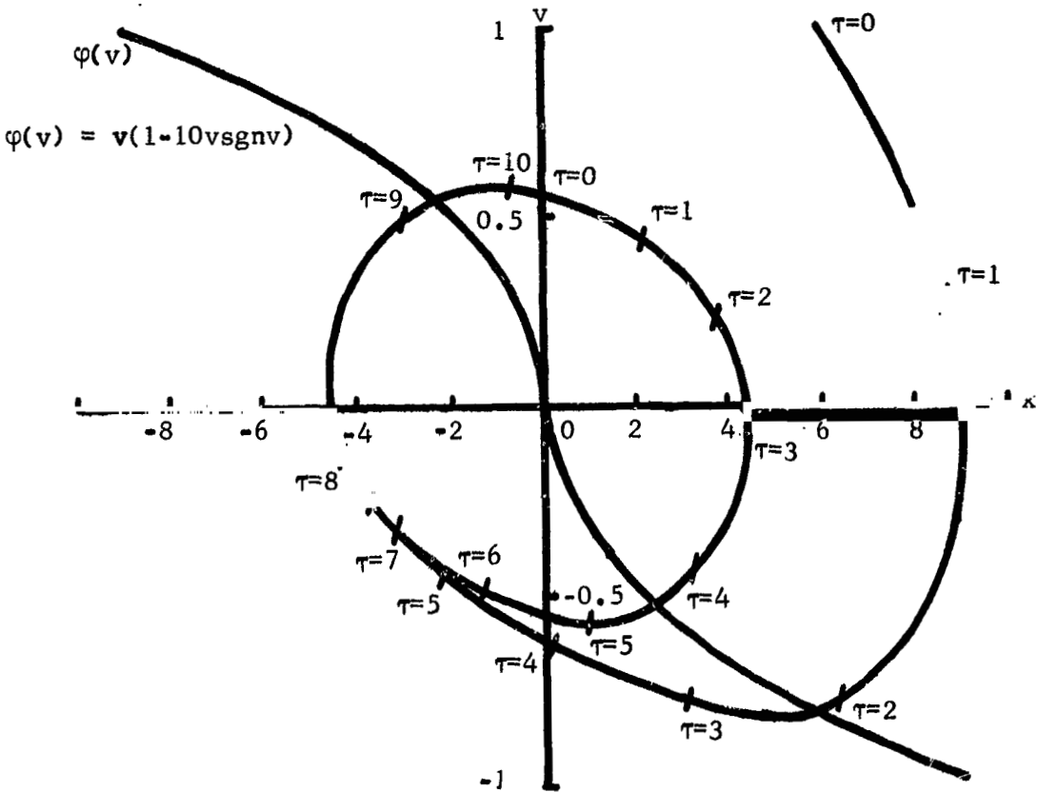

FIGURE 18b LIMIT CYCLE AND TRAJECTORY

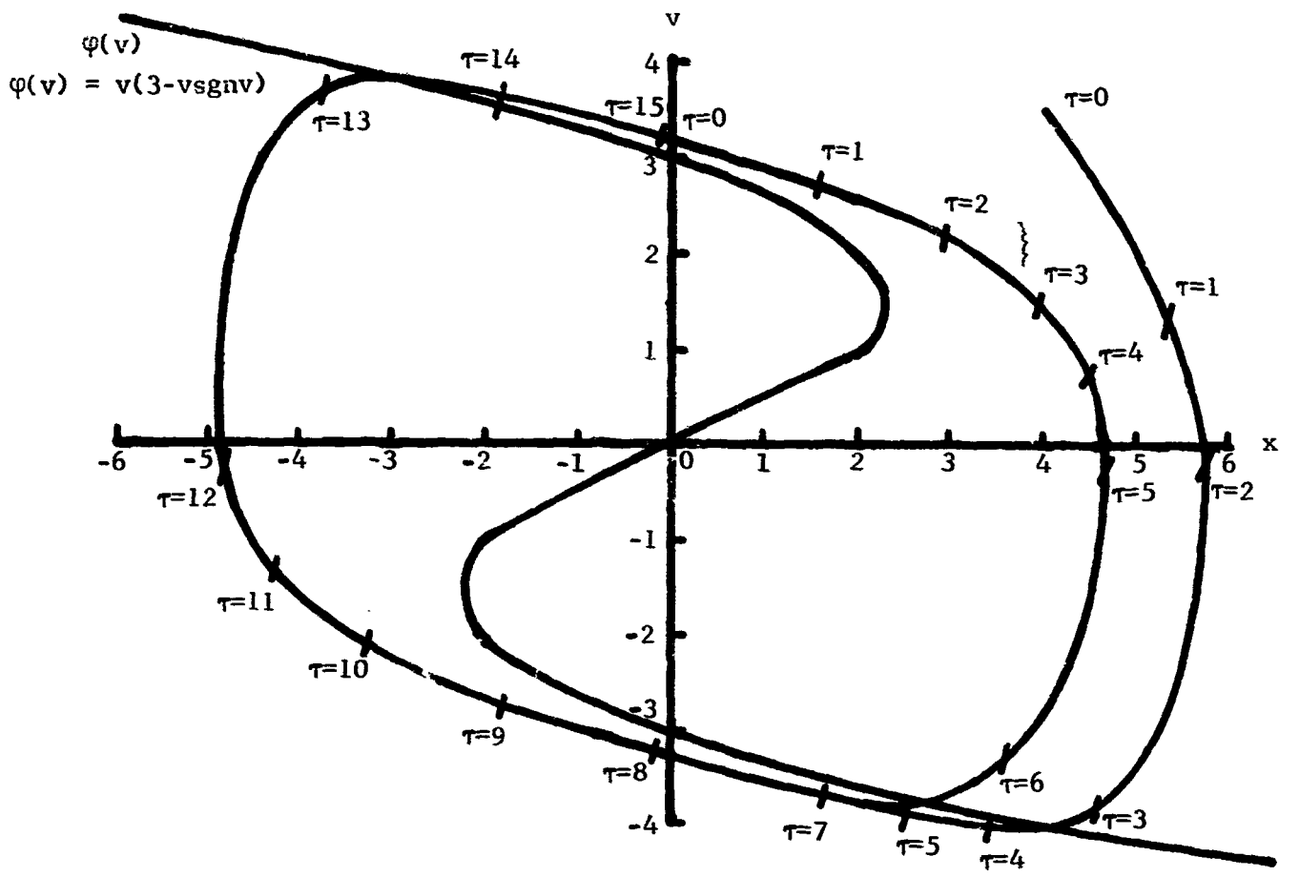

FIGURE 19a LIMIT CYCLE AND TRAJECTORY

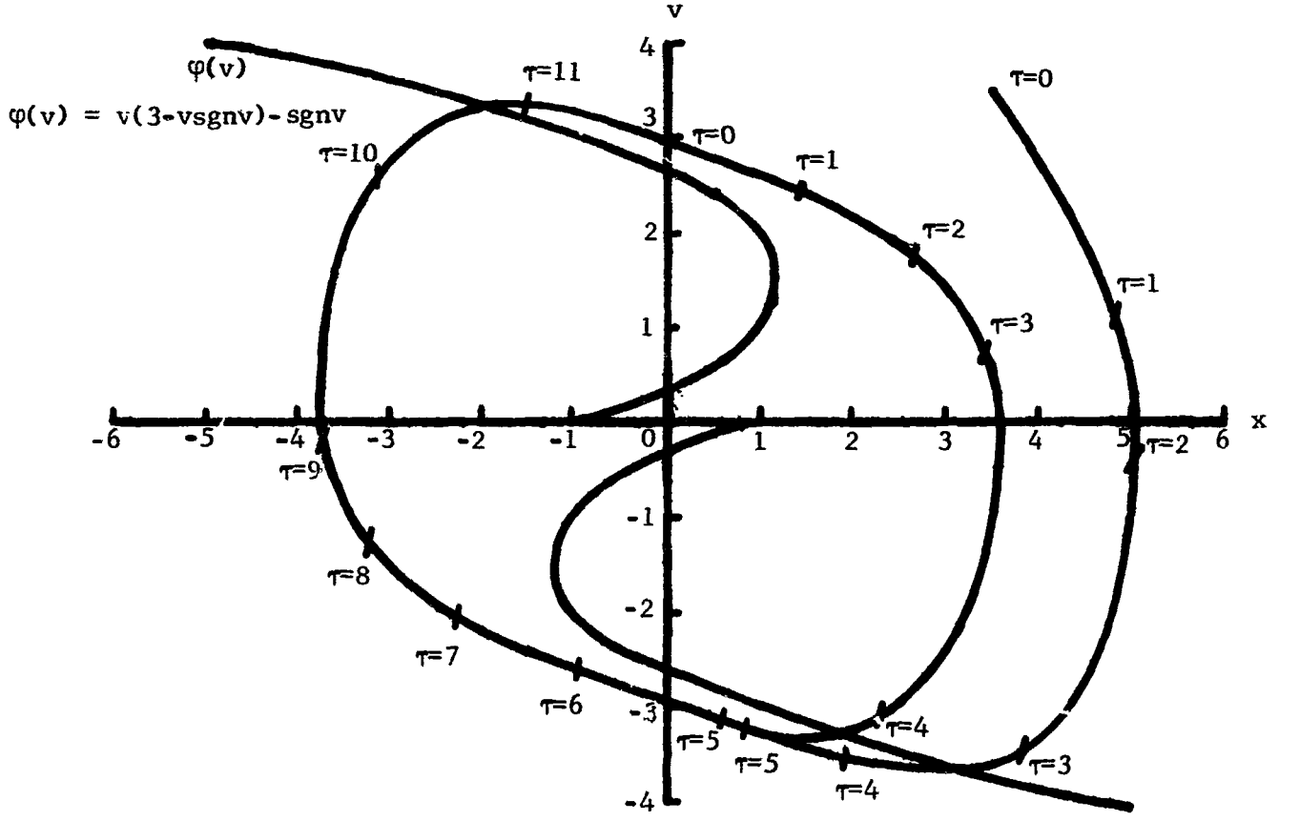

FIGURE 19b LIMIT CYCLE AND TRAJECTORY

"stable" oscillations. The time taken for the trajectory to reach the limit cycle may be taken as a measure of the severity of the impact level.

Typical limit cycles and trajectories for different values of system variables are shown in Figures 18 a,b, 19 a,b. The limit cycles indicate the variations in the frequency (cardiac rate) and heart thrust of the system with different values of dynamic friction, coulomb friction and energy to heart muscle. The trajectories represent the directional and time dependent elements of the transient motion of the "representative point" (P') following impact.

4.2.2 Linearized Model of Limit Cycle Oscillator

The governing equation of motion [8] may be simplified by linearizing the quadratic damping term $\alpha^2\dot{x}$ sgn$\dot{x}$ and by ignoring the coulomb damping term Fsgn$\dot{x}$. In addition, the forcing term $\lambda^2\dot{x}$ may be replaced by a harmonic excitation F sinwt. With these simplifications, equation [8] reduces to

$$m\ddot{x} + c\dot{x} + kx = F\sin wt \qquad [17]$$

Equation [17] agrees qualitatively with the equation obtained by Malindzak and Stacy (14). Their equation representing the dynamic behavior of a mathematical analog of the human arterial system is

$$P_1 = M\ddot{P}_o + V\dot{P}_o + SP_o \qquad [18]$$

where P_1 is the input
P_o is the output
M is the lumped mass term
V is the lumped viscous term
and S is the lumped stiffness term

Impact of the "steady state" linearized model described by equation [17] alters the dynamic equilibrium of the system. If we assume the impact to be represented by the rectangular pulse shown in Figure 20 , the transient response is given by (15).

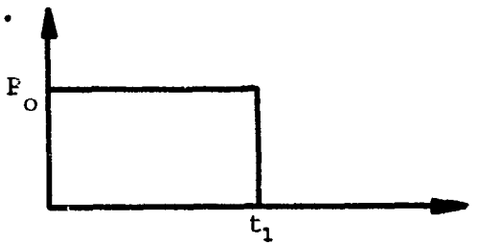

FIGURE 20 RECTANGULAR PULSE

$$x = \frac{P_o}{k}\left[1 - \frac{e^{-\zeta\omega_N t}}{\sqrt{1-\zeta^2}} \cos\left(\sqrt{1-\zeta^2}\,\omega_N t - \Phi\right)\right] \quad 0<t<t_1$$

$$x = \frac{P_o}{k}\left(\left[1 - \frac{e^{-\zeta\omega_N t}}{\sqrt{1-\zeta^2}}\left(\cos\sqrt{1-\zeta^2}\,\omega_N t - \Phi\right)\right]\right. \qquad [19]$$

$$\left. - \left\{1 - \frac{e^{-\zeta\omega_N (t-t_1)}}{\sqrt{1-\zeta^2}} \cos\left[\sqrt{1-\zeta^2}\,\omega_N (t-t_1) - \Phi\right]\right\}\right) \quad t>t_1$$

where $\omega_N = \sqrt{\frac{k}{m}}$ is the natural frequency of the undamped system

$\zeta = \frac{c}{2\sqrt{km}}$ is the damping factor

and φ is the phase angle

Malindzak and Stacy (14) in studying the transient response of the human arterial system have obtained a time constant of 0.16 sec. This value represents the time for oscillations to fade away to 37% of their initial value.

4.3 AORTIC DYNAMICS

The properties of the aortic wall in vitro have been characterized by purely rubber-like behavior by King (16) and elastic behavior by Womersley (17) and Iberall and Cardon (13). Although both approximations have been useful for studying aortic dynamics, neither approach has predicted the flow-deformation-pressure relationships in vivo. Rushmer (18), in his study of pressure-circumference relations in the aorta has experimentally demonstrated that in the living animal the maximum dilatation is followed by the pressure peak. This finding can be explained by considering the equation of conservation of mass [1]. If the term $\int d\omega_{in} - \int d\omega_{out}$ during the acceleration of flow is positive then the considered segment will distend resulting in a change of pressure as defined by the pressure-volume relation [2].

4.3.1 Aortic Dilatation

McDonald (19) has given an approximate equation relating the radial dilatation to the velocity of flow. The relation is

$$\frac{\bar{V}}{C} = \frac{2W}{r_o} \qquad [20]$$

where $\bar{V}$ is the average flow velocity

C is the wave velocity

W is the radial dilatation

and r_o is the resting radius

To obtain the approximate radial dilatation at the junction of the aortic arch and the descending thoracic aorta for the monkey, we have the average velocity from equation [15] during impact as

$$\bar{V} = \frac{Q}{(\pi r_o^2)\tau} = \frac{3.84}{\pi \times \frac{1}{4} \times .01} = 489 \text{ cm/sec} \qquad [21]$$

The wave velocity C as defined by the Moens - Korteweg relation is

$$C = \sqrt{\frac{Eh}{2r_o\rho}} \qquad [22]$$

where ρ is the wall density

h is the aortic wall thickness

E is the Young's modulus

Assumed values for the monkey are:

$E = 3.93 \times 10^6$ dynes/cm^2

$h = 0.1$ cm

$\rho = 1$ gm/cm^3

$r_o = 1/2$ cm

These values yield the wave velocity at the junction of the aortic arch and the descending aorta

$$C = \sqrt{\frac{3.93 \times 10^6 \times 0.1}{2 \times 1/2 \times 1}} = 626 \text{ cm/sec} \qquad [23]$$

From equation [20] and the values of $\bar{V}$ and C from [21] and [23], we get the approximate radial dilatation as

$$W = \frac{489}{626} \times \frac{1}{4} = 0.1958 \text{ cm}$$

For the monkey subject, we therefore get an aortic diametral dilatation of 40% for a rectangular forcing function of duration 0.01sec and intensity 100 G.

4.3. Aortic Pressures

Analytical determination of the dynamic pressures in the aorta at impact is difficult since the dynamic response factor for a given acceleration pulse depends on the natural frequency of the system.

The maximum static pressure (p_{static}) in the aorta can be obtained from the relation

$$p_{static} = \rho A l$$

where ρ is the density of the fluid
and l is the effective length of the fluid column in the direction of the acceleration A.

Calculated values of p_{static} at the junction of the aortic arch and descending aorta for a column length of 10 inches (25 cm) for G levels of 9 G (Run No. 1) and 15 G (Run No. 2) are

$$p_{static} = 170 \text{ mm Hg}$$
$$p_{static} = 280 \text{ mm Hg}$$

A numerical comparison with the experimental values in Figures 6a and 6b indicates dynamic response factors of 1.35 and 1.185 respectively. However, comparisons with Figures 8a to 8c do not furnish a correlation.

A significant finding is that the duration of the pressure pulse in the aorta from Figures 6 to 8 ranges from approximately 70 to 120 milliseconds. This transient duration of the pressure pulse is confirmed by the limit cycle oscillator phase plane trajectories (Figures 18 and 19) which predict recovery in time durations that are small in comparison with the duration of the heart beat.

4.3.3 Aortic Dynamic Response

The preceeding analysis is approximate as it is based on a number of simplifying assumptions. In reality there is a considerable amount of damping in the aortic wall. This possibility suggests that the radial aortic wall motion is non-linear and behaves as a mechanical relaxation oscillator with the modified van der Pol equation as the governing equation of wall motion. In this connection, Lawton's (20) data and observations by Remington (21) show that the elastomeric properties of the aorta lead to dissipation of energy in less than half a second after forcible circumferential or longitudinal elongation.

A linear viscoelastic model of the aortic wall, consistent with recent investigations (22), is shown in Figure 21 . The muscle fibers are taken to be physically parallel to the elastin and collagen fibers. This system can be reduced to a single-spring system with viscous damping.

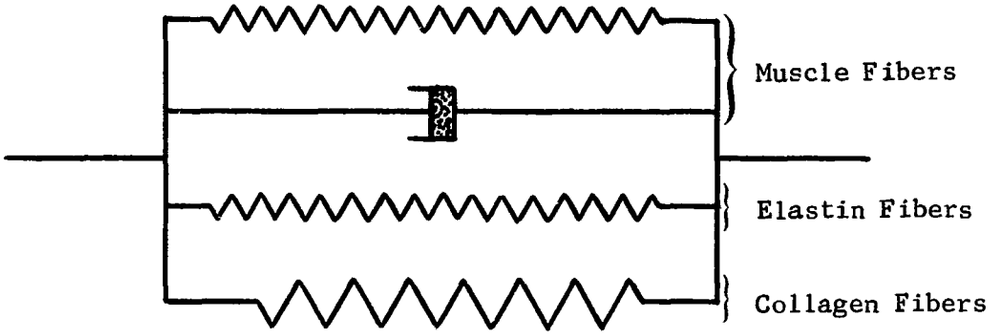

FIGURE 21 MODEL OF BASIC COMPONENTS OF THE AORTIC WALL

To obtain the equation governing radial motion of the aortic wall corresponding to this linearized model, the aorta is assumed to be a long, thin-walled, homogeneous and isotropic circular shell.

Considering an element of the shell as shown in Figure 22, the dynamic equations governing axisymmetric radial-wall motion are

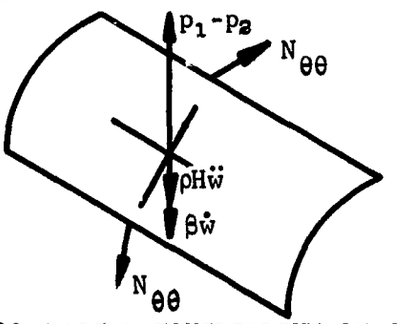

FIGURE 22 RADIAL EQUILIBRIUM OF SHELL ELEMENT

Equilibrium

$$\rho H\ddot{w} + \beta\dot{w} + \frac{N_{\theta\theta}}{r_o} = p_1(t) - p_2(t) \qquad [24]$$

Stress-Strain

$$N_{\theta\theta} = \frac{Eh}{1-\nu^2}\,\varepsilon \qquad [25]$$

Strain-Displacement

$$\varepsilon = \frac{w}{r_o} \qquad [26]$$

where

$N_{\theta\theta}$ = Shell stress, considered constant thickness through shell thickness.

ε = Strain

h = Shell thickness

E = Young's modulus

r_o = Shell radius

w = Radial displacement

$p_1 - p_2$ = Pressure difference across shell wall

ν = Poisson's ratio

β = Damping coefficient

ρ = Shell density

and dots denote differentiation with respect to time

Equation [24] accounts for the inertia of the mass of the tissue in which the aorta is embedded. The quantity H in this equation is defined by

$$H = h + h_1 \frac{\rho_1 R_1}{\rho r_o}$$

where h_1, ρ_1 and R_1 denote the uniform radial thickness, density and mean radius of the surrounding tissue.

Substituting equations [25] and [26] in equation [24], and simplifying, we get

$$\ddot{w} + \frac{\beta}{\rho H}\dot{w} + \frac{Eh\,w}{\rho(1-\nu^2)Hr_o^2} = \frac{p_1(t)-p_2(t)}{\rho H} \qquad [27]$$

Equation [27] governs the motion of a damped spring-mass system excited by a force. The solution to this equation for an arbitrary pressure pulse can be obtained by Duhamel's integral (15).

For $\beta = 0$, and a sinusoidal pressure pulse defined by Figure 23, the dynamic response factor is shown in Figure 24.

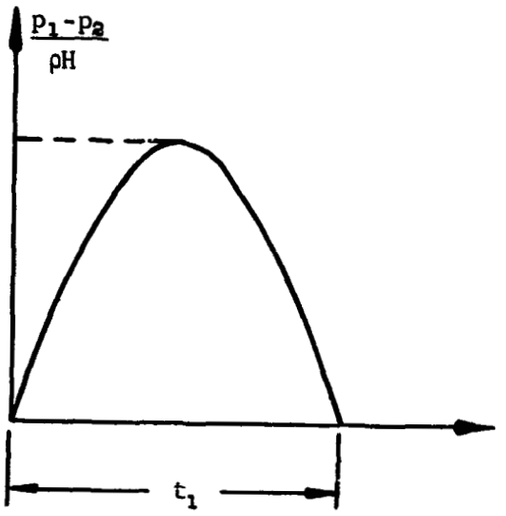

FIGURE 23 SINUSOIDAL PRESSURE PULSE

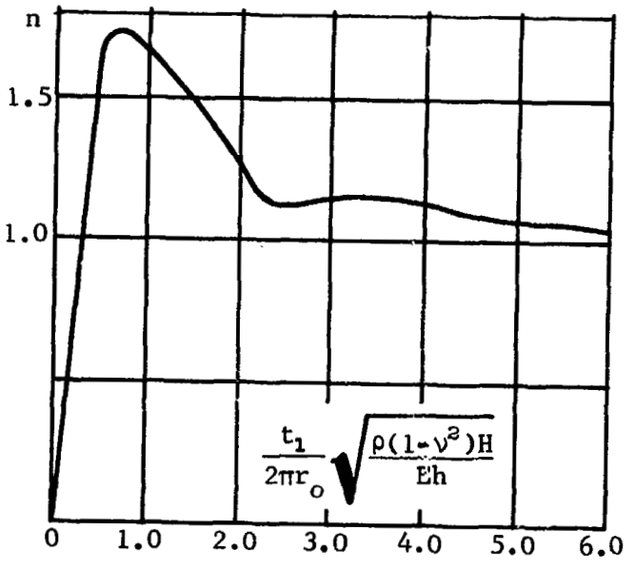

FIGURE 24 DYNAMIC RESPONSE FACTOR

4.3.4 Lateral Vibrations of Aorta

In the preceeding analysis, the axisymmetric breathing mode (expansion and contraction) was studied. We will now proceed to investigate the lateral vibrations of the aorta where in each cross section moves as a rigid body. Mollo-Christensen (23) has obtained an expression governing the stability of wave for the lateral deflection of an elastic tube embedded in an elastic medium. His condition for wave instability is

$$\frac{\bar{V}^2}{1 + \frac{\rho A}{m + Jk^2}} > \frac{1}{\rho A}\left(k^2 EI + T + SG + \frac{K}{k^2}\right) \qquad [28]$$

where $\bar{V}^2$ is the average axial velocity of flow in the tube

EI is effective flexural rigidity

T is the axial tension force

SG is the effective shear rigidity

K is the spring stiffness of medium in which tube is embedded

m is the effective mass of tube per unit length

J is the effective mass moment of inertia of tube

A is the cross sectional area of tube

ρ is the tube density

and k is the wave number $\left(\frac{2\pi}{\text{wave length}}\right)$

We note from the inequality [28] that increasing blood flow velocity $\bar{V}$ at impact in the aorta can lead to wave instability. In this connection Mollo-Christensen (23) comments "Impediments to the transmission, generation and absorption of such waves, even if they are not caused by changes in geometry of blood vessels, may cause malfunctioning in circulation. Local changes may cause local malfunctioning, while overall changes in elasticity or supporting structure of the arteries may change the efficiency of peripheral circulation".

SECTION 5.0
DISCUSSION

The primary objective of the two phases which constitute this program, namely to develop a theoretical analog of the mechanisms of injury to the heart and great vessels of subjects exposed to $-G_z$ impact to the degree that it can be used to predict the preinjury levels (of impact), has been achieved. The experiments in Phase I yielded some unexpected results for both the guinea pig and the monkey subjects. Many complications regarding equipment, instrumentation, and response of subjects were encountered and resolved. The basic premise that the heart and great vessels would rupture was invalidated and experimental design was changed to determine the reason. Analytical studies conducted in Phase II also yielded some very interesting results which, as used to explain the mechanisms of injury of the test subjects in Phase I, appear to be potentially valid for the mathematical model to predict human preinjury levels. However, the remaining Phases III and IV of the overall research should be accomplished to verify and refine the model before it can be applied to predict the preinjury levels for man.

5.1 IMPACT EXPERIMENTS

This section presents a discussion of the results (clinical, ECG, and pathological) of the guinea pig and monkey runs.

5.1.1 Guinea Pig Experiments

This series of tests, in which numerous subjects were used in an exploratory manner within the scope of the project, provided information which, if valid for larger animals, could be useful in establishing the theoretical analog of the mechanisms of injury. The number of variables governing the impact deceleration profiles with the three velocities economically limited the amount of detailed information derivable from the tests. However, more data was obtained than could be reported in detail. This additional data has been used in the formulation of opinions on generalized injury and survivability. Scattered small contusions, lacerations, abrasions, congestions, etc., are details recorded but not reported herein.

The injuries when present, at the 20 ft/sec velocity change were considered to be minor. Injuries at velocity changes of 40 and 60 ft/sec increased in severity along with the severity of impact, with severity in both instances being difficult to define. To visualize the relation of the impact variables and survivability, a bar chart is shown in Figure 25. The threshold of non-survival appears to be 80-100 G at ΔV of 60 ft/sec. Two animals did expire post run at 40 G with a ΔV of 20 ft/sec. However, these two animals definitely were suffering from a respiratory infection indicating that survival limits can be altered considerably by such infections. The gross pathology indicates that the lungs, central nervous system, and the large blood vessels in the neck are areas of acute serious injury at the higher levels of G and duration of G (ΔV).

Analysis of the clinical results obtained reveals that at a velocity change of 20 ft/sec all the survivors appeared normal after the run. Evidence of damage to the CNS producing clinical symptoms was noted in the test subjects at a velocity change of 40 ft/sec at a higher G levels. At a velocity change of 60 ft/sec, 62 per cent of 77 subjects tested presented one or more symptoms of neurological damage. Comparison of the three groups tests at 100, 120 and 140 G, indicates that the rate of onset may be a contributory factor in producing the symptoms as there is an increase in the percentage of subjects showing neurological manifestations at an onset rate of 20,000 G/sec. Trauma to the limbs of the test subjects post run was also observed, which restricted mobility during post run examination.

Bradycardia of varying degrees is a consistent finding throughout the series. While present even at the lowest G levels used, it decreases slightly at higher velocity changes, but is more severe when present (Figures 26 and 27). Other changes in ECG pattern post run (evidence of subendocardial damage, auricular flutter, atrioventricular block, extrasystoles, and asystole) were noted. The transient nature of these findings is indicated by the fact that subjects on reexposure showed no significant differences from the single exposure subjects at the same level. Because these findings are of a transient nature they may be indicative of or contribute to cardiac lesions. Changes in the ST segment due to "current of injury," indicating subendocardial damage, increased with G from infrequent at ΔV of 20 ft/sec to

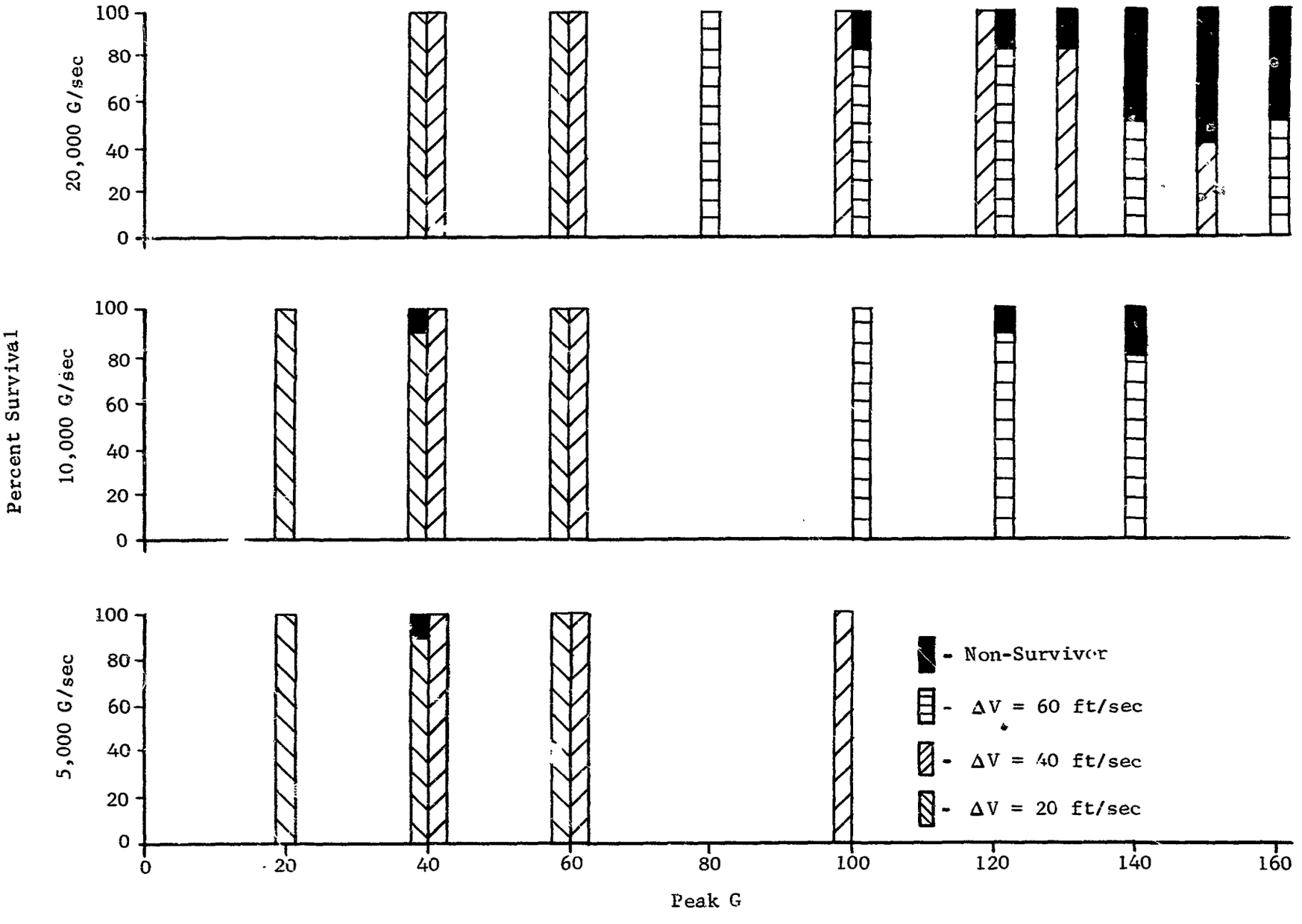

FIGURE 25 PERCENT SURVIVAL VERSUS PEAK G

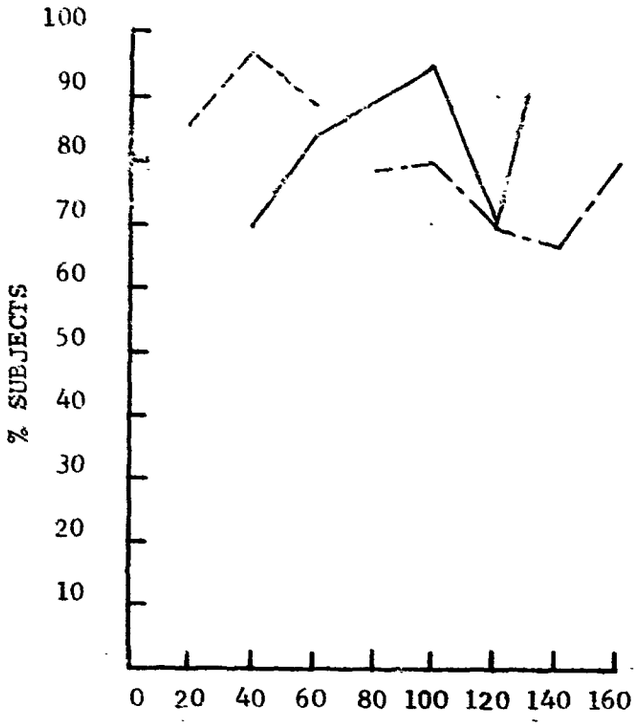

FIGURE 26 BRADYCARDIA

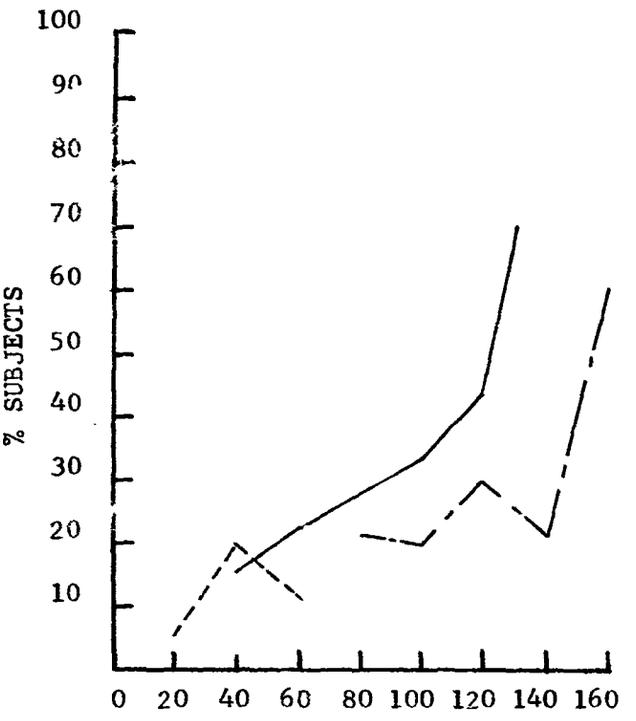

FIGURE 27 SEVERE BRADYCARDIA

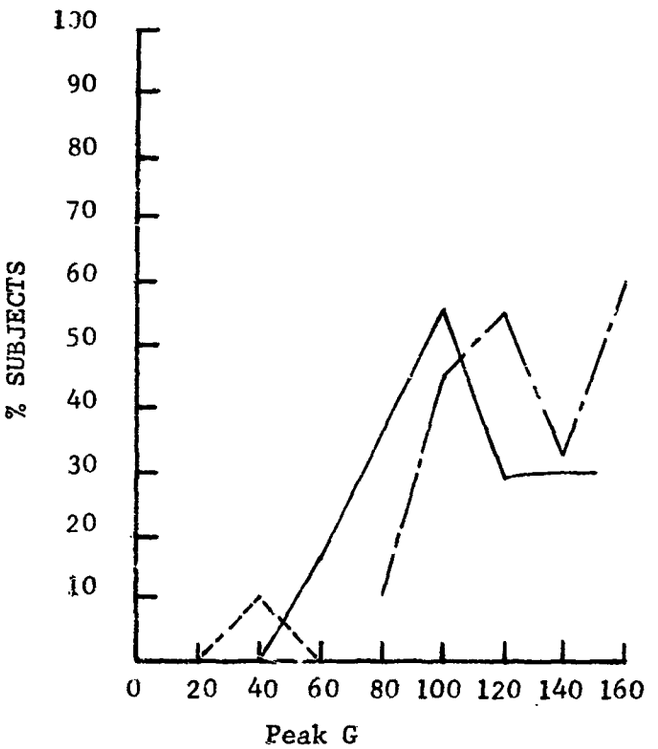

FIGURE 28 EVIDENCE OF SUBENDOCARDIAL DAMAGE

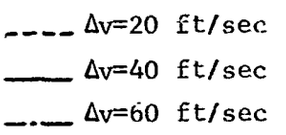

common at the higher velocity changes (figure 28). This indicates potential permanent cardiac lesions may be incurred and, as such, is an unknown worthy of investigation. Conversely, perhaps $-G_z$ impact can be used to induce a cardiac "strain" in experimental animals used as subjects in cardiac research. Cardiac lesions induced by such strain may be progressively serious depending upon many variables. Ventricular tachycardia is considered to occur due to development of a rapidly discharging focus in the myocardium. Unless such arrhythmia is converted as soon as possible, mortality rates are expected to be very high. Ventricular fibrillation is a far more serious condition than ventricular tachycardia and may possibly be converted into a sinus rhythm by defibrillation.

5.1.2 Monkey Experiments

These experiments were more informative due to the body shape, increased size, and cardiovascular reflexes of the subject. This provided more direct information on the problem of $-G_z$ impact exposure of man. All of the test subjects (Macaca speciosa) exposed to the $-G_z$ impacts survived, even though some were reexposed several times as shown under pathology. One subject after multiple exposures has been held for several months and shows no subsequent signs of ill health. The clinical signs and symptoms and the pathology of the subjects indicate that the injuries incurred, even at highest G and highest velocity change (60 ft/sec), were reversible. Bradycardia, unlike the guinea pig experiments, was produced consistently only at high G levels at ΔV of 60 ft/sec. This indicates that considerable variations may exist in the species of test subjects selected and that subjects representing man will require careful selection. Failure of the large vessels to rupture under $-G_z$ impact was determined to be due to a "protective" intrathoracic counterpressure. Restraint of the torso by the thighs at higher levels of G caused fracture of the femur when this portion of the retention load was too high.

Multiple Exposures - The effects of multiple exposure to $-G_z$ impact are shown by comparing pathological findings in five subjects with single two with two, four with three, one with four, and two with six exposures. The lesions of major concern are pulmonary hemorrhage, hematoma around thoracic vertebra, and laceration of internal organs. Pulmonary hemorrhage was severe at the higher G levels (280, 300, and 325) at a velocity change of

60 ft/sec as evidenced by single exposure and in one case of multiple exposures in which the final exposure was at 300 G. Two monkeys with prior exposures at a lower velocity change were exposed at 200 G with ΔV of 60 ft/sec. One showed severe pulmonary hemorrhage but the other did not. One subject with low multiple exposures, but with a final exposure at 166 G with ΔV of 60 ft/sec showed no pulmonary hemorrhage. Only one subject showed such hemorrhage after impact at 250 G with 40 ft/sec velocity change following six previous exposures at lower G. Pulmonary hemorrhage was not observed at lower levels indicating a surprisingly high threshold, even on multiple exposures. Hematoma around thoracic vertebra, severe to moderate, closely parallels occurance of pulmonary hemorrhage. This may be indicative of severe "buckling" of the torso in this area injuring both the lungs and the spinal column. The exact nature and extent of injury to the spinal column was not determined in this exploratory project, although, the spinal segments were saved for possible future studies. Lacerations of internal organs were noted, once in the liver after an exposure of 280 G at ΔV of 60 ft/sec, once in the spleen at 250 G at ΔV of 40 ft/sec, and once in the lungs at 280 G at ΔV of 60 ft/sec. Collapse of the lungs or portions, indicative of lacerations, occurred in two subjects with single runs at high G (300 and 325) with ΔV of 60 ft/sec and in one multiple test in which the final exposure was 170 G with a ΔV of 60 ft/sec. One subject showed collapse of the mid-lobe of the right lung following a final exposure of 450 G with ΔV of 40 ft/sec.

Bradycardia has been considered as a warning sign of possible injury as the level and duration of $-G_z$ impact are increased. The injuries observed at the necropies appear to be reversible in character and are believed to be due to direct loading during the impact. However, these studies show that bradycardia may be a concurrent finding with moderate to severe injury, especially of the lungs, in the Macaca speciosa. The level and duration of G required to produce bradycardia in this monkey is most interesting, appearing to be based on a definite level of energy

transfer as shown in the log log representation of G_{mean}^{*} versus impact duration (Figure 29). No such threshold of bradycardia was observed in the guinea pigs, since it was produced even at the lowest levels used and well below the injury levels. The question arises as to the sensitivity of cardiovascular reflex mechanisms of animals that walk on all fours and those holding the torso erect. Perhaps those having erect postures may have the same reflex sensitivity as man and could be used to pursue the study of bradycardia as a sign of preinjury level in $-G_z$ exposure.

Severe bradycardia was found to be concurrent with severe pulmonary hemorrhage in five out of five test and in which ECG was obtained. Hematoma around the thoracic vertebra was observed in four out of six tests in which an ECG showing severe bradycardia was obtained. In two tests when severe pulmonary hemorrhage and thoracic vertebral hematoma occurred no ECG was obtained. In one instance, severe bradycardia occurred without either the hemorrhage or the hematoma. Thus, it is believed that these injuries and severe bradycardia occur concurrently during exposure to $-G_z$ impact at the same level of energy transfer of ΔV = 60 ft/sec.

The results of these tests and a rather extensive review of the literature indicates that during $-G_z$ impact, the stimuli which influence the vagal tone to produce bradycardia need not come exclusively from the baroreceptors in the aortic arch and carotid sinus. Ample evidence exists to support the contention that bradycardia so produced would be abolished by either surgical or pharmacological vagatomy.

Slowing of the heart rate of human subjects immediately following impact with a $-G_z$ vector component was noted by Brown (1): "The greater the negative z resultant the greater the average slowing of the heart rate". The heart rate decreased sharply at impact and gradually returned to

---

*G_{mean} is defined by the relation

$$G_{mean} = G \frac{(\frac{1}{2} t_1 + t_2)}{(t_1 + t_2)}$$

where G is the peak force
t_1 is the onset duration
and t_2 is the duration of the peak force

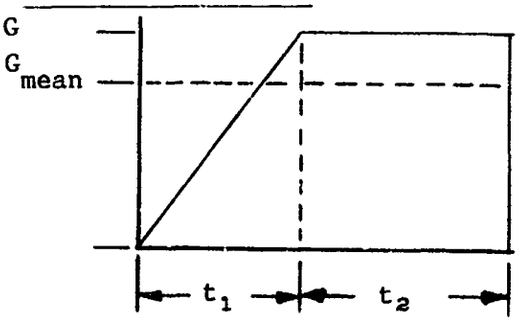

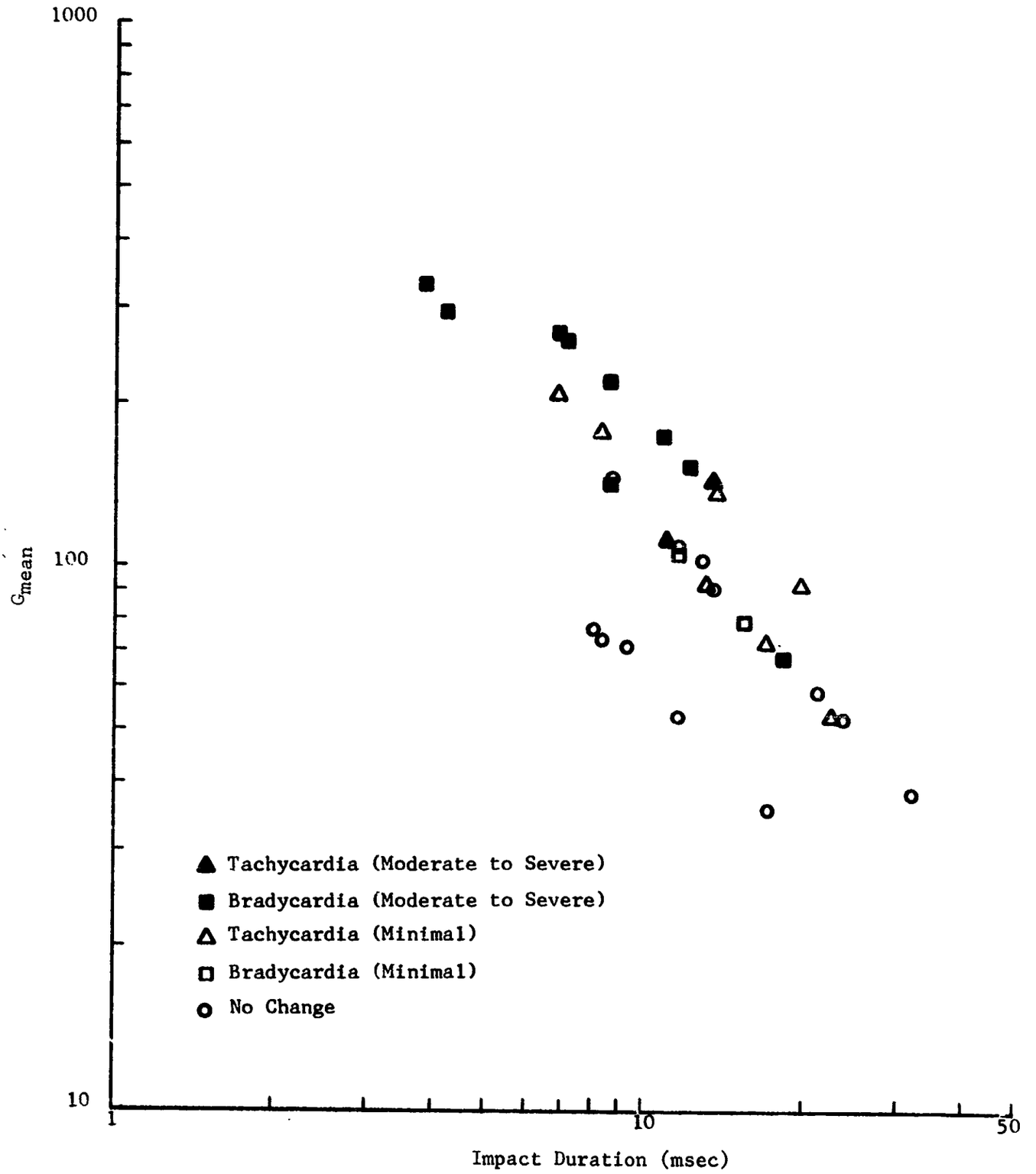

FIGURE 29 BRADYCARDIA THRESHOLD IN YOUNG MACACA SPECIOSA EXPOSED TO $-G_z$ IMPACT IN SEATED POSTURE IN GOOD SUPPORT AND RESTRAINT SYSTEM

preimpact levels in 5 to 20 seconds, except for the full $-G_z$ orientation which was limited to exposure in the lower range to approximately -10 G_z. These two subjects showed a 20% decrease in heart rate. However, these tests also show bradycardia with lateral orientations from 15 to 30 G but to a lesser degree than when a $-G_z$ vector is present. With most of the lateral orientations bradycardia was noted in the 15 to 30 G range, whereas the lower range of 10-15 G caused an increase in heart rate. This indicates the presence of both the cardioaccelerator and cardioinhibitor stimuli with overriding by the cardioinhibitor stimuli at the higher G range.

The "sinus tachycardia", attributed to anxiety and probably associated with transient sharp pain, was noted by Headley (24) in simulated B-70 capsule ground impact tests. In these experiments, human subjects seated upright were exposed to controlled deceleration profiles up to 35 G with the forcing function directed positions within a 90 degree cone, e.g. within 45° of vertical. This was not considered deleterious. The extensive tests of Weis (25) in the same "cone" of orientations using human subjects up to 27 G showed only a few subjects having any remarkable events as recorded by ECG, three with premature ventricular contractions (several) and one with bradycardia for five seconds following impact with all conditions being considered tolerable.

The initiation of the reflexes which produce the bradycardia is probably from stimulated baroreceptor endings of afferent nerve fibers in the carotid sinus and the aortic arch. The behavior of the baroreceptor endings is of particular interest in this $-G_z$ impact study since the effects of the short duration and the high levels of the pressure pulses associated with the impacts upon the baroreceptor mechanism(s) are unknown. The work of Bronk and Stella, as referenced by Heymans and Neil (26), is of great interest in this study since they showed the effect of both the increase in the level and the rate of change of pressure, although in much longer periods of time and much smaller pressure changes. These reflexes and other responses to $-G_z$ stress are discussed in more detail in the Appendix.

5.2 MECHANICAL ASPECTS OF IMPACT INJURY

Injury produced by impact accelerations is caused by the dynamic visco-elastic response of internal organs and hydraulic and pneumatic pressure

(volume) changes in the flow system. To define mechanisms of such injury, it is necessary to investigate the mechanical forces at impact. These mechanical forces are of two types; transient body forces (inertia force/body volume) and transient surface tractions (force/surface area).

Transient body forces from inertial loading cause injury by inertial deformation and/or flow. The energy of body forces produces organ laceration, tissue distortion, and hemorrhage. Damage is primarily caused by shear distortion, tension, compression, bending, hydraulic and pneumatic loading, and rotatory inertial effects. Transient surface tractions from restraint and other surface loadings are in dynamic equilibrium with the body forces. The surface energy potential produces hemorrhage, contusions, and, in some cases, organ laceration. In general, for a given acceleration profile, organs with very low natural frequencies have dynamic response factors of less than unity, while the dynamic response factors are greater than unity for organs with natural frequencies near or above the forcing frequencies.

Dynamic hydraulic and pneumatic pressure imbalances result from surface and body forces. Transient pressure imbalances account for a redistribution of blood volume within tissues, areas of hemorrhage, ischemia and shock.

The following discussion deals with analytical considerations of experimental findings in an attempt to evaluate mechanisms of injury or non-injury.

5.2.1 Aortic Non-Rupture

The failure of the aorta to rupture at high $-G_z$ impact accelerations can be explained by reviewing current investigations and considering the possible stresses that can produce an aortic rupture.

Roberts (27) has shown that pressure surges and blood pressure levels arising from blunt trauma of the thorax are not responsible for aortic rupture. They attribute tears of the aorta and great vessels to the displacement of the heart into the left chest. According to Murdock, cited by Evans (28), "the forces responsible for closed injury to the aorta are (a) inertia or 'drag' resulting from sudden deceleration, and (b) compression with momentary disruption of an open circulation. The inertia force exerted on the blood column either directly or in a torsional plane, produces frictional forces which cause wrinkles, tears, or cracks in the aortic intima."

In general, the stresses responsible for aortic rupture are:

a. Longitudinal stresses acting in a direction perpendicular to the cross-section of the aorta. These stresses are further augmented by tensile stresses resulting from the movement of the heart.

b. Transverse stresses acting in the plane of the circular cross-section of the aorta parallel to the aortic wall. In the curved segment of the aorta, part of this stress results from the transverse bending of the aortic wall as it becomes elliptical in shape.

c. Shear stresses in the aortic wall which result from a combination of the following loading conditions; externally imposed torsional loads, externally imposed shear loads, and out of plane bending moments.

The fact that the great vessels did not rupture in the $-G_z$ impact experiments is conjectured to be due to a concommitant increased intrathoracic pressure and experimental evidence has been obtained to sustain this theory. Figures 8a, b, and c conclusively demonstrate that the transient aortic pressures are externally compensated by the intrathoracic pressures. Consequently, the pressure differential across the aortic wall is minimized, thereby minimizing longitudinal and transverse stresses in the aorta. Since localized trauma is absent, bending moments and torsional and shear loads are non-significant and there is no shear deformation of the aortic wall.

5.2.2 Pulmonary Injury

The incidence of pulmonary injury of various degrees in the guinea pig and monkey subjects exposed to $-G_z$ impact accelerations suggests that injury is caused by the dynamic interplay of hydraulic and pneumatic pressures.

Dynamic analysis of the mechanisms of pulmonary injury is difficult because it depends on several factors, namely geometric configuration, properties of distributed mass and viscoelastic elements, and coupling of longitudinal and lateral motion of elements. From a purely mechanical point of view, the abdomen can be assumed as a fluid filled container in series with the diaphragm, while the chest wall may be considered as divided into two elements operating in parallel, the rib cage and the abdomen-diaphragm. Hence, the static pressures are related by

$$P_{\text{chest wall}} = P_{\text{rib cage}} = P_{\text{abdomen}} + P_{\text{diaphragm}}$$

As a result, the static volume change due to the abdomen-diaphragm movement plus the static volume change due to the rib cage movement yields the static volume change contained within the chest wall.

According to Mead (29), dynamic pressure volume relations of various components of the respiratory system can be stated in the generalized form

$$P = f_1(V) + f_2(\dot{V}) + f_3(\ddot{V}) \qquad [29]$$

where $f_1(V)$ is a function describing the positional (elasticity, gas compressibility, weight, surface tension) component of motion,

and $f_2(\dot{V})$ is a function describing the frictional resistance of flowing fluids and moving solids,

$f_3(\ddot{V})$ is a function describing inertia of all masses being accelerated.

Equation [29] is analogous to the equation governing motion of a spring mass with the displacement being expressed as volume and the pressure as force. The intrathoracic pressure profiles illustrated in Figures 7 and 8 demonstrate this spring mass characteristic following impact.

At impact, the transient pressure head of the fluid column acting on the diaphragm and the intrathoracic pressure. Since the forcing function duration is small, the intrathoracic pressure increase is possibly governed by an adiabatic relation and the pressure profile is similar to a series of blast pulses. The volume of the thoracic cavity, governed by the intrathoracic pressure, is deformed laterally and longitudinally into a frustrum of a cone with an increased angle, as shown in Figure 30. The restoring force provided by the restraint and tissue elasticity limits the amount of such change.

The major mechanisms responsible for pulmonary injury under these conditions may be spalling and implosion. These mechanisms lead to instability of air spaces and a departure of the lung surface energy from its minimum value.* The spalling effect is a phenomena wherein shock fronts

*An equilibrium state of the lung surface is reached only when the surface energy is a minimum for the conditions of restraint imposed by the configuration of elastic fibers and a pressure difference applied to the lungs.

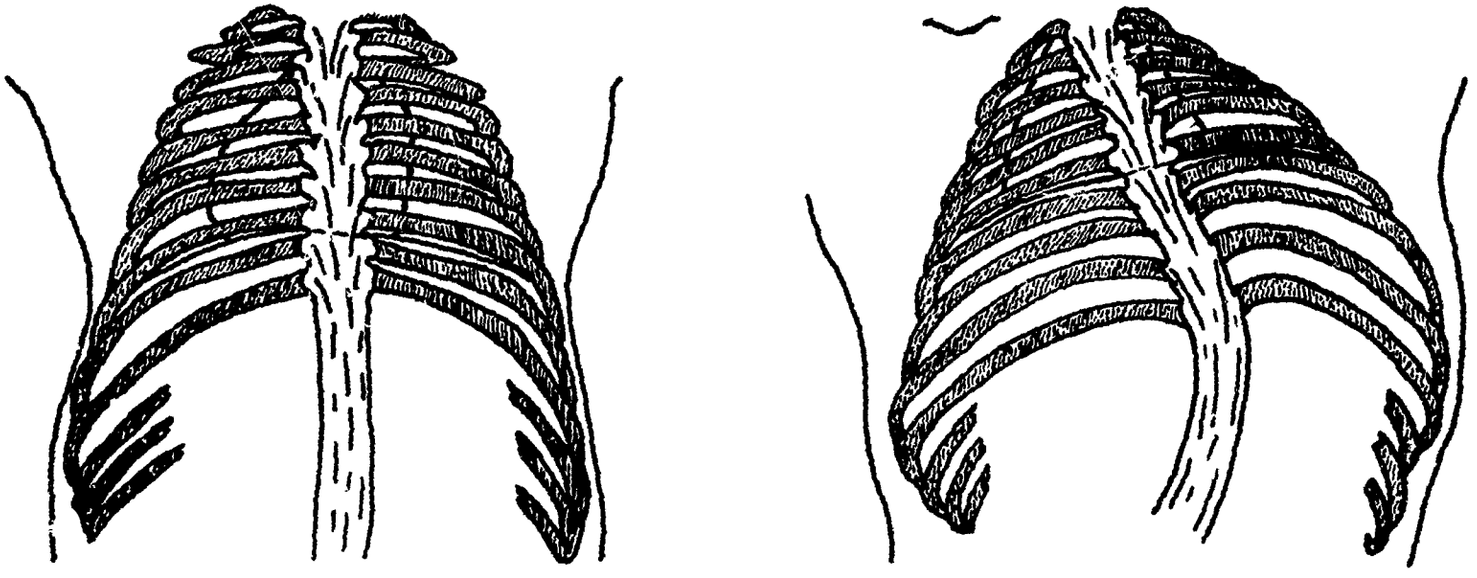

A. NORMAL PRONE ($+1G_x$)

B. DURING IMPACT ($-65G_z$)

FIGURE 30 MODIFIED TRACINGS OF MICRONEX X-RAY PHOTOGRAPHS OF 12 POUND CHIMPANZEE TAKEN AT $+1G_x$ (NORMAL PRONE) AND DURING $-65G_z$, ΔV - 243 ft/sec (30).

traveling to the periphery are reflected back at the junction of two media of different densities. The implosion effect relates to the events which follow a small detonation in fluid with gas bubbles. When the shock reaches the bubbles, they behave as localized explosive sources. Since the mechanisms of spalling and implosion are active at the junction of tissues of different densities, the lesions occurring at the junction between the alveolar tissue and the vascular and the bronchial trees can be attributed to these phenomena.

Spalling and implosion are concluded to be the major cause of injury in blast by Schardin, as referenced by White (31). The pathology incurred from air and water blast pulses has been studied by several investigators (32), (33). Most of these investigators agree that the physical principles of water blast are more clearly defined than the air blast. For such tests, dogs, rabbits, rats, sheep and calves have been used as experimental subjects. The most critical factor that emerges from these studies is that for the same forcing function the pathological findings does not vary much with the species. According to Desaga, as cited by Rossle (32), the susceptibility to injury of young calves is not significantly greater than that of smaller animals. Therefore, it may be assumed that quantitatively similar pathological lesions may occur in humans.

5.2.3 Injury to the Central Nervous System

Concussion is a violent jar or shock, or a condition which results from it, and we must expect all symptoms or injuries resulting from the $-G_z$ impacts to be those of concussion, e.g., concussion of the brain, spinal cord, lungs, etc. The injuries giving rise to the symptoms could be due to: (a) direct mechanical distortions and (b) indirect post impact events or reactions. Denny-Brown (34) and Trotter (35) believe that direct mechanical effects on the nerve cells give rise to the paralytic and other neurological manifestations of concussion. Diffuse cerebral injury by hydraulic pressure changes as advanced by Moritz (36) is probably a combination of both direct and indirect post impact effects. Indirect effects such as those by post impact circulatory disturbances are discussed by Cannon and Scott, as referenced by Moritz (36). Gurdjian (37) provides a broad discussion of both direct and indirect mechanism of injury. Judging from the interplay of forces

associated with impact, both the direct and indirect mechanisms of injury which lead to neurological manifestations, are complex and will be the subject of many reports of basic investigations now in process and in the future. These injuries need not be caused by $-G_z$ impact only to be germain, i.e., $\pm G_{x,y,z}$ impacts may cause some or all of these injuries, depending on the energy.

Injury to the brain can be explained by considering the two most fundamental states of strain, namely, dilatational and distortional. In these experiments of whole body deceleration during $-G_z$ impact, with the head restrained laterally only by soft material, distortion of the skull is minimized and the dilatational mode is limited to the potential volume disparity at the atlanto-occipital joint. Since the bulk modulus of the brain is very high (close to water) and its shear modulus (viscosity 20 dynes-sec/cm^2) relatively low, damage is presumably small when the rotation of the brain (distortional mode) within the cranial cavity is limited or minimized.

In previous experiments, Lombard (6), using guinea pig subjects, observed that hyperflexion at the atlanto-occipital joint while the head was restrained by a two-point suspension during $-G_x$ impact caused a high percentage of fatalities presumably due to cerebrospinal shock. This could be due to a distortional mode, but no anatomical evidence was obtained at necropsy. Likewise, Lombard, in the same experiments, observed the fatal effects of the dilitational mode incurred by rebound of the head against a hard head rest when using a loose or no head restraint. In this instance, cerebral injury with hemorrhage was observed at necropsy. Denny-Brown (34) pointed out that without the presence of signs of local trauma or hematoma formation, subdural or subarachnoid hemorrhage of moderate degrees may produce cerebral damage. The symptoms are brought about due to a change in momentum of the head during acceleration. During acceleration, a sudden rise in intracranial pressure could occur, creating a pressure gradient through the region of the brain stem and the cerebellum toward the foramen magnum (37), producing a shearing stress. Damage may be incurred to nerve cells and may not be detected even microscopically until after degeneration, in case the subject survives long enough. This was shown by Friede (38) using cats as subjects.

5.3 MATHEMATICAL MODEL APPLICATIONS TO HUMANS

Historically, mathematical model applications to humans have been devoted to the arterial system. The arterial system has been represented by a distributed system and extensive studies have been performed on pulse wave transmission, non-linear effects, reflected waves, etc. A majority of the personnel associated with aerospace programs, however, are interested in less refined information directly applicable in the evaluation of alterations in pathological and physiological responses following known input forcings. Of particular interest is the information relating dynamic variables such as pressure-flow characteristics in major blood vessels, cardiac rate, stroke volume, time duration required for recovery to steady state values following a known transient disturbance etc.

The quantitative applicability of the modified van der Pol equation [8] (Paragraph 4.1) necessitates evaluation of the "average steady state" values of the system variables m, λ^2, α^2, k and f. The quantity λ^2 is proportional to the energy available to the heart muscles and is obtainable from the stroke volume and pressure and velocity profiles in the aorta. The quantities α^2 and f representing the dynamic and static friction coefficients can be determined approximately from pressure changes in the resistance beds. The quantity k representing the lumped elasticity of the system is derivable from the cardiac rate and mass of the blood. In this context, Malindzak and Stacy (14) have determined the following values of lumped mass (M), lumped viscosity (V) and lumped stiffness (S) for equation [18]

$$M = 7.13 \times 10^{-4} \quad sec^{-2}$$

$$V = 9.09 \times 10^{-3} \quad sec^{-3}$$

$$S = 0.87$$

These constants were determined from human data at the Mayo Clinic and they represent average values for the normal human arterial system.

Determination of the steady state values m, λ^2, α^2, k and f both humans and larger animals will furnish their fixed limit cycle representations under normal conditions. Experimental studies and analytical correlation of pressure-flow changes in larger animals following impact will provide the altered representation of the phase plane trajectory (characterizing the time dependent and directional element of blood motion) for given values of

the forcing function variables. Unless injury occurs the displaced trajectory returns to the limit cycle oscillator because of the inherent stability of the mechanical oscillator. Consequently, the oscillator can be used to establish impact limits for reversible injury. The representation of the phase plane trajectory for larger animals can be transferred to the corresponding phase plane representation for man by scaling principles to yield the transient response and duration of this transient response for man.

The relaxation oscillator can also be used to qualitatively predict peripheral circulatory failure or shock following impact. In this connection, Harrison (39) remarks that peripheral failure results from a decline in inflow load which subsequently leads to a decrease in cardiac output and inadequacy of the blood flow to the tissues. The compensatory mechanisms attempt to keep the blood flow constant through certain organs, or at least above a critical minimum. Mathematically this condition can be interpreted by by placing constraints on the average blood velocity $\bar{V}$ defined by equation [11].

SECTION 6.0
CONCLUSIONS

As the result of experiments conducted using young adult guinea pigs and monkeys (Macaca speciosa) and by correlating the findings with data from other sources it has been possible to develop a theoretical analog of mechanisms of injury to the heart and great vessels, during exposure to $-G_z$ impact. The theoretical model as described by the modified van der Pol equation (Paragraph 4) and the subsystem study of aortic dynamics (Paragraph 4.3) furnishes good data on the pathophysiological responses of the cardiovascular system subjected to $-G_z$ impact. Before it can be accurately applied to man, however, further verification with larger animal surrogates is necessary. Direct "integration" of the central nervous system and cardiovascular system has not been attempted, since their mathematical coupling is beyond the scope of this project.

The use of bradycardia as a symptom of pending injury as the "level" of exposure to $-G_z$ is increased does not appear to be feasible in the two species of subjects tested, since it occurs much too early in the guinea pig and too late in the monkey. Specific changes in the ECG indicative of subendocardial damage may be more useful but will require further investigations.

Rupture of the heart and great vessels does not occur as predicted during exposure to $-G_z$ impact due to compensatory pressure increase in the thoracic cavity which acts as a "closed box" during the brief impact period. The neck vessels may not be so protected. Laceration of some pulmonary vessels does occur at very high G levels due to distortions, etc.

With the head protected by soft cloth or fabric restraint laterally only and a padded head rest intracranial injury was limited to minor hemorrhage in the meninges at the highest velocity changes and G levels. The subjects at levels of 300 G with ΔV of 60 ft/sec (velocity change) were dazed but not unconscious.

Support-restraint of the subject must consider distribution of the load to prevent; overload with compression of thorax, fracture of legs in bending

while holding the body in-tension, bending the torso by lack of lateral support, injury of head and neck by the use of soft lateral supports only, and careful selection of structures of support-restraint system. In addition, distribution of the load must minimize dynamic displacements.

It is believed that with a proper support-restraint system, the level of survival of man to $-G_z$ exposure with recoverable injuries should be approximately 100 G with velocity changes up to 60 ft/sec. Tolerance limits with perhaps some minor injuries should be from 20 to 30 G with velocity changes up to 60 ft/sec. Onset could be a factor that limits tolerance level more than survival level. Size of the subject, at present, does not appear to be an adverse factor, i.e., man size need not be more prone to injury. Fear of easy rupture of great vessels and the heart during $-G_z$ impacts appears to be unfounded.

The objectives of Phases I and II have been achieved and the results are very encouraging, especially since rupture of the heart and large vessels does not appear to be a factor. The possibility that the analog developed could be verified, using large animals, and refined so that it could be applied to man is very good. However, support-restraint system development will require a concomitant effort.

REFERENCES

1. Brown, W. K., et al: Human Response to Predicted Apollo Landing Impacts Selected Body Orientations. Aerospace Med., 37:394, 1966.

2. Stapp, J. P. and Taylor, E. R.: Space Cabin Landing Impact Vector Effects on Human Physiology. Aerospace Med. 35:1117, 1964.

3. Taylor, E. R. et al; Effect of Atropine Upon the Relative Bradycardia Associated with Impact. ARL-TDR-62-13, August 1962.

4. Lombard, C. F., et al: The Influence of Orientation and Support-Restraint Upon Survival from Impact Acceleration. NSL 66-110, July 1966. (In press as ARL-TDR-).

5. Lombard, C. F., et al: Impact Tolerance of Guinea Pigs Related to Orientation and Containment. Aerospace Med., 35:1, 1964.

6. Lombard, C. F., et al: Pathology and Physiology of Guinea Pigs Under Selected Conditions of Impact and Support-Restraint. Aerospace Med., 35:860, 1964.

7. Woodward, K. E., et al: Some Engineering Considerations of the Human Cardiovascular System, Diamond Ordnance Fuze Laboratories, TR-1075, February 1962.

8. Warner, H. R.: The Use of an Analog Computer for Analysis of Control Mechanisms in the Circulation. Pro. IRE, 46:1913, 1959.

9. Macey, R. I.: The Excitation of the Heart and its Modification under the Influence of the Chemical Mediators and the Cardiac Nerves: II. A Particular Case of the One-Factor Theory. Bull. Math. Biophys. 15:547, 1953.

10. Van der Pol, B. and Van der Mark, J.: The Heart Beat Consdiered as a Relaxation Oscillation, and an Electrical Model of the Heart. Arch. Neurl. Physiol. L'Homme Anim. 14:418, 1929.

11. Brinks, W. J.: Non-linear Differential Equations in Circulatory System Modelling. Harry Diamond Laboratories, February 1965.

12. Minorsky, N.: Non-linear Oscillations. D. Van Nostrand Co. Inc., New York, 1962.

13. Iberall, A. S. and Cardon, S. Z.: Analysis of the Dynamic Systems Response of Some Internal Human Systems. NASA CR-141, January 1965.

14. Malindzak, G. S. and Stacy, R. W.: Dynamic Behavior of a Mathematical Analog of the Normal Human Arterial System. J. Med. Elec., pp. 28-34, January - March 1965.

15. Flugge, W.: Handbook of Engineering Mechanics. McGraw Hill, New York, 1962.

16. King. A. L.: Pressure - Volume Relation for Cylindrical Tubes with Elastometric Walls: The Human Aorta. J. Appl. Physics, 17:501, 1946.

17. Womersley, J. R.: Oscillatory Flow in Arteries. The Constrained Elastic Tube as a Model of Arterial Flow and Pulse Transmission. Physics in Med. and Biol., 2:178, 1957.

18. Rushmer, R. F.: Pressure - Circumference Relations in the Aorta. Amer. J. Physiol. 183:545, 1955.

19. McDonald, D. A.: Blood Flow in Arteries. The Williams & Wilkins Co., Baltimore, 1960.

20. Lawton, R. W.: Measurements of the Elasticity and Damping of Isolated Aortic Strips of the Dog. Circ. Res., 3:403, 1955.

21. Remington, R. W.: Hysteresis Loop Behavior of the Aorta and Other Extensible Tissues. Amer. J. Physiol., 180:83, 1955.

22. Apter, J. T.: Mathematical Development of a Physical Model of Some Visco-Elastic Properties of the Aorta. Bull. Math. Biophys., 26:367, 1964.

23. Mollo-Christensen, E.: Energy Exchange and Stability Considerations in the Circulatory System. MIT Fluid Dynamics Res. Lab. Rept. No. 61-7, May 1961.

24. Headley, R. N., et al: Human Factor Response During Ground Impact. Aerospace Med., 33:141, 1962.

25. Weis, E. B., Jr., et al: Human Response to Several Impact Acceleration Orientations and Patterns. Aerospace Med., 34:1122, 1963.

26. Heymans, C. and Neil, E.: Reflexogenic Areas of the Cardiovascular System. Little, Brown and Company, Boston, p. 78, 1958.

27. Roberts, V. L., et al: Blunt Trauma to the Thorax - Mechanisms of Vascular Injuries. Ninth Stapp Car Crash Conference (University of Minnesota) pp. 3-12, 1966.

28. Evans, F. G. and Patrick, L. M.: Impact Damage to Internal Organs. Impact Acceleration Stress Symposium, pp. 159-171, November 1961.

29. Mead, J. and Milic - Emile, J.: Theory and Methodology in Respiratory Mechanics with Glossary and Symbols. Handbook of Physiology, Amer. Physiol. Soc., Sec. 3, I:363, 1964.

30. Stapp, J. P.: "Tolerance to Abrupt Deceleration", Collected Papers on Aviation Medicine. Butterworths Scientific Publications, London, pp. 122-169, 1955.

31. White, C. S.: Biological Effects of Blast. Technical Progress Report, Contract No. DA-49-416-XZ-055, December 1961.

32. Rossle, R.: "Pathology of Blast Effects". German Aviation Medicine World War II , U.S. Government Printing Office, Washington, DC, II:1260, 1950.

33. Schardin, H.: "The Physical Principles of the Effect of a Detonation". German Aviation Medicine World War II, U.S. Government Printing Office, Washington, DC, II:1207, 1950.

34. Denny Brown, D. and Russell, W. R.: Experimental Cerebral Concussion. Brain, 64:93, 1941.

35. Trotter, W.: On Certain Minor Injuries of the Brain. Lancet, 1:933, 1942.

36. Moritz, H. C.: The Pathology of Trauma. Lea and Febiger, Philadelphia, p. 319, 1954.

37. Gurdjian, E. S. and Webster, J.E.: Head Injuries. Little, Brown, and Company, Boston, 1958.

38. Friede, R. L.: Experimental Concussion Accelerations. Arch. Neurol., 4:449, 1961.

39. Harrison, et al, editors: Principles of Internal Medicine. McGraw Hill Book Co. Inc., New York, 1958.

APPENDIX

PATHOPHYSIOLOGICAL RESPONSE TO $-G_z$ IMPACTS

The production of pathophysiological cardiovascular and central nervous system manifestations at lower levels and the additional production of anatomical injury at higher levels of exposure of experimental animals to $-G_z$ impact has raised a considerably doubt as to the safety of human subjects during experiments to establish tolerance levels or limits. Correlations between objective symptoms and injuries occurring in animal subjects and the variables of the $-G_z$ impact will give greater insight into the problem. The areas of prime concern are the potential production or induction of "potentiated" injury of the a) heart, b) central nervous system, and c) vascular tonicity. These "potentiated" injuries such as ventricular tachycardia, cerebral concussion, and shock may or may not be more frequent in occurrence due to $-G_z$ exposure than in any other orientation. The lack of adequate data on either animal or human subjects in the $-G_z$ orientation makes it necessary to pay particular attention to these "potentiated" types of injuries such that signs and symptoms, indicative of preinjury level, could be established prior to extensive use of human subjects. Bradycardia, a common occurrance following $-G_z$ exposure to acceleration, has been considered to be a possible measure of pending cardiovascular injury such as the above. A discussion of the reflex control of heart rate and a brief literature review of bradycardia is, therefore, given.

A.1 REFLEX CONTROL OF HEART RATE

The pulsation (beat) of the heart is a result of action potentials which depolarize the cell membrane of the cardiac muscles causing them to contract. These action potentials are generated in the sinoatrial (S-A) node which is situated in the right atrium (Figure A1). The impulses spread throughout the atria to the atrioventricular (A-V) node and are then conducted through the bundle of His and the Purkinje network to the ventricles. The S-A node, however, is not the only area of the heart capable of generating action potentials since this is an inherent characteristic all types of cardiac muscle. After the muscles have depolarized they must be repolarized before they can discharge spontaneously. The time required for repolarization

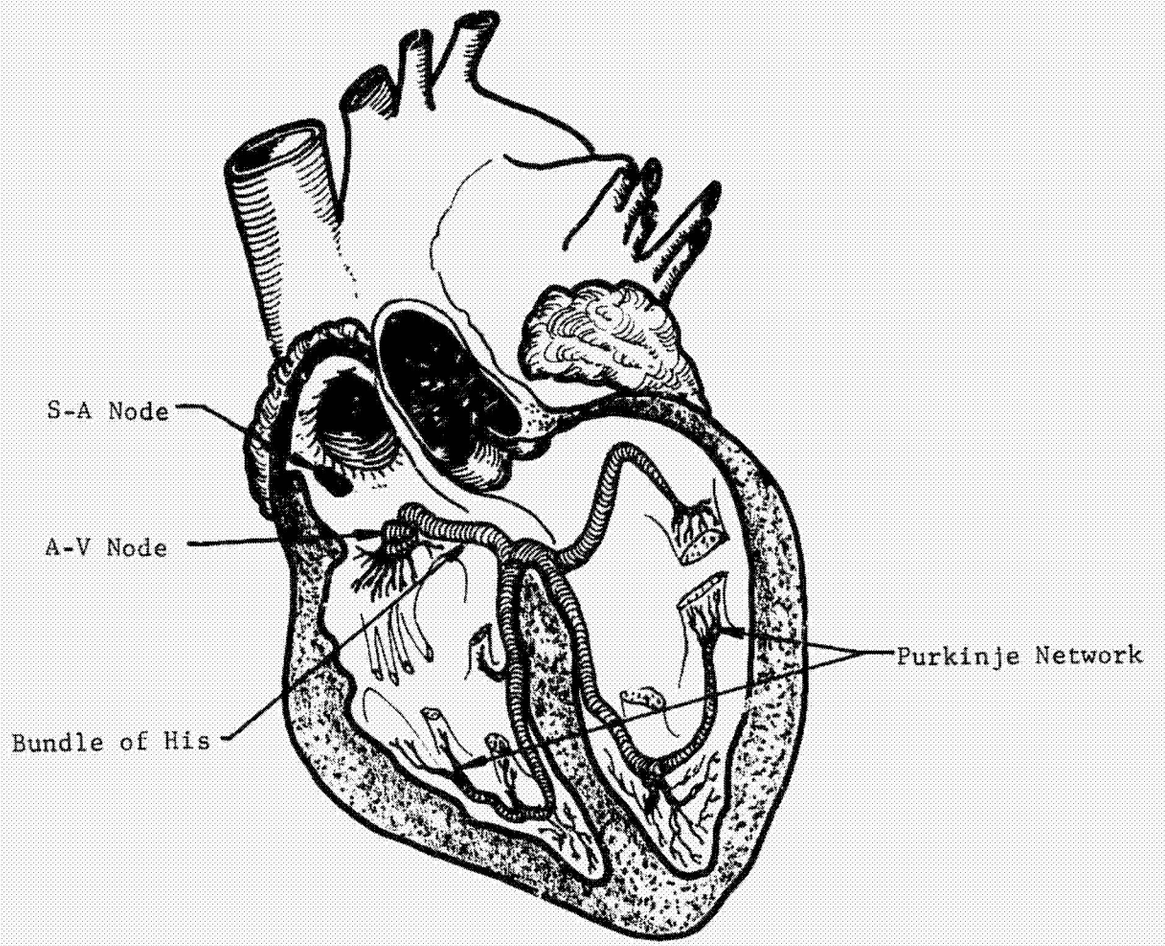

FIGURE A1 SCHEMATIC DIAGRAM OF HEART WITH IMPULSE CONDUCTING SYSTEM

varies with the different types of cardiac muscle (ventricular muscle, atrial muscle, etc.). This specialized property permitts the S-A node, which has the highest intrinsic rhythm, to regulate the rhythmic discharge of the other areas of the heart. The S-A node discharges, depolarizing the remainder of the heart, then recovers and discharges again before any other cardiac muscle can fully repolarize and discharge. Thus, the cardiac muscles are continuously depolarized in rhythm with the S-A node and are prevented from establishing their own basic rhythms. For this reason the S-A node is referred to as the pacemaker.

The heart rate is controlled physiologically by the balancing influence exerted on the pacemaker cells (S-A node) by the slowing effects of discharges along the parasympathetic nerves and the accelerating effects of discharges along the sympathetic nerves. The action of the sympathetic and parasympathetic nerves in altering the basic rhythmic discharge of the pacemaker cells is, in a large measure, reflex in origin.

To appreciate the basic mechanism of reflex control, an understanding of the reflex arc is essential. The reflex arc consists of an afferent limb, a center, and an efferent limb. The afferent limb is composed of receptors, which on excitation give rise to nerve impulses, and neurons which conduct impulses to the center. The center situated in the gray matter of the central nervous system, consists of a group of cell bodies which transmit impulses to the efferent limb. The efferent limb is comprised of motor neurons which convey impulses to stimulate the effector organ(s).

The cardiac reflexes act in a similar manner, but are considerably more complex. The afferent pathways are situated in numerous regions of the body with the probable exception of the skin (1)*. The centers, located in the medulla, are known as card centers. The efferent pathways consist of the inhibitor (vagi) and accelerator (sympathetic) nerves which act on the heart. The vagus nerves are cardioinhibitory and their stimulation causes bradycardia. They convey fibres, belonging to the parasympathetic division of the involuntary nervous system, from the cardioinhibitory center in the medulla to special tissues of the heart (S-A node, A-V node, etc.). The accelerator or augmentor nerves are part of the sympathetic nervous system. The preganglionic fibres enter the gangliated chain of the sympathetic system to connect with cells in the inferior, middle, and superior cervical ganglia which supply fibres to the heart. Changes in heart rate are

*Appendix References given at end of Appendix

effected by an adjustment in the balance between the effects of the two sets of nerves as shown in Figure A2. It has been observed that if both vagi and sympathetic nerves to the heart are cut, the heart rate increases. Thus it can be concluded that vagal effects predominate at rest.

Probably the first idea of a reflex regulation of the cardiovascular system exercised via afferent nerve endings situated in the heart and blood vessels occurred to Cyon and Ludwig (2) with the discovery of the depressor nerve (Figure A3). They found that stimulation of the central end of the nerve produced marked bradycardia in a rabbit. Paintal (3) has confirmed the work of Cyon and Ludwig recently. It has been shown that this reflex bradycardia can be abolished by the use of atropine.

It was proved by Koster and Tschermak (2), with degeneration experiments, that the principal site of origin of the aortic nerve (one of the afferent paths to the cardioinhibitory center) was from the arch of the aorta (Figure 3) and the roots of the great vessels. They demonstrated that action potentials could be generated in the nerve by distending the isolated aorta with saline (2). Bradycardia in animals could be caused by distending an isolated innervated segment of the aortic arch (2). Similar reflex responses have also been reported by Daly (2) and Sutton (2). Heymans and Ladon (2) conducted some classical experiments with the establishment of cross-circulation in dogs. They used a donor dog to perfuse the head of a recipient dog, whose head was completely separated from its trunk (maintained properly for respiration and circulation) except for the vagi nerves. A rise in pressure in the trunk of the recipient dog produced bradycardia in the recipient dog. Following section of the vagi, however, no bradycardia was found concomitant with a rise in pressure in the trunk of the recipient dog. This indicated that the bradycardia response was reflex in origin with both afferent and efferent stimulation being carried in the vagi.

Nakayama (2) has shown that a rise in pressure in the right subclavian area of dogs induced reflex bradycardia. This findings was corroborated in cats by Neil (2). Although bradycardia could be induced by raising the blood pressure in the perfused carotido-cephalic circulation (2), it was left to Hering (2) to make the discovery that this was reflexogenic in origin. He found that light pressure on one of the carotid arteries evoked

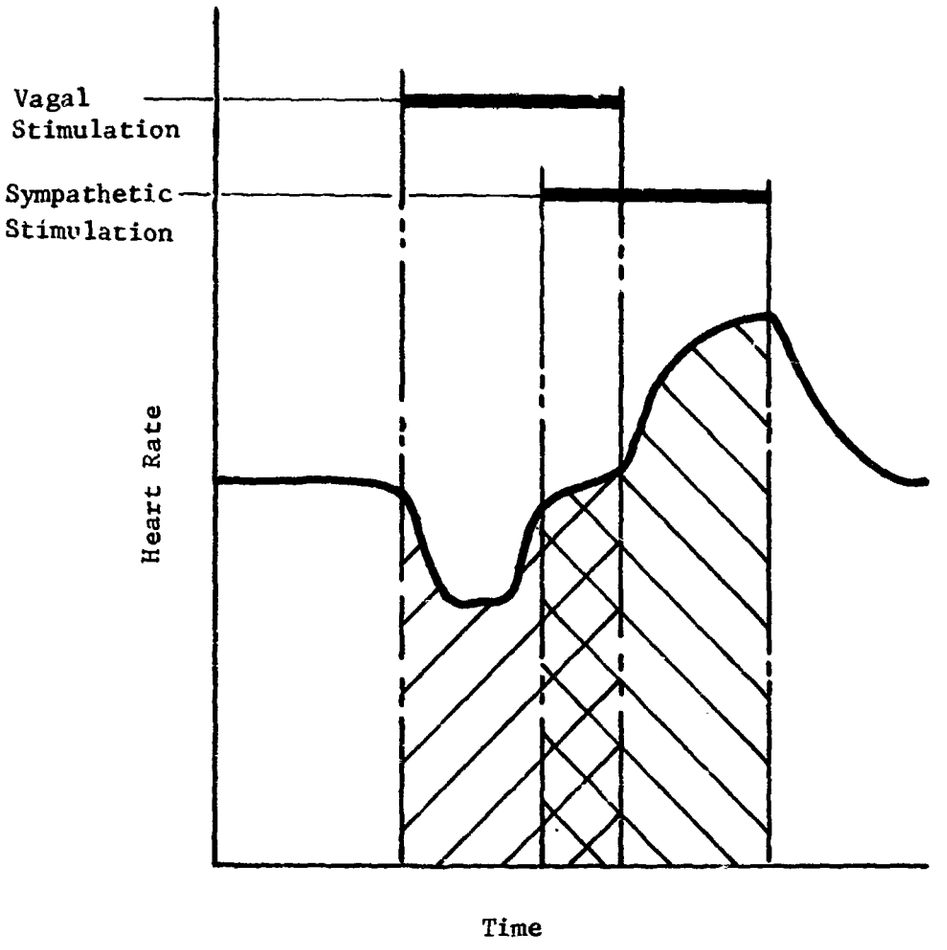

FIGURE A2 VAGAL AND SYMPATHETIC EFFECTS ON HEART RATE

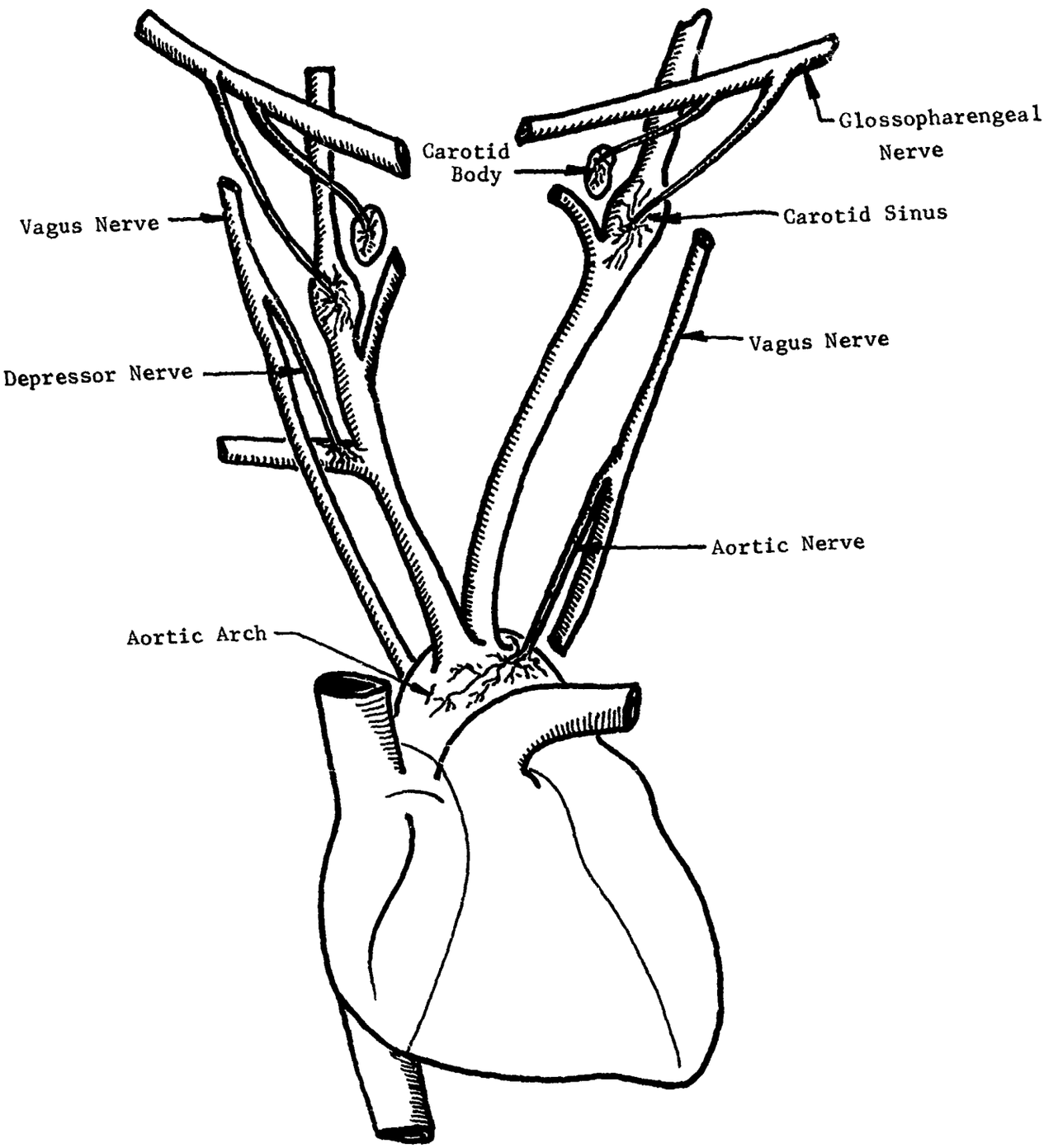

FIGURE A3 IMPULSE CONDUCTING SYSTEM FROM AORTIC ARCH AND CAROTID SINUS

marked slowing of the heart. Bronk and Stella (4) observed that the mean level of blood pressure was not the sole cause of stimulation of the baroreceptors. Different baroreceptors were found to have different thresholds, not only to pressures at the steady state but also to the rate of rise of pressure with higher pressures demanding increased frequencies of discharge (2). In this respect the sinus receptors are similar in behavior to muscle spindles in that the frequency of discharge (impulses) is directly influenced by the rate of rise of tension or stretch (stress or strain rates).

In experiments designed by MacLeod and Scott (5) to determine the efferent pathways through which bradycardia could be evoked, it was observed in cats that division of the cervical vagosympathetic nerves reduced, but did not always abolish slowing of the heart in response to stimulation of carotid bodies. Therefore, they concluded that bradycardia occurring during carotid body excitation is due both to an increase in vagal tone and to a decrease in sympathetic tone. This finding is in agreement with the results obtained by other workers in previous experiments conducted on dogs (6, 7).

In man, dramatic reflex cardiovascular effects have been observed as a result of unavoidable traction and manipulation of vessels and nerve trunks during neck surgery. Local anesthetic block of the afferent fibres of vagus nerve have eliminated such undesirable responses (8).

The effects of direct electrical stimulation of the carotid sinus nerve in man by Carlsten (9) produced a reflex bradycardia, a decrease in the pulse amplitude and decrease in both systolic and diastolic pressures. There was a concomitant marked fall in the resistance to blood flow within the forearm vascular bed. The events are illustrated in Figure A4.

All the literature cited above is devoted to the mechanisms of reflex action under steady state. Similar mechanisms governing physiological responses are expected to function under conditions of accelerative stress. Jongbloed and Noyons (10) demonstrated severe bradycardia in rabbits on a small turntable at about -2.5 G_z. They denervated the carotid sinus area and showed that this bradycardia was due to carotid sinus reflex stimulation of the vagus depressor nerves. Rosenfeld and Lombard (11) studied the cardiovascular pressor reflex mechanism in goats, monkeys, and dogs and

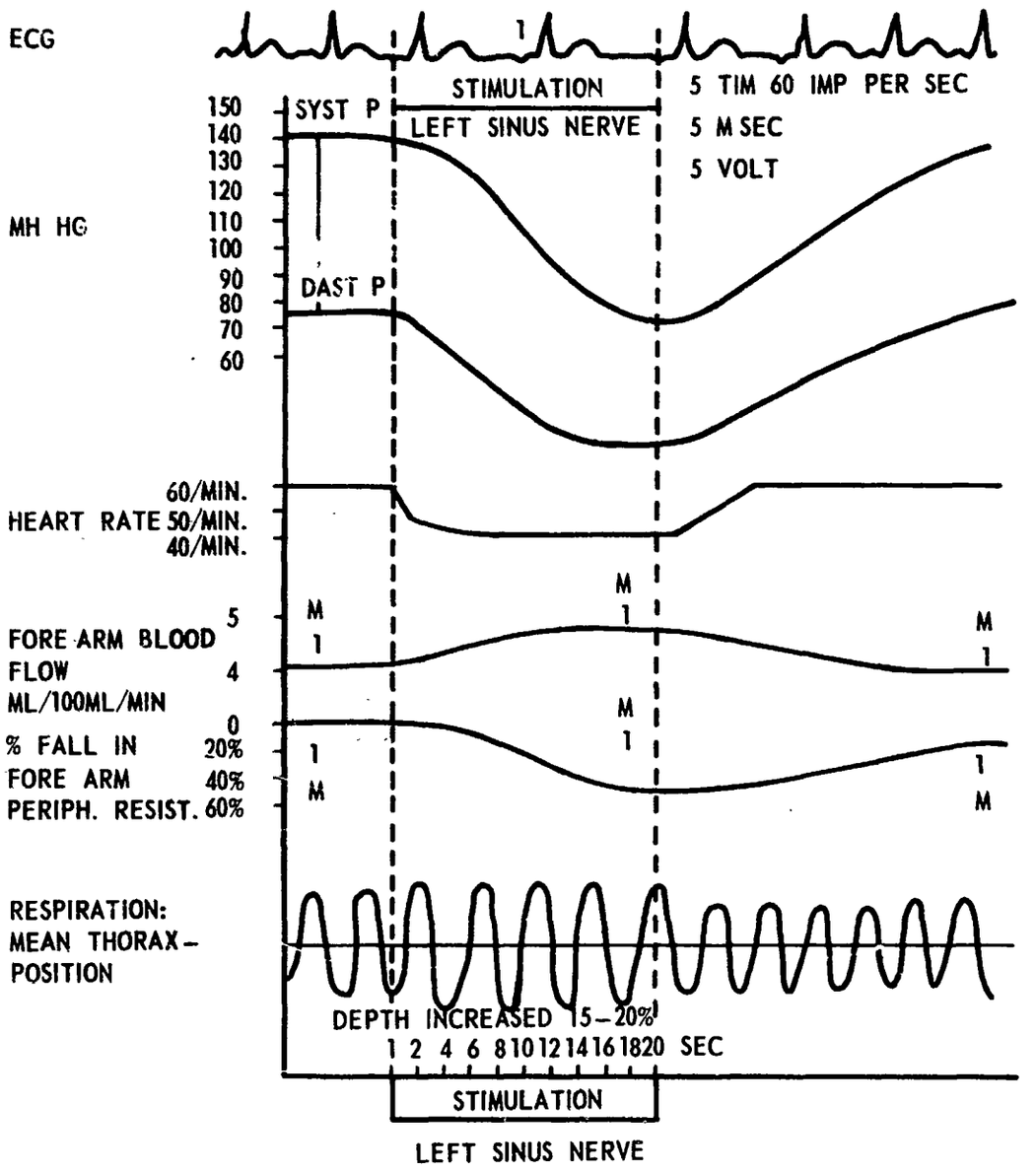

FIGURE A4 A DIAGRAM ILLUSTRATING THE EFFECT OF STIMULATION OF THE LEFT SINUS NERVE IN MAN. NOTE THE ECTOPIC PACEMAKER OF THE HEART AT STIMULATION (9).

compared the effect of exposure to -5 G_z on the centrifuge to that of man exposed to -3 G_z. The animals were exposed both vagotomized and nonvagotomized. The oscillograph records are shown in Figures A5 thru A10 and the reduced data is shown in Tables AI, AII and AIII. These records indicate that the response of the cardiovascular pressor reflex in the three animals tested is similar to that of man. The dog and monkey (rhesus) are most similar since the control of the arterial pressure was least effective in the goat. After bilateral vagotomy of the three animals the bradycardia was essentially abolished during the $-G_z$ exposures, but the arterial pressure in the dog dropped to a lowered level indicative of poor venous return or hypovolemia. Individual variations and techniques may account for some of these differences.

A carotid sinus reflex bradycardia of less than 30 seconds duration results from headward force vectors of whole body single impact exceeding 15 G magnitude, which probably triggers the carotid sinus by an abrupt rise in hydraulic pressure (12).

The bradycardia response is not limited to $-G_z$ exposures since it has also been demonstrated in $\pm G_x$ impacts. Rhein (13) found bradycardia in humans following exposure to +15 G_x impacts. Ruff (14) using human subjects in impact exposures in the $-G_x$ orientation up to 18 G (1500 Kg) with total time of impact around 0.1 sec., and using a wide abdominal belt (40 cm - 16 in) reports no injuries to organs or tissues. However, above 12 G the impacts were "subjectively unpleasant" and produced a reduction in heart rate indicating increased vagal activity. An examination of slow motion pictures of the impacts revealed that the torso rotated forward about the abdominal belt. This indicates a $-G_z$ terminal orientation of the torso.

Slowing of the heart rate in man as a result of accelerative forces has been reported by Brown and his colleagues (15) in a recent study. Similar reports have been published by other investigators (16 and 17).

A.2. SHOCK

Clinical shock following impact is perhaps the best known pathophysiological response besides baroreceptor reflex mechanism and trauma. The shock can and often does occur without any structural failure and is

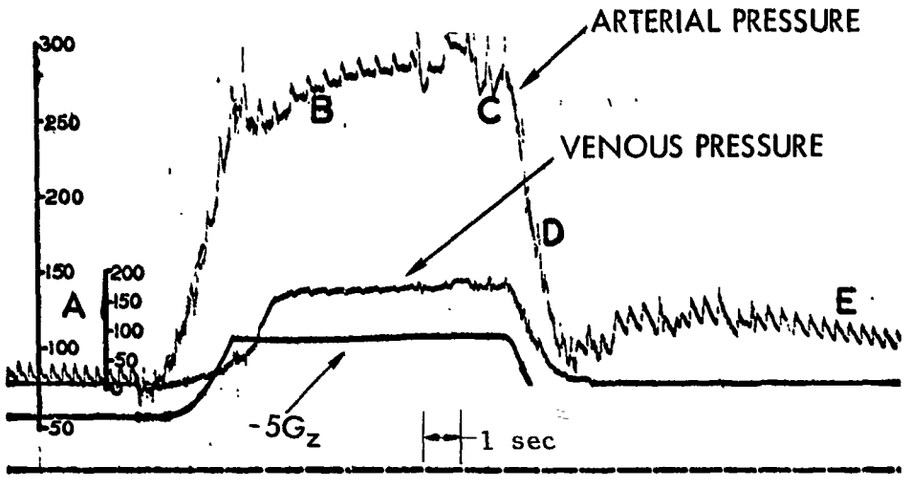

FIGURE A5 - OSCILLOGRAPHIC RECORDINGS OF CAROTID AND JUGULAR PRESSURE OBTAINED DURING EXPOSURE OF A GOAT TO $-G_z$. CAPITAL LETTERS ARE EXPLAINED IN TABLE I.

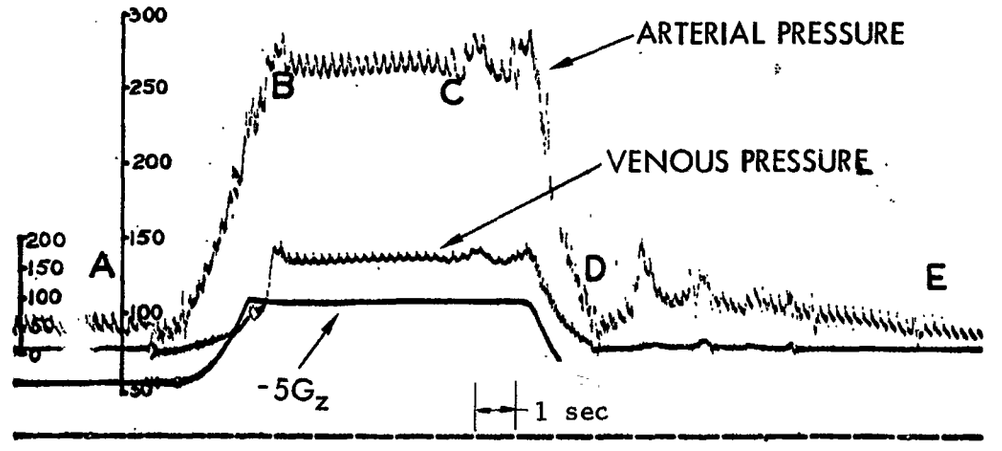

FIGURE A6 - OSCILLOGRAPHIC RECORDINGS OF CAROTID AND JUGULAR PRESSURE OBTAINED DURING EXPOSURE TO $-5G_z$ AFTER THE GOAT OF FIGURE 5 WAS BILATERALLY VAGOTOMIZED. CAPITAL LETTERS ARE EXPLAINED IN TABLE II.

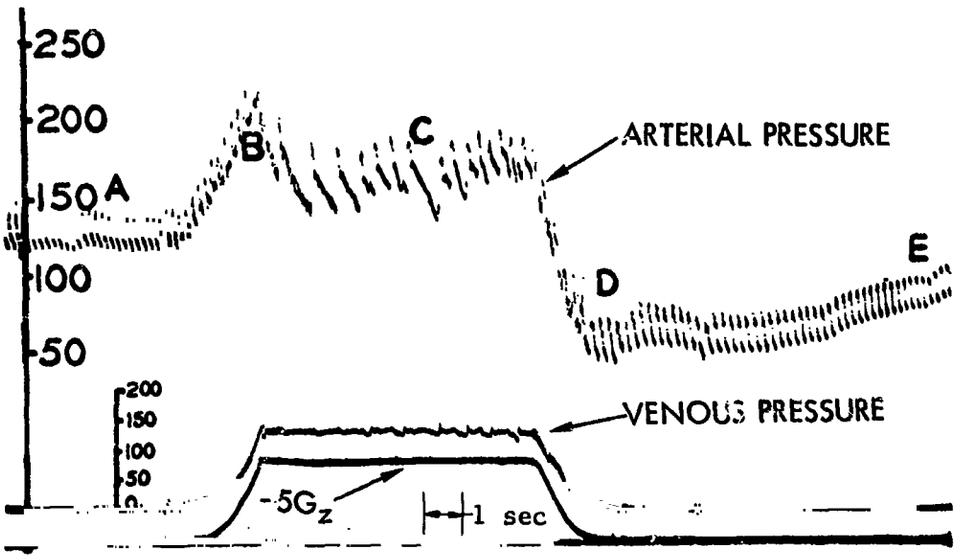

FIGURE A7 - OSCILLOGRAPHIC RECORDINGS OF CAROTID AND JUGULAR PRESSURE OBTAINED DURING EXPOSURE OF A DOG TO $-5G_z$.

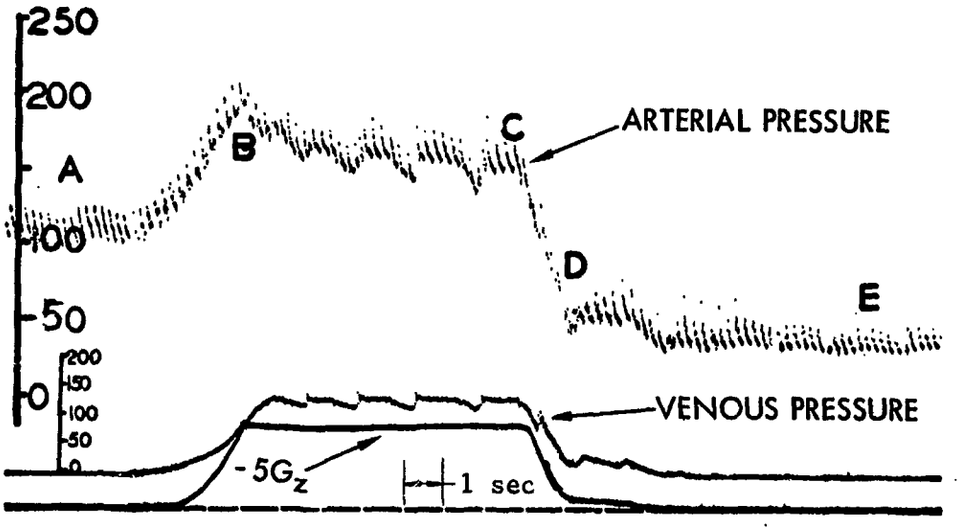

FIGURE A8 - OSCILLOGRAPHIC RECORDINGS OF CAROTID AND JUGULAR PRESSURE OBTAINED DURING EXPOSURE TO $-5G_z$ AFTER THE DOG OF FIGURE 7 WAS BILATERALLY VAGOTOMIZED.

TABLE AI NORMAL RESPONSE OF CARDIOVASCULAR REFLEXES TO NEGATIVE 5G (EXPRESSED IN mm Hg)

		A*	B	C	D	E
		Before Acceleration	During Acceleration		After Acceleration	
			1st 5 sec	Last 5 sec	1-4 sec	20 sec
GOAT	Arterial Pressure	90/75	278/268	300/275	155/145	110/90
	Venous Pressure	10	170	175	80	10
	Pulse Pressure	15	10	30	10	20
	Arterio-Venous Diff.	72	97	155	70	90
	Pulse	96	60	36	--	96
DOG	Arterial Pressure	140/115	235/200	190/160	75/45	110/80
	Venous Pressure	-5	140	130	9	-5
	Pulse Pressure	25	35	30	30	30
	Arterio-Venous Diff.	130	78	45	50	100
	Pulse	165	80	48	120	156
MONKEY	Arterial Pressure	105/90	145/115	120/95	78/60	65/40
	Venous Pressure	20	20	50	25	20
	Pulse Pressure	15	30	25	18	15
	Arterio-Venous Diff.	75	110	66	44	37
	Pulse	228	84	84	168	228

NORMAL RESPONSE OF CARDIOVASCULAR REFLEXES TO NEGATIVE 3G (EXPRESSED IN mm Hg)

		Before Acceleration	During Acceleration		After Acceleration	
			1st 5 sec	Last 5 sec	1-2 sec	10 sec
MAN **	Arterial Pressure	140/90	205/165	175/150	125/70	135/85
	Venous Pressure	10	70	90	60	8
	Pulse Pressure	50	40	25	55	50
	Arterio-Venous Diff.	150	115	73	37	102
	Pulse	96	72	48	96	96

DATA PRESENTED ABOVE IS REPRESENTATIVE OF TYPICAL RESPONSE ELICITED BY VARIOUS SPECIES STUDIED

* CAPITAL LETTERS represent points makred in capital letters in Figures 5, 7, and 9.

** Data extracted from oscillographic record illustration (11).

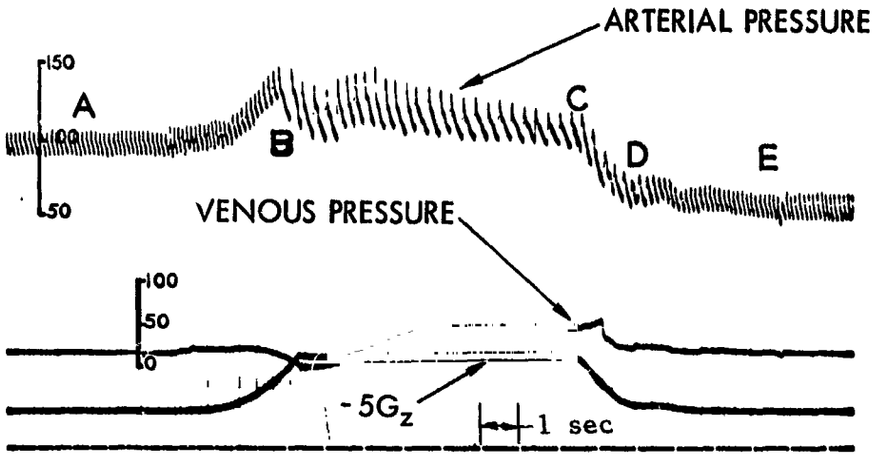

FIGURE A9 - OSCILLOGRAPHIC RECORDINGS OF CAROTID AND JUGULAR PRESSURE OBTAINED DURING EXPOSURE OF A RHESUS MONKEY TO $-5G_z$.

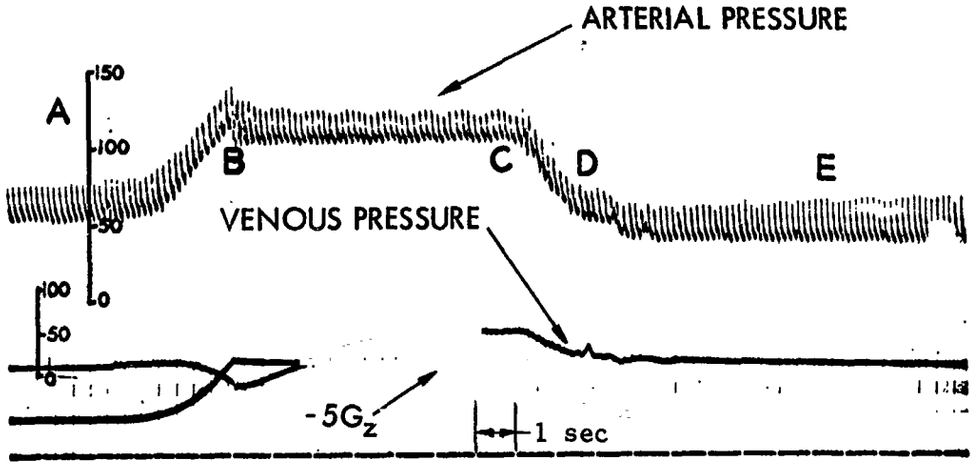

FIGURE A10 - OSCILLOGRAPHIC RECORDINGS OF CAROTID AND JUGULAR PRESSURE OBTAINED DURING EXPOSURE TO $-5G_z$ AFTER THE MONKEY OF FIGURE 9 WAS BILATERALLY VAGOTOMIZED.

TABLE AII RESPONSE OF CARDIOVASCULAR REFLEXES TO NEGATIVE 5G AFTER BILATERAL VAGOTOMY (IN mm Hg)

		A*	B	C	D	E
		Before Acceleration	During Acceleration		After Acceleration	
			1st 5 sec	Last 5 sec	1-4 sec	20 sec
GOAT	Arterial Pressure	100/85	286/250	275/255	100/70	102/70
	Venous Pressure	0	190	164	0	32
	Pulse Pressure	15	26	20	30	32
	Arterio-Venous Diff.	92	85	101	85	86
	Pulse	120	120	120	120	120
DOG	Arterial Pressure	120/100	205/185	170/150	64/45	62/37
	Venous Pressure	15	65	130	25	-5
	Pulse Pressure	20	20	20	20	25
	Arterio-Venous Diff.	115	130	30	30	55
	Pulse	144	132	132	140	144
MONKEY	Arterial Pressure	75/55	130/115	125/105	75/55	65/40
	Venous Pressure	10	0	50	30	10
	Pulse Pressure	20	25	20	20	25
	Arterio-Venous Diff.	55	127	65	35	42
	Pulse	184	183	180	180	189

DATA PRESENTED ABOVE IS REPRESENTATIVE OF TYPICAL RESPONSE ELICITED BY VARIOUS SPECIES STUDIED.
*CAPITAL LETTERS represent points marked in capital letters in figures 6, 8, and 10.

TABLE AIII CALCULATED AND RECORDED BLOOD PRESSURES

	Heart to Base of Brain in cm. (approx. values)	"G"	Calculated Pressure in mm Hg.		Recorded Pressure in mm Hg.			Actual Arterial Pressure Exclusive of Hydrostatic Pressure	
			Venous*	Arterial**	Venous	Arterial			
						1st 5 sec	Last 10 sec	1st 5"	Last
Goat	38	5G	148	1. 148+ 82=230 2. 148+ 90=238	170	Mean 273 Syst. 278	290 300+	Mean 125 Syst. 130	[illegible] 152+
Dog (large)	38	5G	148	1. 148+128=276 2. 148+140=288	140	Mean 217 Syst. 235	175	Mean 69 Syst. 87	27 42
	38	3G	89	1. 89+127=216 2. 89+140=229	85-90	Mean 203 Syst. 222	180 192	Mean 114 Syst. 133	91 103
Man	28-32***	3G	70	1. 70+115=185 2. 70+140=210	70-90	Mean 185 Syst. 205	162 175	Mean 115 Syst. 135	92 105
Monkey	17	5G	56	1. 56+ 97=153 2. 56+105=161	20-50	Mean 130 Syst. 145	107	Mean 74 Syst. 89	51 64

* Hydrostatic Pressure at G

** 1. Hydrostatic Pressure + Pre Run Mean Arterial Pressure

2. Hydrostatic Pressure + Pre Run Systolic Pressure

*** No Figures Available for Subject Used, Average Values Used

wholly accompanied by transient bradycardia. According to Harrison (18), the clinical signs and symptoms of shock (peripheral type of forward failure or primary decrease of cardiac inflow load) may vary with the severity and accuteness of the condition. When forward failure is predominant, a reduction in pulse pressure is one of the earlier signs. He further remarks that initially the decrease in pulse pressure and the accompanying faintness may be observed only in the standing and seated positions. Considering these observations, the shock noted by Stapp (19) and Lombard (20) in animals exposed to $-G_z$ and also $-G_x$ orientacions in the absence of hemorrhage must have been the result of reflexes with primary loss of vascular tone and inadequate venous return. The reflex mechanism involved in the production of this primary shock may be more than the afferent vasopressor stimulation of the vagus and glossopharyngeal nerves. Lombard (20) found that animals allowed to remain upright after a $-G_x$ impact had symptoms of inadequate circulation and expired in 5 to 10 minutes. If the animals were immediately pronated after exposure symptoms of inadequate circulation disappeared and the animals would recover in about 10 minutes. Thus, one can seriously question any support-restraint system which after escape impact (parachute or windblast) or landing impact does not protect against the secondary effects of primary shock. This means that the long axis of the body must be at right angles to the gravity vector to restore circulation after impact.

A.3. CEREBRAL CONCUSSION

The loss of consciousness due to impact of the head is called concussion and must be considered. Denny-Brown (21) extensively studied cerebral concussion using cats, dogs and monkeys as experimental subjects and concluded that his subjects show features of cerebral concussion directly comparable with cerebral concussion as observed clinically in man. Acceleration concussion was produced in the monkey and the cat when the head was struck by a heavy mass with the velocity of approximately 28 ft/sec. One of his numerous conclusions of particular interest is "Subthreshold blows often stimulate the vago-glossopharyngeal system, and in this way result in depression of cardiac, vasomotor and respiratory function for ten to thiry seconds, occasionally longer. This is a possible explanation for the 'knockout blow' in boxing." He attributes lack of recovery from the effect on vago-glossopharyngeal mechanism in inducing primary shock as the main cause of of failure of blood pressure leading to death from acceleration concussion.

A.4. SUMMARY

The exact mode of action for the production of the bradycardia due to $-G_z$ impact lacks conclusive proof. However, from the experiments conducted and the [illegible]rature reviewed it is believed to be due to a combination of afferent stimuli reflexly [illegible]pressing the heart (rate) through the efferent pathways, the vagus nerves. Both the elevated pressures in the blood vessels (especially in the carotids) and the mechanical distortions of the body tissues (viscera) during the $-G_z$ impact could give rise to the afferent stimulus. In addition to bradycardia, $-G_z$ impact exposures may lead to other serious reflex complications such as cerebral concussion and shock with mortality.

APPENDIX

REFERENCES

1. Rushmer, R. F.: Cardiovascular Dynamics. W. B. Saunders, Philadelphia, 2nd Ed., Chapt. 3, 1961.

2. Cited by - Heymans, C. and Neil, E.: Reflexogenic Areas of the Cardiovascular System. Little, Brown and Co., Boston, 1958.

3. Paintal, A. S.: A Study of Ventricular Pressure Receptors and Their Role in the Bezold Reflex. Quart. J. Exp. Physiol., 40:348, 1955.

4. Brown, D. W. and Stella, G. J.: Afferent Impulses in Carotid Sinus Nerve Relation of Discharge from Single End Organs to Arterial Blood Pressure. J. Cell and Comp. Physiol., 1:113, 1932.

5. MacLeod, R. D. M. and Scott, M. J.: The Heart Rate Responses to Carotid Body Chemoreceptor Stimulation in the Cat. J. Physiol., 175:193, 1964.

6. Daly, M. DeB. and Scott, M. J.: The Effects of Stimulation of the Carotid Body Chemoreceptors on Heart Rate in the Dog. J. Physiol., 144:148, 1958.

7. Downing, S. E., Remensnyder, J. P., and Mitchell, J. H.: Cardiovascular Responses to Hypoxic Stimulation of the Carotid Bodies. Circ. Res., 10:676, 1962.

8. Wang, S. C. and Borison, H. L.: An Analysis of the Carotid Sinus Cardiovascular Reflex Mechanism. Amer. J. Physiol., 150:712, 1947.

9. Carlsten, A., et al: Cardiovascular Effects of Direct Stimulation of the Carotid Sinus Nerves in Man. Acta Physiol. Scand., 46:138, 1958.

10. Cited by - Duane, T. D., et al: Studies on Cerebral Physiology of Monkeys at 12 Negative G. J. Aviation Med., 23:479, 1952.

11. Rosenfeld, S. and Lombard, C. F.: Cardiovascular Pressor Reflex Mechanism and Cerebral Circulation Under Negative G Head-to-Tail Acceleration. J. Aviation Med., 21:243, 1950.

12. Stapp, J. P. and Taylor, E. R.: Space Cabin Landing Impact Vector Effects on Human Physiology. Aerospace Med., 35:1117, 1964.

13. Rhein, L. and Taylor, E. R.: Relative Bradycardia After Impact. ARL-TDR-63-12, Aug. 1962.

14. Ruff, S.: "Brief Acceleration: Less than One Second." German Aviation Medicine World War II, U.S. Government Printing Office Washington, DC, I:584, 1950.

15. Brown, W. K., et al: Human Response to Predicted Apollo Landing Impacts in Selected Body Orientations. Aerospace Med., 37:394, 1966.

16. Taylor, E. R., et al: Effects of Atropine Upon the Relative Bradycardia Associated with Impact. ARL-TDR-62-13, Aug. 1962.

17. Weis, E. B., Jr., et al: Human Response to Several Impact Acceleration Orientations and Patterns. Aerospace Med., 34:1122, 1963.

18. Harrison, et al, editors: Principles of Internal Medicine. McGraw Hill Book Co., Inc., New York, 1958.

19. Stapp, J. P.: "Tolerance to Abrupt Decelerations." Collected Papers on Aviation Medicine, Butterworths Scientific Publications, London, pp. 122-169, 1955.

20. Lombard, C. F., et al: Pathology and Physiology of Guinea Pigs Under Selected Conditions of Impact and Support-Restraint. Aerospace Med., 35:860, 1964.

21. Denny-Brown, D. and Russell, W. R.: Experimental Cerebral Concussions. Brain, 64:93, 1941.